UNIVERSITEIT VAN PRETORIA
UNIVERSITY OF PRETORIA
YUNIBESITHI YA PRETORIA

DOCTORAL THESIS

Sedimentology, palaeoenvironment and structural interpretation of the Cretaceous SW Anambra Basin, Nigeria

Author:

Erepamo J. Omietimi

Student number: 19390514

Supervisors:

Prof. Nils Lenhardt

Prof. Adam Bumby

Prof. Renchao Yang

A thesis submitted in partial fulfillment of the requirements for the

degree of Doctor of Philosophy in Geology

In the Faculty of Natural and Agricultural Sciences

University of Pretoria

Pretoria

August 24th , 2022

Declaration

I, Erepamo J. Omietimi declare that the thesis, which I hereby submit for the degree of Doctor of Philosophy (PhD) in Geology at the University of Pretoria, is my own original work and has not previously been submitted by me for a degree at this or any other tertiary institution.

Parts of this thesis have been published as:

Omietimi, E. J., Chouhan, A. K., Lenhardt, N., Yang, R., Bumby. A. J. (2021) Structural interpretation of the south-western flank of the Anambra Basin (Nigeria) using satellite-derived WGM 2012 gravity data. Journal of African Earth Sciences, 182, 104290. https://doi.org/10.1016/j.jafrearsci.2021.104290).

Omietimi, E.J., Lenhardt, N., Yang, R., Götz, A.E. & Bumby, A.J. (2022) Sedimentary geochemistry of Late Cretaceous-Paleocene deposits at the south-western margin of the Anambra Basin (Nigeria): Implications for paleoenvironmental reconstructions. Palaeogeography, Palaeoclimatology, Palaeoecology. 600, 111059. https://doi.org/10.1016/j.palaeo.2022.111059

Omietimi, E.J., Lenhardt, N., Yang, R., Götz, A.E. & Bumby, A.J. (2022) Organic geochemistry, palynofacies, maceral analysis, and petroleum potential of Campanian-Paleocene deposits of the western Anambra Basin (Nigeria). Journal of Petroleum Science and Engineering [Status: in review]

Signed:————————————————————————————-

Date:————————————————————————————-

Abstract

The Inland Anambra Basin of Nigeria, formed on the western segment of the Lower Benue Trough, represents the sag phase of the Trough. Its basin infill comprises shallow to marginal marine and freshwater sedimentary clastic deposits of the Cretaceous to Paleogene age. The basin forms part of the larger rift systems of sedimentary basins of the West and Central African Rift Systems (WCARS), a geological chain of faulted and rifted structures that are genetically related. An important part of this study is to investigate the paleosedimentary history of the basin, paleoclimatic implications, paleowater depth, subsurface structures, formation of source beds, petroleum potentials, and evidence for the genetic link between the Anambra Basin and the Benue Trough and other WCARS basins. In order to address this scientific contribution, an integration of multi-proxy tools involving sedimentary geochemistry, mineralogy, organic petrography, rock evaluation, and satellite gravity survey was used in this thesis to provide robust data and new insights.

Satellite-derived gravity data based on the total horizontal derivative technique records anomalous Bouguer values ranging from -58 and +28 mGal in generic directions of NE-SW and NW-SE, and the CRUST 1.0 model reports a Moho depth of 37 km. Seven high-anomaly zones (HR1-HR7) and four low-anomaly areas were identified in the research area (HL1-HL4). Additionally, the sedimentary basin depth ranged from 3.5 to 5.0 km, indicating adequate depths for source rock formation and hydrocarbon accumulation. Furthermore, all Cretaceous and Paleogene Formations were influenced by the primary structural trends that dominated the basin's formation history.

The transgressive units of the Nkporo, Mamu and Imo Formations in the western segment of the basin from subsurface data revealed dominantly warm, humid tropical paleoclimates with high rainfall in the Late Cretaceous-Paleogene epoch, which corresponds to geologic events in WCARS Cretaceous basins in West Africa. Thus, the geologic record in West Africa indicates intense precipitation and high temperatures during the Cretaceous. The paleoenvironment was reconstructed as predominantly brackish to shallow-marine with some freshwater incursions. Deposition under an oxic environment is detected using a combination of paleoredox markers. On the other hand, anoxic conditions only occurred infrequently in the study area. The presence of wavy laminations in the mudrocks reveals receding seawater and strong paleohydrodynamic conditions. In addition, poor to medium primary productivity was recorded due to terrestrial clastic

influx and hydrodynamic settings. Ultimately, the southwestern Anambra Basin is characterized by shallow sea deposits influenced by strong hydroenergy circulation.

Furthermore, a high-resolution petroleum investigation suggests that the source rocks have a high potential for conventional gaseous hydrocarbons. An integrated approach based on palynofacies, maceral data, and rock eval interpretations supports type III kerogen in a marginal thermal stress stage. The results of this study contrasted favorably with other Cretaceous WCARS basins and showed that type III kerogen predominated. The basin's northern portion shows good shale gas potential. Finally, shallow marine to marginal marine transgressive, maximum flooding surface, and highstand deposits were detected in this study. The Anambra Basin and the other WCARS basins are genetically linked, as evidenced by similarities in paleoweathering, paleoclimate, paleowater depth, paleosalinity, paleoredox conditions, palynofacies assemblage, and structural trends, despite differences in sediment origin, paleogeographic positions, and the exposure of some WCARS basins to thermal fracture and crustal upheaval.

Acknowledgements

I am grateful to my supervisor, Prof. Nils Lenhardt, for accepting me as a PhD student at the Department of Geology, University of Pretoria. Nils was extremely helpful, with insightful discussions, Corel Draw plots, constructive and timely feedback, coffee sections, and publications, among other things, all of which contributed significantly to the success of my research here in Pretoria, as well as my overall well-being during my studies. My thanks to my co-supervisor and the head of the Department of Geology, Prof. Adam Bumby, for allowing me to work with him, for supervising me, and for editing, proofreading, and assisting with language corrections on all of my papers and thesis. Prof. Renchao Yang, my co-supervisor, deserves praise for allowing me to collaborate with him, providing constructive and timely reviews, and revising all papers.

I want to thank all of the co-authors, including Avinash K. Chouhan, Nils Lenhardt, Renchao Yang, Annette E. Gotz, and Adam J. Bumby, for their contributions to the publications.

Dr. Joel A. Edegbai, thank you for sparking my interest in sedimentary geology and as a continuing source of knowledge and inspiration.

Finally, I'd like to thank Dr Nimibofa Ayawei for all his affection and financial support, as well as my siblings and friends, who helped me get through this 4-year era in my life, for their unwavering support and for offering some much-needed relief from work.

Chapter One

1.1. Introduction

Sedimentary basins are areas of the Earth's surface where sediments have collected in tens of square kilometers or more, and they are the source of nearly all commercial hydrocarbons on the planet (Selley, 1997; Miall, 2013; Zhao et al., 2016; Li et al., 2020a). The Cretaceous epoch was an important period in the geologic record in Africa because of the separation of Gondwana and the subsequent opening of the Atlantic Ocean (Fig. 1.1), as well as high global mean temperatures and the development of sedimentary basins (Burke and Whiteman, 1973; Burk and Dewey, 1974; Trurnit, 1988; Benkhelil, 1989; Selley, 1997; Frazão et al., 2015; Hay and Floegel, 2012; Scotese et al., 2021). Warm temperatures typical of tropical regions were reported in West Africa's geologic record (Omietimi et al., 2022). In the Cretaceous period, a few rift systems opened, while others failed and were filled with thick sedimentary strata that most often contained organic-rich mudstones deposited in marine, brackish, and freshwater paleosedimentary environments (Burke et al., 1972; Selley, 1997). As a result, failed rifted sedimentary basins are frequently significant petroleum regions (Macgregor, 1995; Selley, 1997; Abubakar, 2014). The sedimentary basins of the rift systems are an essential component of the West and Central African Rift System (WCARS), a geological chain of faulted and rifted structures that are genetically and physically linked (Binks and Fairhead, 1992; Abubakar, 2014; Ene et al., 2019). These rift systems are extensive, span over 4000 km with marine to freshwater deposits, and are traceable as half-grabens from Nigeria to Niger, Chad, and Sudan (Binks and Fairhead, 1992; Abubakar, 2014; Ene et al., 2019). Nigeria’s Anambra Basin and Benue Trough are linked structures that are part of the WCARS (Anakwuba et al., 2018; Ejeh, 2021). The inland Anambra Basin, the focus of this study, represents the sag phase of the Benue Trough and comprises Cretaceous to Paleogene, shallow to marginal marine sedimentary rocks with high terrestrial influence (Anakwuba et al., 2018; Edegbai et al., 2019a; Ejeh, 2021; Omietimi et al., 2022). The basin is part of Nigeria's inland sedimentary terrain and is an energy-rich province located on the southern portion of the Benue Trough (Adebayo et al., 2018; Anakwuba et al., 2018; Ene et al., 2019; Omietimi et al., 2022). The basin with a syn-rift structure is characterized by its significant stratigraphic heterogeneity in vertical and lateral directions, and sedimentary sequences are over 5 km thick (Anakwuba et al., 2018; Omietimi et al., 2021).

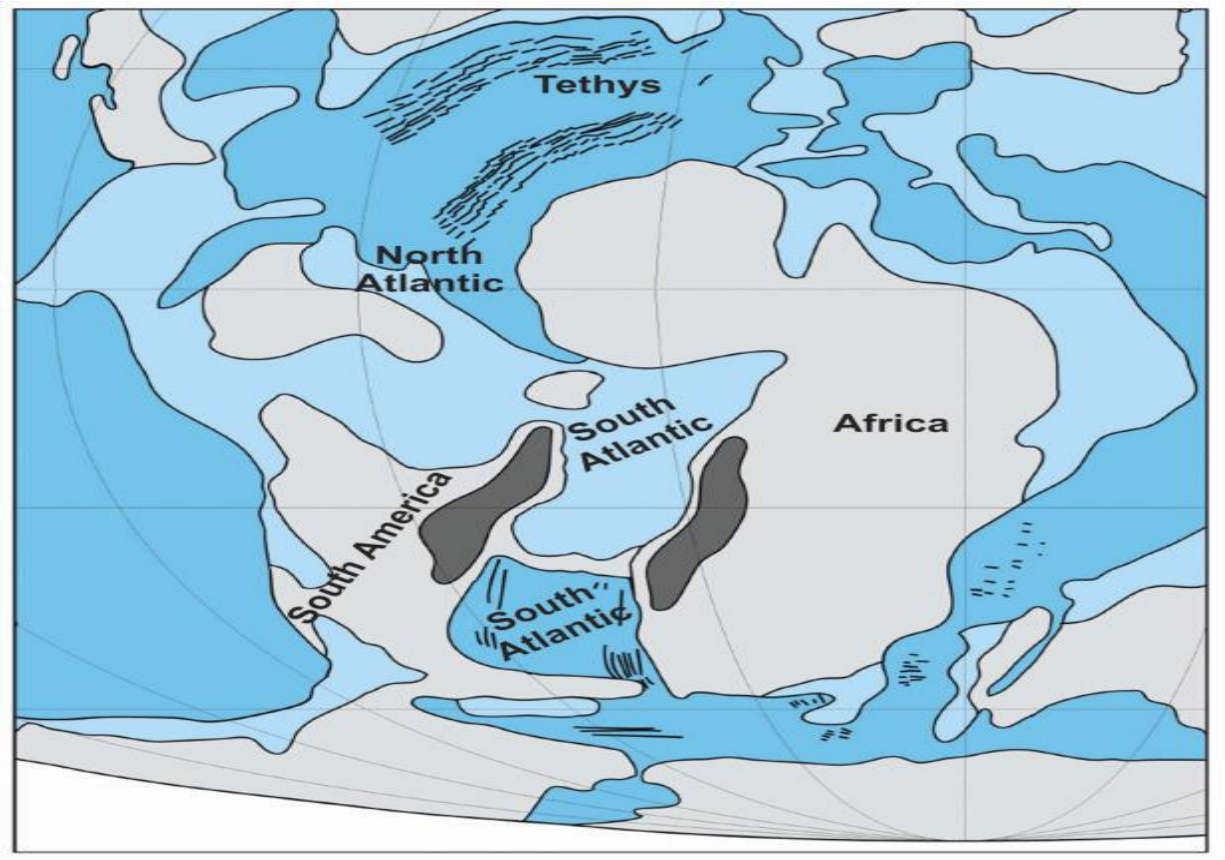

Figure 1.1 Paleogeographic reconstruction of Atlantic Ocean in the Albian (Azevedo, 2004; Parmera et al., 2017)

Petroleum resources account for about 90% of Nigeria's economy (Tuttle et al., 1999; Uwakonye et al., 2011; Monday and Salihu, 2017; Anakwuba et al., 2018). Most of the available exploratory studies on the sedimentary terrain of Nigeria focus on the Paleogene Niger Delta Basin (Obaje et al., 2004; Ene et al., 2019). However, due to continued reliance on fossil fuels for global energy consumption, the government has emphasized the need for exploration in the inland basins of Nigeria (Obaje et al., 2004; Adebayo et al., 2018; Anakwuba et al., 2018; Ene et al., 2019). There has been an increase in the exploration of hydrocarbons in the inland basins over the past decade, and this led to the discovery of oil for the first time in 2019 in northern Nigeria, i.e., the Kolmani River II well of the Gongola Basin, which is a sub-basin of the Upper Benue Trough (NNPC, 2019). The Nigerian National Petroleum Corporation (NNPC) report indicates that the discovery consists of gas, condensate, and light sweet oil of API gravity ranging from 38°-41° found in stacked siliciclastic Cretaceous reservoir rocks of the Yilde Bima sandstone. The discovery of more hydrocarbon resources would boost national reserves and bring significant socio-economic impact and transformation (Obaje et al., 2004; Anakwuba et al., 2018).

Hydrocarbons are formed and preserved when specific geologic requirements are met. The organic-rich source bed is an essential component of the petroleum system and is the first prerequisite for forming fossil fuels (Alalade and Tyson, 2010; Ndip et al., 2019; Mohammed et al., 2020). This must be accompanied by sufficient heat flow to convert organic carbon to hydrocarbons over time (Cappuccio et al., 2021). Such high temperatures can be achieved at depths of 2-4 km or less, depending on the geothermal gradient of the basin (Hunt, 1996; Abubakar, 2014; Omietimi et al., 2021). Furthermore, migration pathways are needed to enable generated hydrocarbons to move to a geologic trap. In addition, suitable reservoir rock with adequate porosity and permeability, an effective seal of impermeable rock above the reservoir, and a closed geological structure that traps are the final components needed for an effective hydrocarbon system (Dim et al., 2017; Anakwuba et al., 2018).

During the last three decades, sedimentary geochemistry studies, together with petrographic, organic geochemistry, and gravity surveys, have increased significantly. Sedimentary geochemistry is now applied to provide valuable insights into the contributions of marine, brackish, and freshwater depositional settings, climatic conditions, basin infill, and petroleum potentials of sedimentary basins worldwide (Zhang et al., 2020; Omietimi et al., 2021; Wei et al., 2021; Omietimi et al., 2022). Fine-grained siliciclastic rocks are important for reconstructing and

interpreting sedimentary processes and provide the most comprehensive records of geologic history (Li et al., 2020a; Wu et al., 2020; Chen et al., 2022; Ding et al., 2022; Omietimi et al., 2022). Mudrocks contain specific immobile elements that can retain the signatures of source materials, making it possible to reconstruct paleo-sedimentary conditions (Li et al., 2020a; Zhang et al., 2020, 2021; Chen et al., 2022). Furthermore, the close-fitting and impervious character of mudrocks preserves the initial geochemical fingerprints of sedimentary source materials, ensuring that they are not affected by extrinsic fluids (Moradi et al., 2016; Li et al., 2020a; Zhang et al., 2020). As a result, mudrocks provide highly useful records of paleo-sedimentary data (Li et al., 2020a; Zhang et al., 2021; Chen et al., 2022). Thus, several researchers have utilized sedimentary geochemistry of mudrocks internationally to determine paleoclimatic conditions, reconstruct paleo-depositional environments, hydrodynamics, paleo-redox settings, terrigenous influx, and hydrocarbon potentials during sedimentation based on the geochemical fingerprints of mudrocks (Pehlivanli, 2019; Overare et al., 2020; Parthasarathy et al., 2020; Li et al., 2020a; Wu et al., 2020; Zhang et al., 2020, 2021; Chen et al., 2021a; Wang et al., 2021c; Chen et al., 2022). Microscopic kerogen studies using palynofacies is an integrated approach applied to the study of particulate organic matter in mudrocks (Achaegakwo and Atta-Peters, 2021; Li et al., 2021a). Palynofacies analysis is important to the hydrocarbon industry and is widely applied in the identification of organic material, sea-level changes, and paleoenvironment, all of which help with the overall evaluation of a sedimentary basin's hydrocarbon potential (Batten, 1982; Götz et al., 2008; Carvalho et al., 2013; Singh et al., 2017; Perner, 2018; Achaegakwo and Atta-Peters, 2021; Li et al., 2021a). Also, I applied the gravity surveying technique, which is a non-destructive method of determining variations in rock density in the geological lithosphere using remotely sensed data (Chouhan, 2020; Fairhead, 2020). The gravity technique measures gravitational anomalies (Chouhan, 2020). The Bouguer anomaly method is used worldwide to determine subsurface lineaments, trends and sedimentary basin thickness (Zhang et al., 2015; Obasi et al., 2018; Zhang et al., 2019b; Chouhan, 2020; Fairhead, 2020; Omietimi et al., 2021; Wang et al., 2021b). Petroleum and organic geochemistry is an interdisciplinary discipline that identifies prospective and non-prospective regions, as well as the qualities of source rocks, thermal stress interpretation, shale oil potential, indigenous and non-indigenous hydrocarbons, migration and oil/gas accumulation and alteration (Adebayo et al., 2018; Ndip et al., 2019; Mohammed et al.,

2020; Cappuccio et al., 2021; Chen et al., 2021a; Wei et al., 2021; Adeyilola et al., 2022; Wu et al., 2022).

The southwestern portion of the Anambra basin is characterized by the Campanian to Paleogene deposits of the Nkporo, Mamu, Ajali, Nsukka, and Imo Formations (Omietimi et al., 2022). The Maastrichtian Ajali and Mamu Formations and a thin ironstone unit, representing the Nsukka Formation, are exposed at the surface (Edegbai et al., 2019a, 2019b). There is a paucity of research works on the paleosedimentary environment, climatic conditions, hydrothermal influence, paleowater depth, hydrodynamic conditions, lineaments and shale oil potential from subsurface studies in the western segment and also in the central and eastern segments (Edegbai et al., 2019b, 2020; Omietimi et al., 2021, 2022). In contrast, many researchers have concentrated their efforts on the southeastern portion of the basin, focusing on provenance studies, tectonic interpretations, palynology, source rock prospects, coal studies, and mineralogy of the Nkporo, Mamu, and Imo Formations (Akande and Mücke, 1993; Gebhardt, 1998; Antolinez-Delgado and Oboh-Ikuenobe, 2007; Tijani and Nton, 2009; Anakwuba and Onyekwelu, 2010; Tijani et al., 2010; Ogala, 2011; Adebayo et al., 2018; Adeleye and Daramola, 2018; Chiadikobi et al., 2018; Obasi et al., 2018; Dim et al., 2019; Ejeh, 2021).

Only a few of the publications on the western segment (i.e., Benin Flank) focused on outcrop samples (Olabode, 2014; Edegbai et al., 2019b, 2020; Ilevbare and Omodolor, 2020; Ogungbesan and Adedosu, 2020), which are prone to alteration. Therefore, this research focused on subsurface samples (ditch cuttings/core samples and gravity data) to provide new insights and further appraise the basin. A multi-parameter approach that comprises sedimentary geochemistry, lineament interpretations, gravity modelling, palynofacies analyses, petrographic maceral investigations, and organic geochemistry, was applied for Late Cretaceous to Paleogene paleoclimate deductions. Furthermore, paleosedimentary environment implications, marine redox/biogeochemical conditions, reconstruction of paleodepth, paleosalinity, and paleohydrodynamics, structural interpretations and determination of the depth of the Mohorovičić discontinuity (Moho), source rock characterization, thermal stress interpretations, the potential for unconventional petroleum, and implications for petroleum prospecting for the subsurface deposits of the western segment of the Nigerian Anambra Basin.

The paleoclimate, palynofacies, stratigraphy heterogeneity, and inorganic and organic geochemical interpretations of the Anambra Basin indicate a close resemblance with other WCARS basins, i.e., in Chad, Niger, and Sudan, where commercially viable hydrocarbons have been discovered. The Late Cretaceous to Paleogene Formations in the western segment of the Anambra basin has been studied in this research to provide insight for prospective exploratory initiatives in the basin.

1.2. Objectives

New data and methods are used in this thesis to provide new insights on the paleosedimentary conditions and conventional and unconventional hydrocarbon potential of the Campanian to Paleogene deposits of Nigeria's Anambra Basin. To access the petroleum potential, industry and academia-based studies commonly use geochemical techniques because they offer fast and inexpensive results (Tyson, 1993; Perner, 2018). On the other hand, optical kerogen analysis is still relatively new in the industry (Perner, 2018; Mohammed, 2020), due to its elevated cost and schedule, regardless of the fact that it produces more comprehensive data. A combination of optical, geochemical, and gravity techniques is applied to develop an elaborate and highly accurate interpretation of the paleosedimentary environment and oil and gas potential in the western segment of the Anambra Basin. A multi-proxy concept is widely recommended to account for the possibility of errors from single data types (Perner, 2018; Zhang et al., 2018; Mohammed, 2020; Chen et al., 2021a; Wang et al., 2021c). To achieve highly accurate and precise results, the multi-proxy method necessitates the use of more than one analytical method to evaluate sedimentary basins (Mohammed, 2020; Li et al., 2021a; Wei et al., 2021; Adeyilola et al., 2022; Ma et al., 2022).

In the western segment of the basin, major and trace elemental geochemistry, mineralogy, structural modelling, organic geochemistry, and optical methods have been integrated to provide more detailed and robust data on paleodepositional systems, climatic reconstructions, sedimentary basin infill, and hydrocarbon source development. Furthermore, high mean global temperatures occurred during the Late Cretaceous and early Paleogene epochs, and these geologic records are preserved in sedimentary rocks and reconstructed in this thesis (Sellwood and Valdes, 2006; Tan et al., 2017; Zhang et al., 2018; Scotese et al., 2021; Omietimi et al., 2022). The constituents of the organic matter types (OM) and geochemical analyses can then be used to make substantial inferences about the kerogen types, thermal stress and petroleum source prospects

(Singh et al., 2017; Mohammed et al., 2019; Cappuccio et al., 2021; Chen et al., 2021a; Wei et al., 2021; Adeyilola et al., 2022; Ahmed et al., 2022). As part of my study, I linked the Anambra Basin, the Benue Trough, and the WCARS basins. Consequently, the findings of this research have broad implications for regional research, sedimentary basin evaluation, and liquid and gaseous petroleum exploration. In this thesis, I provide an improved understanding of how sedimentary systems evolve as well as the sedimentary facies' paleo-bioproductivity and sea level changes. Hence, I focus on transgressive carbonaceous shallow-marginal units, which provide the best source sections.

1.3. Summary of research gaps in literature

Critical deductions of the published literature on the tectonic structures, lithofacies, paleoclimate, paleoxygenation, paleo-redox, and hydrocarbon prospects of the Anambra Basin have shown aspects that justify further research.

1. Paleosedimentary conditions in the western segment of the Inland Anambra Basin and implications on a regional scale have not been addressed in previous studies.
2. The tectonic framework and lineaments in the western segment of the Anambra Basin were not addressed in the previous studies.
3. Structural relationships between the subsurface lineaments and their vital role as potential hydrocarbon traps that would influence exploration in the basin are not established.
4. Palynofacies assemblage studies at the western margin of the Anambra Basin to help delineate transgressive events, maximum flooding surfaces and highstand deposits are not established.
5. Paleohydrodynamic, paleo-water depth, and paleosalinity reconstructions of the Anambra Basin using high accuracy elemental proxies have not been undertaken in the past.
6. Paleoproductivity and redox conditions of the Cretaceous Nkporo and Mamu Formations and the Paleocene deposits of the Imo Formation in the western segment, from subsurface data within the Anambra Basin arising from elemental proxies are not yet established in previous studies.
7. A detailed description of the paleoclimatic conditions during the formation of the Anambra Basin and the relationship with the Benue Trough and WCARS basins are poorly understood.

8. Hydrocarbon prospectivity owing to the maceral types, kerogen types, sources of the kerogen, thermal stress from optical and Rock-Eval measurements from subsurface data within the western portion of the Anambra Basin are not yet addressed in previous studies.

1.4. Thesis framework and format

The research is divided into four sections: geologic setting and stratigraphy of the Anambra Basin, structural interpretation of the basin, paleoenvironmental conditions, and kerogen composition, and implications for petroleum prospecting. To reconstruct paleoclimatic regimes and interpret paleoenvironmental implications, paleoenvironmental and paleoclimate proxies were used. The structural modelling and sedimentary basin infill involved the use of a satellite gravity survey. High resolution WGM 2012 gravity data were integrated for structural modelling and sedimentary basin infill to delineate structural lineaments, sediment thickness and reveal the depth of Moho. The research is based on subsurface samples from the Owan-1 and Ubiaja wells in the western Anambra Basin. Fig. 1.2 depicts the applied research framework. Petrographic analysis was also employed to reconstruct and interpret paleoenvironmental data. The kerogen assessment necessitates determining the organic material (OM) content and variations across the research region. Microscopy (palynofacies, maceral data) and geochemical (TOC, Rock-Eval data) techniques were used for kerogen interpretation. In addition, calculated vitrinite reflectance and Tmax geochemical data were used to investigate thermal maturation as well as the effect of depth on thermal stress in the basin. The source rock development and hydrocarbon potential can be calculated based on these three components. The sea level fluctuations were determined using palynofacies ratios.

For the mudrocks, I incorporated guidelines by Loubser and Verryn (2008), Espitalié et al. (1977, 1985), Tissot and Welte (1984), ASTM (2014), and SANS 7404–3 (2016)/ ISO 7404-3 (2009). The guidelines by Lowrie (2007) and Blakely (1996) were adopted for the gravity survey. The following are the four main components of this methodology:

- **Inorganic geochemistry techniques**
  - Major, trace and rare element analysis XRF and ICP-MS
  - Mineralogy analysis (XRD)
- **Gravity data**
  - Data processing and modelling
  - To determine the structural lineaments Total horizontal derivative THD was used

- 2.5D forward gravity technique was used for depth and dimensions of sedimentary infill
- **Organic geochemistry technique**
- TOC and Rock-Eval methods
- **Petrographic techniques**
- Palynofacies analysis
- maceral analysis

The thesis is divided into six chapters, the **first** of which covers the introduction, objectives, research gaps, methods used, and research framework.

Chapter two discusses the regional geologic setting and tectonic evolution of the Anambra Basin, the lithostratigraphic formations, and the sedimentary environment.

Chapter three presents new insights on the subsurface structures, structural trends, Moho depth, and sedimentary basin infill in the Anambra Basin's western segment. The chapter is titled: Structural interpretation of the south-western flank of the Anambra Basin (Nigeria) using satellite-derived WGM 2012 gravity data.

Chapter four provides a detailed reconstruction of paleosedimentary changes during basin evolution of Cretaceous to Paleocene deposits in the basin's western segment, as well as regional implications. Chapter four is titled: Sedimentary geochemistry of Late Cretaceous–Paleocene deposits at the southwestern margin of the Anambra Basin (Nigeria): Implications for paleoenvironmental reconstructions.

In **Chapter five**, a high-resolution multi-proxy petroleum analysis is used to analyze organic material (OM) and particulate organic material (POM), hydrocarbon generation potential, and shale oil potential in the Cretaceous Nkporo and Mamu Formations, as well as the Paleocene Imo Formation. New insights into the regularity and dynamics of OM accumulation are important to understanding changes in conventional hydrocarbon and unconventional shale oil quality within the western segment of the basin and their implications on a regional scale. In addition, this study identified shallow marine to marginal marine transgressive, maximum flooding surface, and highstand deposits. Chapter four is titled: Palynofacies, maceral analyses, and unconventional petroleum potential of Campanian-Paleocene deposits in the Anambra Basin's southern segment (Nigeria).

Chapter six presents deductions drawn from the integration of multi-data sets. Based on the study, I present an overview of my conclusions and recommendations.

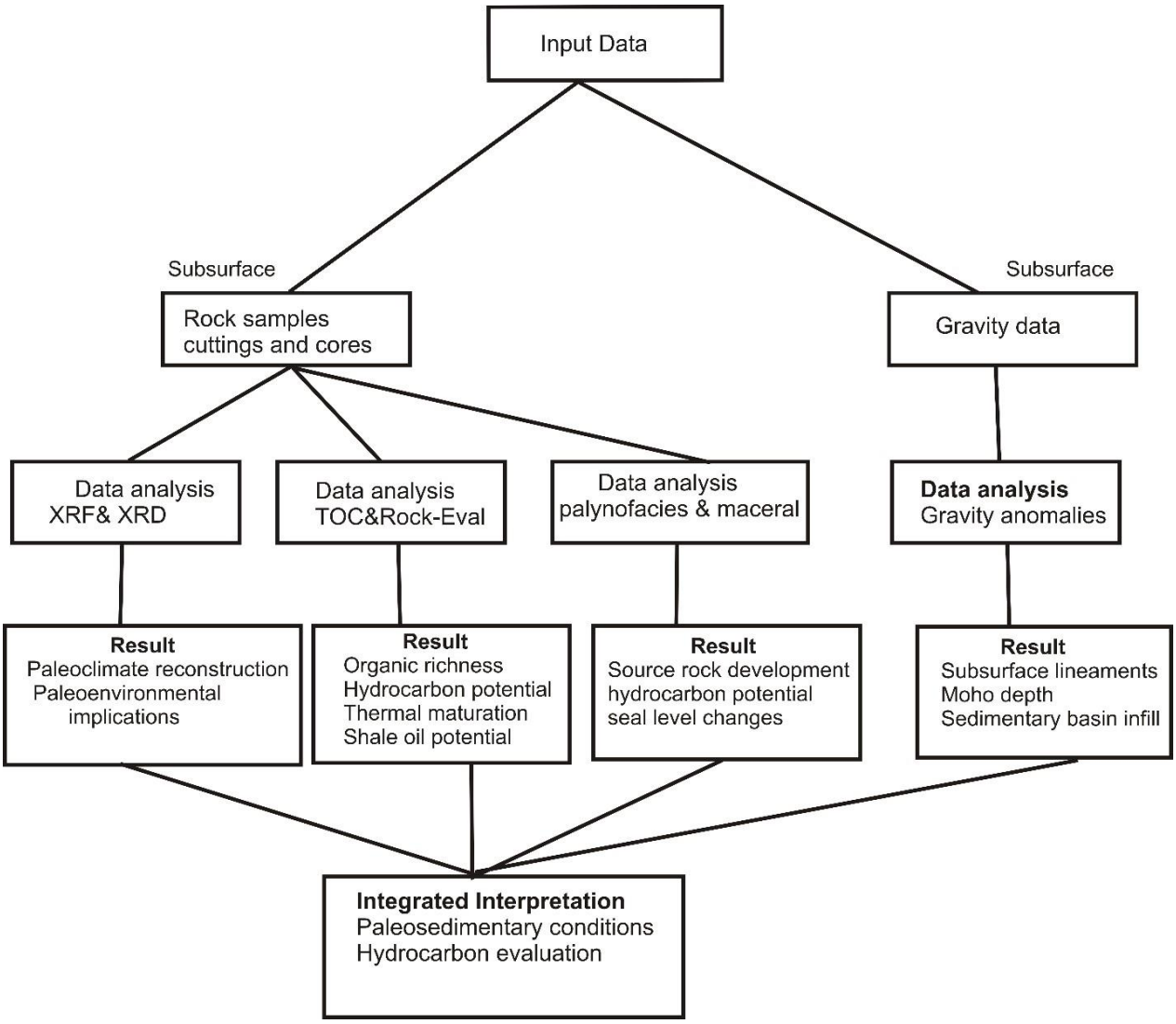

Figure 1.2. This study's work - flow applied a multi-parameter approach combining sedimentary geochemistry (XRF, ICP-MS, XRD), gravity survey (satellite gravity data), petrographic microscopy (Palynofacies and maceral) and geochemical (TOC, Rock-Eval).

Chapter Two

2.1. Regional and tectonic setting

Nigeria's Anambra Basin is part of the West, and Central African Rift System (WCARS) basins (Abubakar, 2014) formed during the Early Cretaceous when Gondwana began to break apart and the South Atlantic Ocean started to open (Burke and Whiteman, 1973; Fairhead, 1988; Benkhelil, 1989). The basin formed during the post-deformational sedimentation period of the Benue Trough's evolution, followed by Santonian inversion tectonics across the basin (Obaje, 2009; Mode et al., 2016; Edegbai et al., 2019a).

The Anambra Basin is one of Nigeria's seven sedimentary basins (Fig. 2.1), featuring a structural depression at the southwestern margin of the Lower Benue Trough. It covers an area of ca. 40,000 km^2 and stretches from Nigeria's Anambra, Enugu, and Ebonyi states, partly southwards to Delta state, partly north to Benue and Kogi states, and partly west to the Edo province (Akaegbobi et al., 2000; Edegbai et al., 2019a). Geological, well/core data, gravity, magnetic and seismic modelling have shown that the Anambra Basin comprises of >6 km thick sedimentary succession, depicting a sequence of continental, deltaic, and marginal marine sedimentation (Agagu and Adighije, 1983; Obasi et al., 2018; Dim et al., 2019; Omietimi et al., 2021). The oldest sediments within the basin date from the Campanian age, and deposition continued through the Late Cretaceous into the Early Paleogene.

2.2. Lithostratigraphy

The Anambra Basin comprises Campanian, Maastrichtian, and Paleocene sediments (Fig. 2.2). The basin subsided during the Santonian stage, which accompanied the main tectonic process, and an E-W prograding deltaic system formed, with the Campanian marine Nkporo and Enugu Formations being the first to be formed, comprising mainly marine dark grey shales, sandy shales, sandstones, and ironstones (Akande and Mücke, 1993; Akaegbobi et al., 2000). Maastrichtian deposits of the Mamu Formation comprise shales, sandstones, siltstones, clays, sandy shales, shaly sands, clayey shales, ironstones, and coal seams of fluvio-deltaic to marginal marine depositional environments (Dim et al., 2019; Edegbai et al., 2019a). The overlying Ajali Formation was deposited in a shallow marine to terrestrial environment (Tijani et al., 2010), and its thickness varies across the basin. The Nsukka Formation, conformably overlying the Ajali Formation, marks the termination of Maastrichtian deposits and the onset of Paleocene

sedimentation. The formation accumulated in the bay, mud flat, lagoonal, shoreface and shallow-marine environments during a period of transgression (Mode and Odumodu, 2015) and is more developed in the basin's eastern portion, where complete sections are available; in the western part, it is only represented by a thin unit that caps the Ajali Formation (Edegbai et al., 2019a). In the late Paleocene, the Imo Formation was deposited, characterized by foreshore and shoreface to delta front deposits (Oboh-Ikuenobe et al., 2005). This formation is considered the subsurface equivalent of the Akata Formation in the Niger Delta Basin (Reijers et al., 1997; Odunze and Obi, 2011; Adeleye and Daramola, 2018). The basin's sedimentary fills range from fairly deep to shallow marine, marginal marine shales, mudstones, carbonates, shoreline sandstones, and coastal fluvial sands (Ola-Buraimo et al., 2016; Dim et al., 2019; Edegbai et al., 2019a; Omietimi et al., 2022).

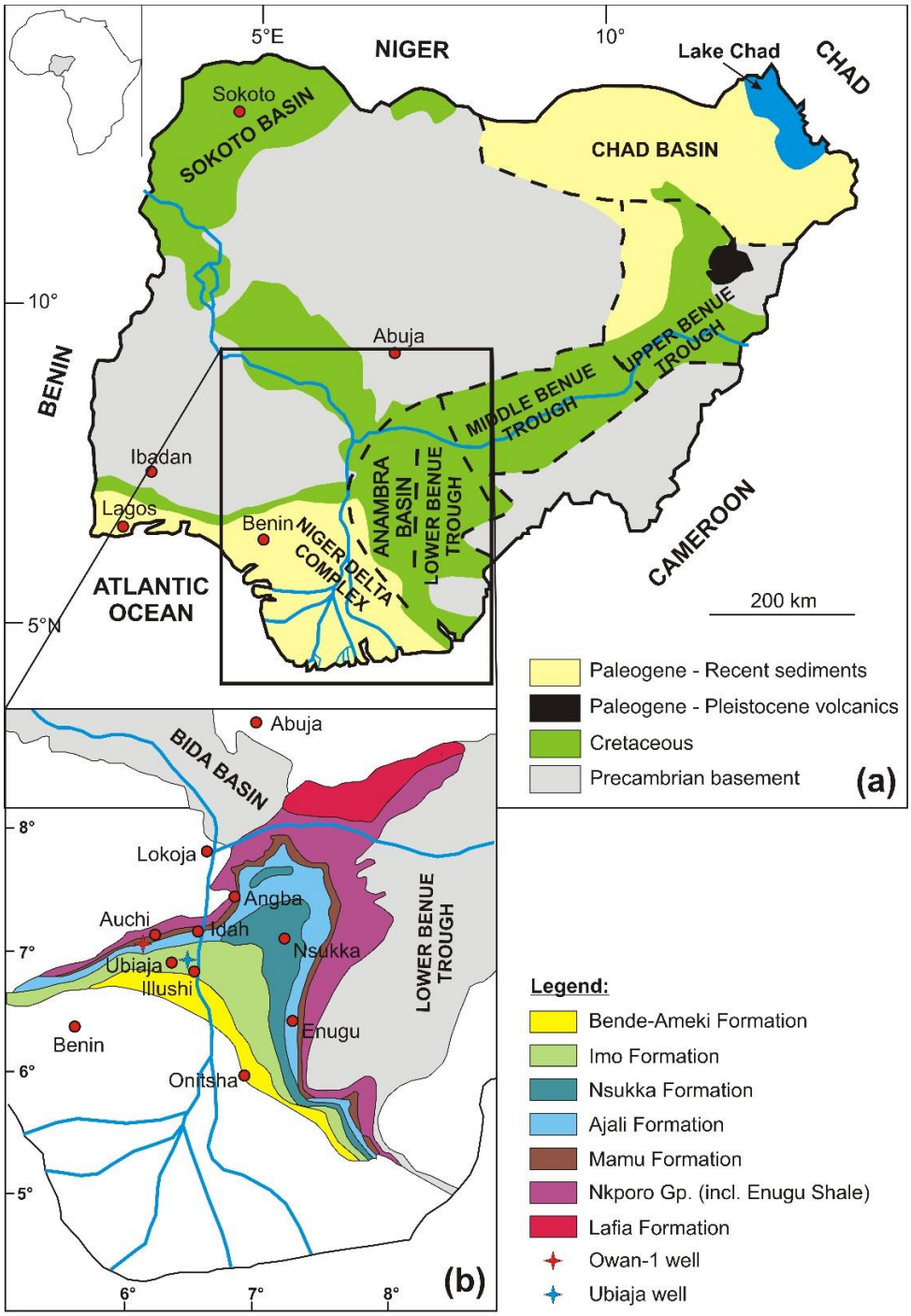

Figure 2.1. (a) Geologic map of Nigeria showing the Anambra Basin (Obaje, 2009); inset: Map of Africa showing the location of Nigeria. (b) Geologic map of the Anambra Basin showing the location of the studied Owan-1 and Ubiaja wells (Nwajide, 1990).

2.3. Sedimentary environment

The Nkporo, Mamu, and Imo Formations are characterized by dark-grey shales and claystones and an alternation of siltstones, sandstones and coal seams (Ola-Buraimo et al., 2016; Edegbai and Schwark, 2020). These lithofacies have been intersected by the studied Owan-1 and Ubiaja wells (Figs. 4.1-4.2, 5.1, 5.5). The Ajali and Nsukka Formations probably thinned out and were not intersected within the studied wells in the western part of the basin Fig, 2.2 (original report from oil companies). In the eastern part of the basin, the lithofacies of the Nkporo Formation represents marine and inner estuarine environments (Odunze et al., 2013). The Mamu Formation comprises brackish sediments at the basin's western margin, while the central basin features marsh and bay depositional environments (Edegbai et al., 2019a). In contrast, Dim et al. (2019) classified the Mamu Formation's lithofacies at the basin's eastern margin into lagoonal, barrier island, shoreface, offshore transition zone and open shelf depositional environments. In the lower Benue Trough, Odunze et al. (2011) classified the lithofacies of the Imo Formation into tidal, estuarine, and marine facies. These authors further described high-frequency regressive and transgressive sequences in lagoonal coastal swampy settings to shelf depositional settings. The distribution of sedimentary facies throughout the basin has been influenced by sea level changes.

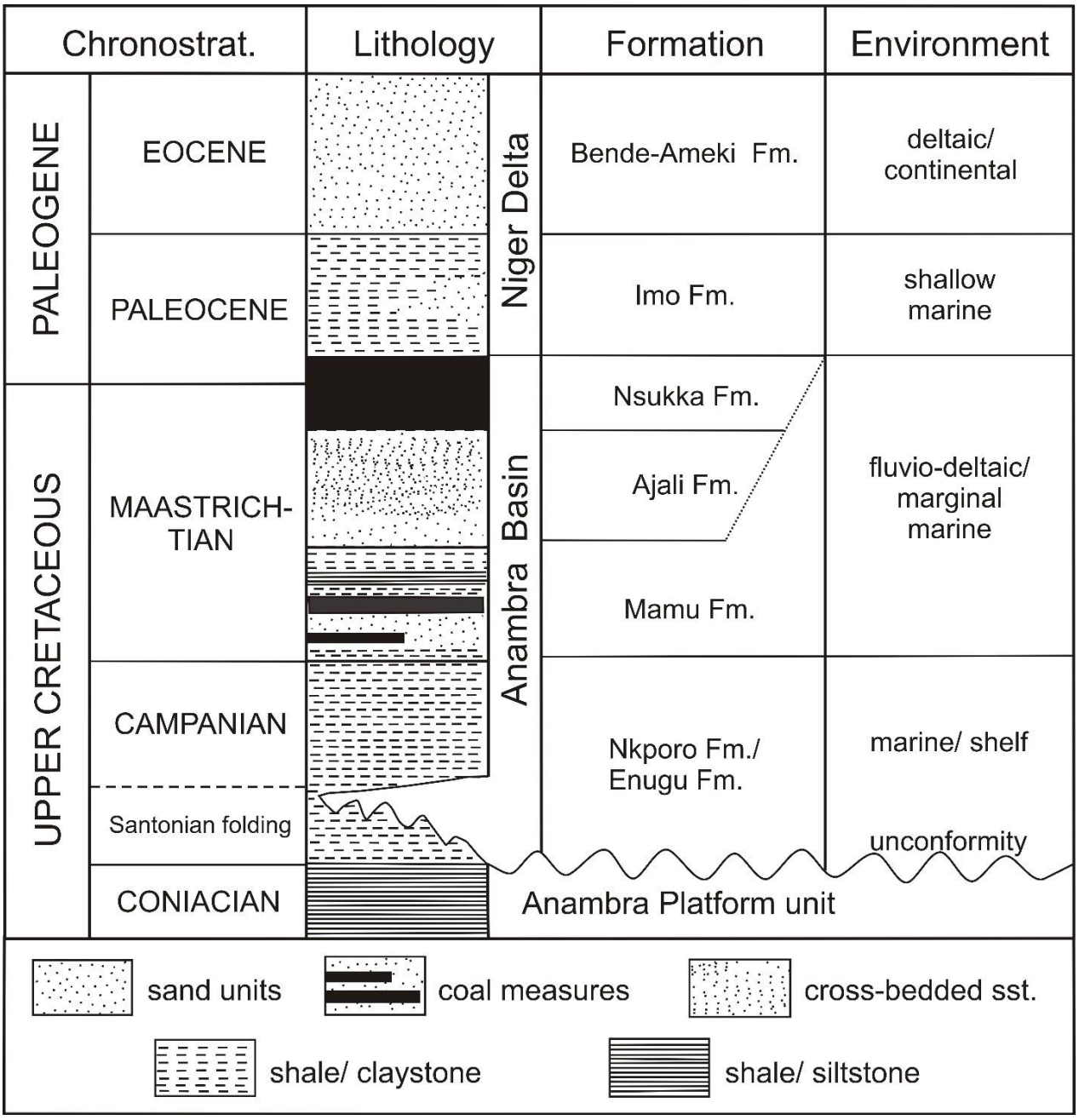

Figure 2.2. Stratigraphy and depositional environments of the Anambra Basin (Ogungbesan and Adedosu, 2020; Omietimi et al., 2022; Tijani et al., 2010). Chronostrat. = chronostratigraphy.

Chapter Three

Structural interpretation of the south-western flank of the Anambra Basin (Nigeria) using satellite-derived WGM 2012 gravity data

3.1. Introduction

The gravity method is a useful geophysical technique for identifying and mapping subsurface geological structures (Abtout et al., 2014; Altinoğlu et al., 2015; Khazri and Gabtni, 2018; Bba et al., 2019; Dilalos et al., 2019). It is commonly used to demarcate lineaments (Hu et al., 2015; Zhang et al., 2015; Mauri et al., 2018; Chouhan, 2020; Chouhan et al., 2020b) . The demarcation of lineaments, e.g. faults, folds, fractures, joints, geological contacts, is a very important step in studying the tectonic framework and the hydrocarbon trapping mechanisms of sedimentary basins (Isyaku, 2018).

The Anambra Basin, situated west of the lower Benue Trough in the southern part of Nigeria, is an inland sedimentary basin and one of Nigeria's most promising hydrocarbon producing fields (Fig. 2.1a, (Obaje, 2009). During the last few decades, the basin has attracted a variety of studies that used a wide range of geophysical and geological methods (Agagu and Adighije, 1983; Cratchley et al., 1984; Benkhelil, 1989; Onwuemesi, 1997; Abbass and Mallam, 2013; Adetona and Abu, 2013; Obiora et al., 2015; Abdullahi and Singh, 2018; Ekwueme et al., 2018; Obasi et al., 2018; Okorie et al., 2019; Oguama et al., 2021). A first power spectrum analysis of magnetic data showed varying thicknesses of sedimentary deposits within the basin between 0.9 and 5.6 km (Onwuemesi, 1997). In contrast, more recent geophysical studies, using an integrated analysis of spectrum analysis and source parameter imaging in the upper part of the basin, corrected the range of sedimentary thickness to a spectrum between 0.08-9.85 km (Adetona and Abu, 2013). Adetona and Abu (2013) also revealed a N-S and NE-SW-oriented structural trend in the upper part of the Anambra Basin. Also, calculations from source parameter imaging provided information on the existence of a magnetic anomaly in the Nsukka region (Fig. 3.1) with depths varying between 0.15 and 3 km (Obiora et al., 2015). Furthermore, the Euler deconvolution of the Nsukka area's magnetic data revealed depths of shallow magnetic sources that vary between 8 and 129 m (Obiora et al., 2015). The magnetic anomalies in the Nsukka area mainly originate from iron-rich minerals, such as limonite, pyrite, hematite, and pyrrhotite. Ekwueme et al. (2018) carried out a study in the region of Idah and Angba that depicts a magnetic source depth between

2.2 km and 6.8 km. Ubiaja and Illushi regions have a NE-SW structural trend of magnetic anomalies with depths varying between 3 and 5.5 km (Okorie et al., 2019). Most recently, Oguama et al. (2020) used magnetic data to study the structural lineaments at the eastern margin of the Anambra Basin. The majority of these lineaments are oriented in a NE-SW direction. Like Oguama et al. (2020), previous studies on the Anambra Basin's lineaments mostly used the delineation's magnetic method. Very few gravity studies are available on the basin (Agagu and Adighije, 1983; Obasi et al., 2018). Therefore, there is a need to determine structural lineaments based on gravity studies to improve the understanding of the subsurface lithologies and determine the sedimentary thickness. Both magnetic and gravity analyses, naturally cannot replace seismic studies that exhibit much higher resolutions (Fairhead, 2012). Nevertheless, in developing countries and remote areas, gravity surveys, recorded from an aircraft or satellite, can provide a very cost-efficient alternative that may provide very reliable data on very large areas (Downey, 2004; Ennen and Hall, 2011; Fairhead, 2012). Therefore, the resulting information may play a key role in hydrocarbon exploration in these areas. Available data indicates that the Anambra Basin could be as rich as the Niger Delta Basin regarding its hydrocarbon potential. In addition to coal, the basin holds an estimated gas reserve of ca. 30 trillion cubic feet and 1 billion barrels of oil (Dublin-Green and Agha, 1999).

Both magnetic and gravity surveys are well suited for detecting lateral variations, faults, etc. In contrast, seismic surveys are more suited for analysing vertical variations in rocks and the boundaries between layers in a sequence of rocks. The gravity method may be more straightforward than the magnetic method because the magnetic anomalies may be affected by small variations in the occurrence and distribution of magnetic minerals such as titano-magnetites, which may have little relation to the overall lithology (Fairhead, 2012). However, the gravity method does not have such a drawback. A gravity survey is a non-destructive remote sensing geophysical method that measures variations of the rock density from the geological subsurface. The Bouguer anomaly is the measured gravity that is corrected for the known gravity effects (Karcol et al., 2017), indicating the response of the entire density fluctuation below the surface. Therefore it is an aggregate of the regional and residual gravity anomalies within the study area (Petit et al., 2002). The Bouguer anomaly technique has been used internationally in the interpretation of subsurface structures, trends, and understanding sedimentary basin infills

(Flinders et al., 2010; Fairhead, 2012; de Castro et al., 2014; Zhang et al., 2015; Alrefaee, 2017; Chouhan, 2020; Chouhan et al., 2020a; Njeudjang et al., 2020; Wang et al., 2021b).

In the past, Shell British Petroleum Development Company and the Nigerian Geological Society Agency carried out a gravity survey to study the basin architecture of the Benue Trough and part of the Anambra Basin (Agagu and Adighije, 1983). However, due to the difficult terrain, the gravity survey could never be completed for the whole basin. For this reason, satellite-derived gravity data are needed for this type of area to provide a complete picture of the basin architecture at the south-western flank of the basin. This area had previously been neglected in former studies (Fig. 3.1b). There are many global gravity models like EIGEN6C4 (Förste et al., 2014), EGM 2008 (Pavlis et al., 2012), XGM 2019 (Zingerle et al., 2020), which have the spatial resolution (of the order of 10 km X 10 km). Study for the extraction of lineaments (Kumar et al., 2019; Sahoo and Pal, 2019; Chouhan et al., 2020a), tectonic features (Kumar et al., 2020; Sahoo and Pal, 2021), mineral exploration (Rani et al., 2019) and density modelling (Chouhan, 2020; Chouhan et al., 2020b) have been done by many researchers using these data in the past. However, the WGM 2012 is the first set of global gravity anomaly maps that takes into account a realistic earth model, and it considers the contribution of most surface masses like atmosphere, land, oceans, inland seas, ice caps, and ice shelves (Kahveci et al., 2019). This gravity model is suitable for mapping lineaments, Moho depth and sedimentary thickness (Alemu et al., 2018). Studies based on WGM 2012 are already done by many researchers for the rift basin with good efficacy (Titi and Minarto, 2017; Alemu et al., 2018; Guo and Gao, 2018; Chouhan, 2020). Therefore, in this study, I have used the WGM 2012 model. The present study used satellite-derived WGM 2012 gravity data and provide this needed information for the Anambra Basin. The purpose of this study is to provide new information on the lineaments of the Anambra Basin, related to residual and regional gravity anomalies, thereby shedding new light on both shallow and deep-seated structures within the basin, respectively.

3.2. Material and methods

3.2.1. Gravity data

The data used for this contribution was gathered from the International Gravimetric Bureau (BGI) gravity database (http://bgi.obs-mip.fr). The World gravity model (WGM 2012) is a joint gravity data set, which includes satellite data based on CHAllenging MiniSatellite Payload (CHAMP), Gravity Recovery and Climate Experiment (GRACE), Earth gravity model 2008 (EGM 2008), Gravity Field and Steady-State Ocean Circulation Explorer (GOCE), Technical University of Denmark 10 (DTU 10) global gravity field, elevation data of the global topography 30 arc-second (GTOPO30), and in-situ gravity data. All the data mentioned above sets are conjoint through the iterative least-squares method and have a maximum spherical harmonic coefficient of up to 2190^{o} and order 2159^{o} (Andersen et al., 2010; Balmino et al., 2012; Pavlis et al., 2012). The WGM gravity data have a spatial coverage with a high-resolution of 9 × 9 km (Balmino et al., 2012; Pavlis et al., 2012). The WGM 2012 is provided in electronic form for educational and research applications (Balmino et al., 2012).

3.2.2. Data processing and modelling

Topographic corrections i.e. Bouguer plate and terrain corrections were performed to process the Free-air anomaly (Appendix 1) data. Once the corrections were applied, the complete Bouguer anomaly was computed using a density of 2670 kg/m^3 for the Bouguer slab and the digital elevation model ETOPO1 for topographical heights. The calculated Bouguer anomalies contain both the anomalies related to shallow (high-frequency anomalies) and deep-seated (low-frequency anomalies) sources (Blakely, 1996; Lowrie, 2007). For detailed interpretations and better delineation of the subsurface structure, a separation of anomalies related to shallow (residual) and deeper (regional) parts is necessary, a process called regional-residual separation (Lowrie, 2007). This is performed by various techniques such as wavelength filtering, polynomial fitting, and continuation of the Bouguer anomaly (Lowrie, 2007). In the present study, the upward continuation technique is adopted. The upward continuation is a classic technique used to calculate the Bouguer anomalies on to a surface, which is higher than that of the surface of observation. It is based on the principle of equivalent stratum (Blakely, 1996). The shorter wavelength anomalies (belonging to shallower features) are attenuated more rapidly than long-wavelength anomalies (belonging to deeper features) during the upward continuation. Thus, the anomaly calculated after the upward continuation and having the long wavelength anomaly can be considered to be a

regional Bouguer anomaly (Lowrie, 2007). Choosing an optimum height for upward continuation is an inherent problem in this method. To resolve this ambiguity, (Jacobsen, 1987) proposed a method to choose an optimum height. Thus, the regional field, determined by the upward continuation of gravity anomaly at height x, is connected to sources situated at half the height of upward continuation, i.e. x/2 (Jacobsen, 1987). This idea is used to select an optimal height and extract the regional anomaly from the Bouguer anomaly.

To determine the lineaments, the total horizontal derivative (THD) of the Bouguer anomaly is calculated. The THD method is widely used as the edge detection using the Bouguer anomaly, and it is reliable in locating the edges of density variation from the gravity data (Blakely, 1996). THD measures the lateral change in density and does not require any prior information about the anomaly sources. The total horizontal derivative is calculated using the following expression:

$$THD = [(\partial p/\partial x)^2 + (\partial p/\partial y)^2]^{1/2} \quad (1)$$

Here, $\partial p/\partial x$ and $\partial p/\partial y$ represent the horizontal derivatives of the Bouguer anomaly p in the x and y directions, respectively. The computed THD is least affected by noise in the data since it is estimated by the two first-order horizontal derivatives of the gravity field (Cordell and Grauch, 1985; Saibi et al., 2019). The THD maximal crest value is noticed vertically over the edges of the source body (i.e. geologic contacts, faults, fractures). Nevertheless, when the source body is not almost vertical or many anomalies are near, at that point, an offset may be noticed in the highest range value of THD (Grauch and Cordell, 1987; Blakely, 1996). Chouhan (2020) has tested the efficiency of the THD technique over theoretical models and found that maximum values lie vertically above the edges of the source body. In the current study, the peak value of the THD was used to demarcate the structural lineament. In theory several other gradient techniques other than THD can be used for this purpose such as tilt-derivative, analytical signal, theta derivative, and balanced horizontal derivative. However, the greatest advantage of THD over the other techniques is that this method is least susceptible to noise in the data because it only requires the calculations of the two first-order horizontal derivatives of the field (Blakely, 1996; Pilkington and Keating, 2004).

The 2.5 dimensional (2.5D) forward gravity modelling of the residual Bouguer anomaly was done using the GM-SYS software in the present study. The GM-SYS software is based on the algorithm of (Talwani et al., 1959) and (Talwani and Heirtzler, 1964), which computes the

gravity reaction of numerous polygonal-structured shapes of finite strike range (Chouhan, 2020). Gravity models along two profiles have been created. The accuracy of the model was tested by comparing the model's gravity response to observed measurements and minimizing the rms error. Details of the rms error calculation can be found in the GMSYS manual (Oasis Montaj GMSYS manual; pages.geo.wvu.edu/~wilson/gmsys_49.pdf)). The models were generated, taking into account our understanding of the geology of the area.

The interpretation of gravity surveys can be done qualitatively and quantitatively. The qualitative interpretation includes the anomalous geophysical information that is extracted from the regional and residual anomalous maps and their correlation with the geology of the basin. In contrast, the quantitative interpretation involves making 2.5D modelling to estimate the depth and dimensions of the sedimentary cover (Hope and Eaton, 2002; Kamguia et al., 2005).

3.3. Results

The Bouguer gravity anomaly ranges from -58 to +30 mGal, as shown in Fig. 3.1. To extract the regional anomaly from the Bouguer anomaly, upward continuation of the Bouguer anomaly was used at the height of 30 km (Fig. 3.2a), corresponding to an anomaly depth of 15 km (cf., Jacobsen, 1987). Thus, the regional Bouguer anomaly in this study provides information below the depth of 15 km. The residual anomaly is calculated after subtracting the regional anomaly from the Bouguer anomaly (Fig. 3.2b). The anomalous regional map (Fig. 3.2a) and the anomalous residual map (Fig. 3.2b) display gravity values ranging from -38.9 to 6.2 mGal, and -6.8 to 7.6 mGal, respectively. An application of the total horizontal derivative of the Bouguer anomaly was calculated for the residual and regional Bouguer anomalies and was used to detect the lineaments. The total horizontal derivative of the Bouguer anomaly is shown in Fig. 3.3a. The THD map derived by using the residual Bouguer anomaly is presented in Fig. 3.4a. The calculated THD map using the regional Bouguer anomaly is shown in Fig. 3.5a. The 2.5-dimensional models were also produced to determine the thickness of the sedimentary rocks and depth to basement in the study area.

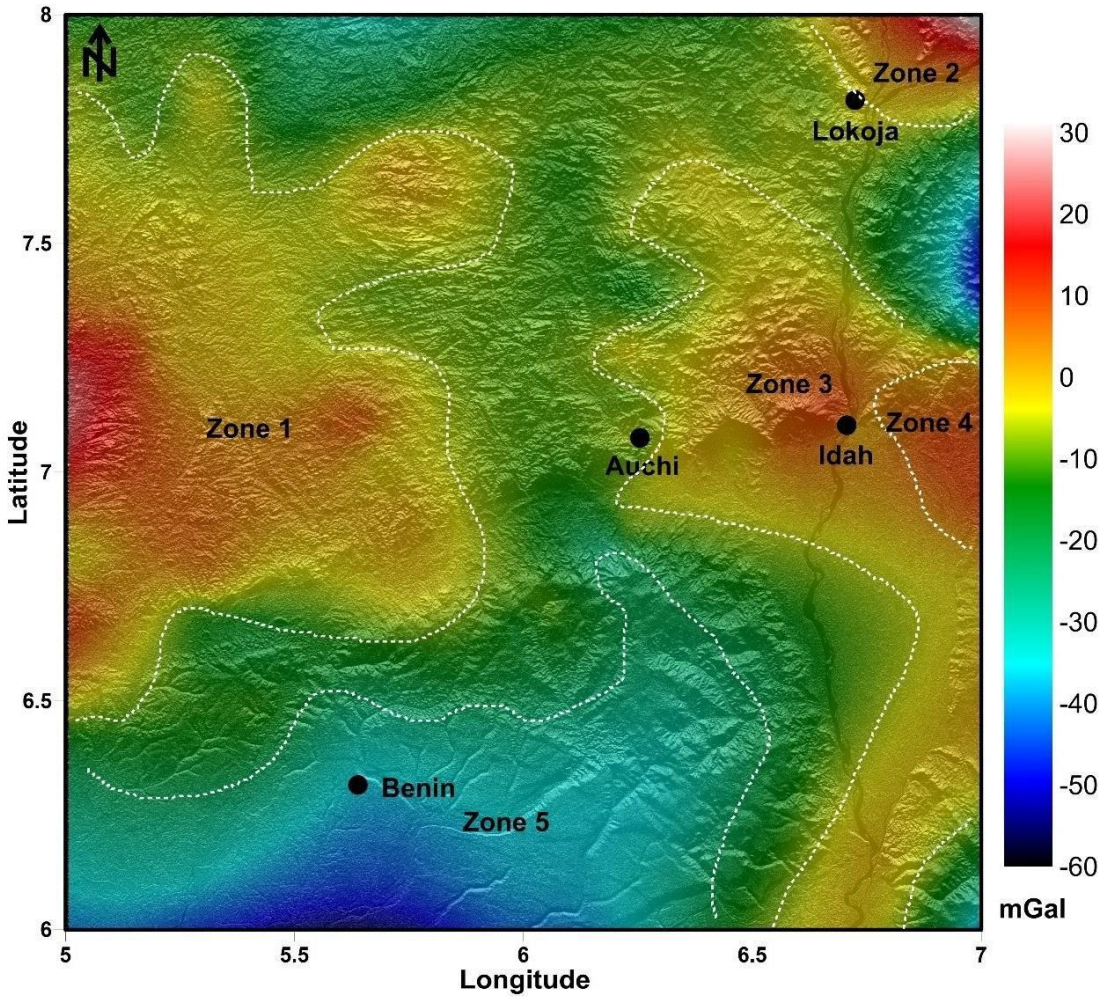

Figure 3.1. The Bouguer anomaly map of the Anambra Basin draped over the digital elevation model (DEM). Based on the anomaly pattern, the whole study area is divided into five zones (Zones 1, 2, 3, 4 and 5) and their boundaries are represented by white dashed lines. Black dots represent the major locations in the study area.

3.3.1. Gravity modelling of profiles lines

The residual Bouguer anomaly was used for the 2.5-dimensional gravity modelling along the profiles AB and CD (Fig. 3.2b). The profiles for modelling were chosen to make sure that they cross the majority of the prominent anomalies (Fig. 3.2b). During the gravity modelling, two layers, the basement and the overlying sedimentary cover, are considered. Opted density of the sedimentary and basement layers were 2400 kg/m^3 and 2700 kg/m^3, respectively (cf., Obasi et al., 2018)

3.3.1.1. Gravity modelling along profile AB

The NE-SW oriented gravity model along profile AB (Fig. 3.2) has a profile length of 300 km and is shown in Fig. 3.6a. During the modelling along profile AB, the root mean square error was kept below 0.16. The variation of basement depth along the profile AB is between 4 and 6 km.

3.3.1.2. Gravity modelling along profile CD

Gravity modelling along profile CD has a profile length of 220 km and is oriented in an E-W direction (Figs. 3.2b, 3.6b). The root mean square error was kept below 0.25 during the modelling along the profile. The forward modelling results reveal that the basement depth along the profile CD varies between 3.5 and 6.5 km (Fig. 3.6b).

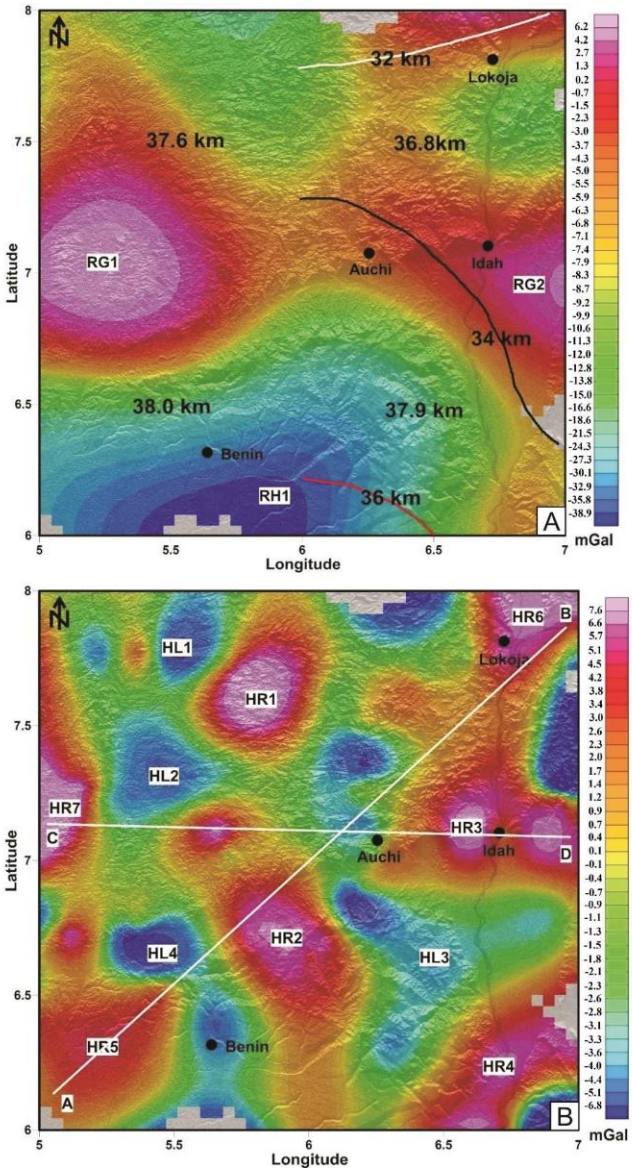

Figure 3.2. (a) Regional gravity anomaly map of the Anambra Basin calculated by upward continuation at height of 15 km draped over the DEM. Black dots represent the major locations in the study area. White, black and red contour lines represent the 32, 34 and 36 km Moho depths, respectively (Djomani et al., 1995). Digits represent the Moho depths from the CRUST 1.0 model. RG1, RG2 and RH1 show the high and low regional Bouguer anomalies. (b) Residual gravity anomaly map of the Anambra Basin draped over the DEM. Black dots represent the major locations in the study area. HR1-HR7 and HL1-HL4 define the identified conspicuous gravity high and low in the study area.

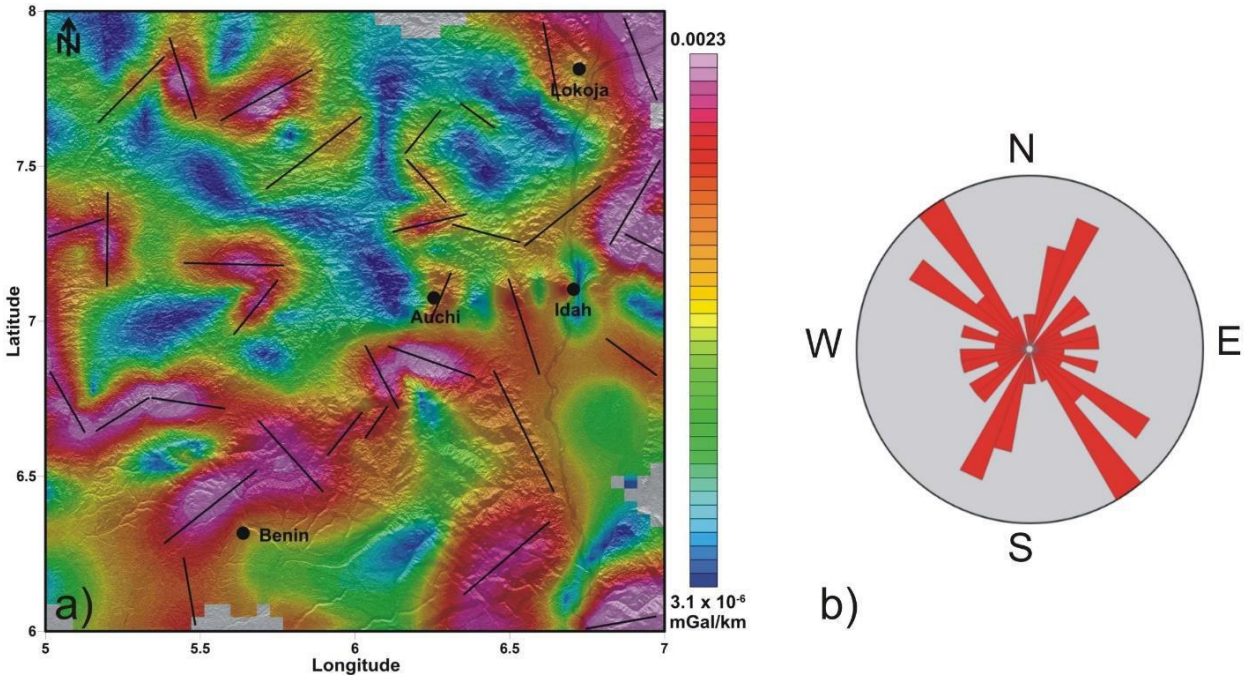

Figure 3.3. (a**)** Total horizontal derivative (THD) of the Bouguer anomaly over the Anambra Basin draped over the DEM. Black dots represent the major locations in the study area. Black lines represent the determined lineaments based on present result. (b) Rose diagram of the determined lineaments using THD of the Bouguer anomaly.

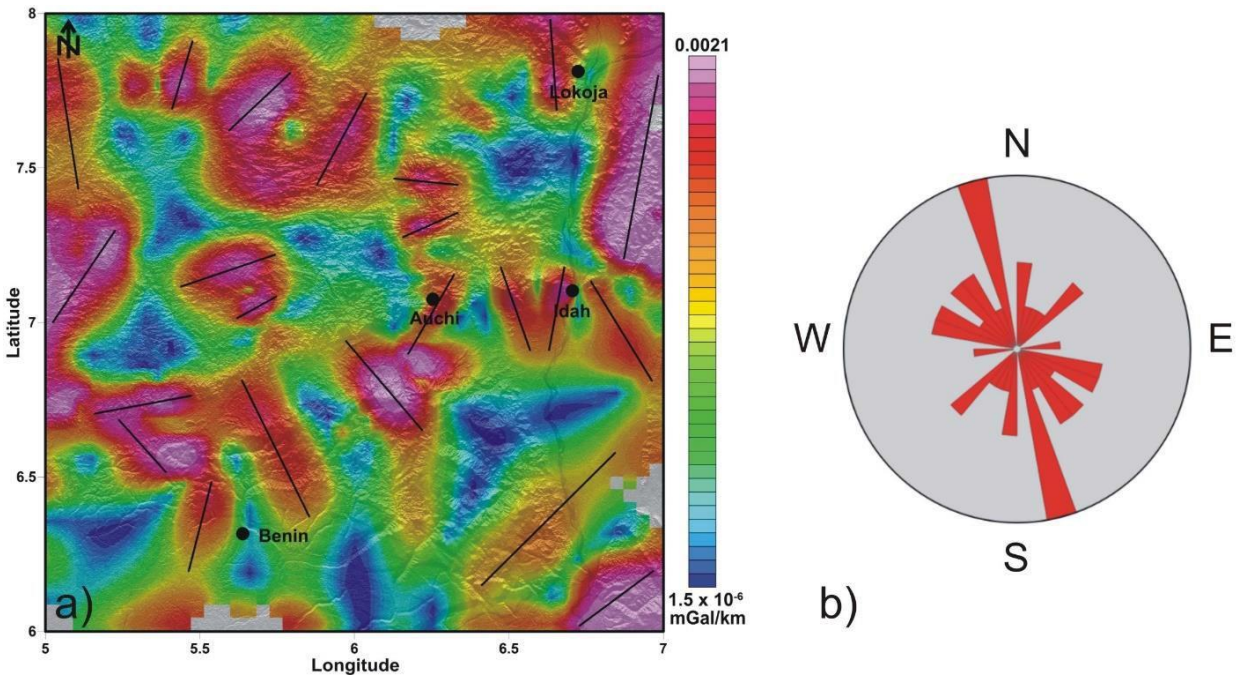

Figure 3.4. (a) Total horizontal derivative (THD) of the residual Bouguer anomaly over the Anambra Basin draped over the DEM. Black dots represent the major location in the study area. Black lines represent the determined lineaments based on present result. (b) Rose diagram of the determined lineaments using THD of the residual Bouguer anomaly.

3.4. Discussion

The Bouguer gravity anomaly is a combination of the regional and residual gravity anomalies within the study area (Blakely, 1996; Petit et al., 2002; Lowrie, 2007). The southern part of the map's anomalous gravity values gradually increases from -58 to more than +20 mGal towards the western and eastern parts of the study area (Fig. 3.1). The Bouguer anomaly pattern of the study area exhibits two general trends in E-W and NNE-SSW directions (Fig. 3.1). The Bouguer anomaly values over the Anambra Basin and its surroundings consist of negative (-ve) and positive (+ve) anomalies. Negative anomalies are generally attributed to materials that are less dense than the surrounding basement. Positive gravity anomalies correspond to denser materials than the surrounding basement (Eyike et al., 2010). Density differentiation between rocks forming the earth's crust gave rise to the various anomalies of low and high amplitudes in the gravity field (Riad, 1977). Based on the amplitude pattern, five zones can be distinguished (Fig. 3.1). Zone 1 is located in the western part of the study area, where the high anomaly values can be observed. The

exposure of the basement complex in Zone 1 might be the possible explanation of this high Bouguer anomaly. A similar interpretation can be given for the high anomaly values of Zone 2. The shallow depth of the basement rocks can be observed throughout the Idah region (Abbass and Mallam, 2013), and the high Bouguer anomaly of Zone 3 is probably associated with this. Zone 4 lies directly over the Nsukka Formation (Fig. 2.1b), and a shallow basement is a possible explanation for that. Finally, Zone 5 is located in the southern part of the studied area and on top of the Niger delta complex (Fig. 2.1b). This zone shows the lowest values within the studied area. This may be attributed to a thick succession of sedimentary rocks. Similar deductions have been made earlier for the eastern margin within the basin (Obasi et al., 2018), where the Bouguer gravity values ranged from -22.1 to 33.5 mGal, interpreted as igneous rocks, lower to middle Cretaceous sediments, upper Cretaceous to Paleogene deposits, and alluvium (Obasi et al., 2018).

The regional Bouguer anomaly from the CRUST1.0 model reveals a Moho depth of 38.0 km, dipping in a SW direction (Fig. 3.2a). This is consistent with the SW trend of the negative anomalous gravity. The prominent high gravity values in the E-W directions are characterized as RG1 and RG2. In contrast, the low gravity value in the south-western direction is determined as RH1. The present regional Bouguer anomaly shows the lower values in the southern part of the study area. Therefore, the low value of the regional anomaly RH1 is associated with the deeper Moho (Fig. 3.2a) (cf., Agagu and Adighije, 1983). The eastern part of the regional Bouguer map is consistent with the calculated Moho depth of Djomani et al. (1995) (contour maps are presented in Fig. 3.2a), which shows a southward dipping Moho. The circular gravity highs RG1 and RG2 are present at the western and eastern margins of the study area, possibly reflecting the presence of one or more intrusive bodies at a lower crustal level (cf., (Adighije, 1981; Ekwueme et al., 2018). Similar deductions of the Moho depth were made by Adighije (1978) for the Lower Benue Trough, where a Moho depth ranging from 20 – 30 km was postulated. A crustal thickness of 22-30 km below the Niger delta was recognized from gravity data (Benkhelil et al., 1988), consistent with our model. The generated residual gravity anomalies signify a distinct gravity variance in the study area, which serves as a pointer to categorize anomalous geological sources' effects. Based on amplitude values, seven high residual anomalies HR1-HR7 and four low anomalies HL1-HL4 have been identified (Fig. 3.2b). Due to an elevated basement floor, zone HR4's basement depth was found to be shallow by Onwuemesi's (1997) magnetic modeling. A deeper basement floor is observed in zone HL3, which resulted in the deposition of a thick sedimentary succession on top

of the basement floor. The power spectrum analysis and source parameter imaging of magnetic data depicts the basement depths in the region of Idah and Lokoja varies between 5 and 5.5 km, i.e. shallower than in many parts of the study area (Abbass and Mallam, 2013). This may also be the possible explanation for the gravity highs HR3 and HR6. The basement depth is shallow over HR1, explaining the gravity high (Ekwueme et al., 2018). The residual anomalous gravity in the basin's western margin is characterized by distinct elliptical, annular and elongated anomalies dispersed throughout the area and determined the subsurface structural orientation impacting the study area. This is denoted by the identified high (HR1-HR7) and low (HL1-HL4) amplitudes. The high residual gravity anomalies are interpreted as hypabyssal igneous rocks such as granites, and granodiorites, from a shallow basement (Adighije, 1981; Cratchley et al., 1984; Benkhelil, 1989; Abdullahi and Singh, 2018). In contrast, the low negative anomalies are attributed to Paleogene and Cretaceous sediments of the Niger delta complex, and the Bende, Imo, Nsukka, Ajali, Mamu and Nkporo Formations (Obasi et al., 2018; Ekwueme et al., 2018).

The THD of the Bouguer anomaly (Fig. 3.3a) indicates that most determined lineaments in the southern part of the study area are oriented in the NE-SW and NW-SE directions. The lineaments in the northern part exhibit a NE-SW and N-W trend (Fig. 3.3a). The rose diagram of the lineaments shows the two orientations in the NW-SE and NE-SW directions (Fig. 3.3b).

To determine the deeper and shallow seated structural features in the western margin, THD is calculated by using both the regional and residual Bouguer anomalies. The determined structural features using the THD of the residual anomaly roughly belong to the depth up to 15 km. The northern part of the THD of the residual map shows the NE-SW and E-W trending structural features. The lineaments in the southern part have a NE-SW and NW-SE trend (Fig. 3.4a), respectively. The rose diagram of the lineaments shows the three orientations in the NNW-SSE, NE-SW and NW-SE directions (Fig. 3.4b).

The calculated THD map (Fig. 3.5a) of the regional Bouguer anomaly belongs to the depth below 15 km and shows the trend of determined lineaments. The northern part of the regional map THD shows the NW-SE trending structural features, and the lineaments in the southern part have a NE-SW trend. The rose diagram of the lineaments shows the orientations in the ENE-WSW, NNE-SSW and NW-SE directions (Fig. 3.5b). Based on the present analysis, a revised tectonic map of the study area is provided in Fig. 3.5c.

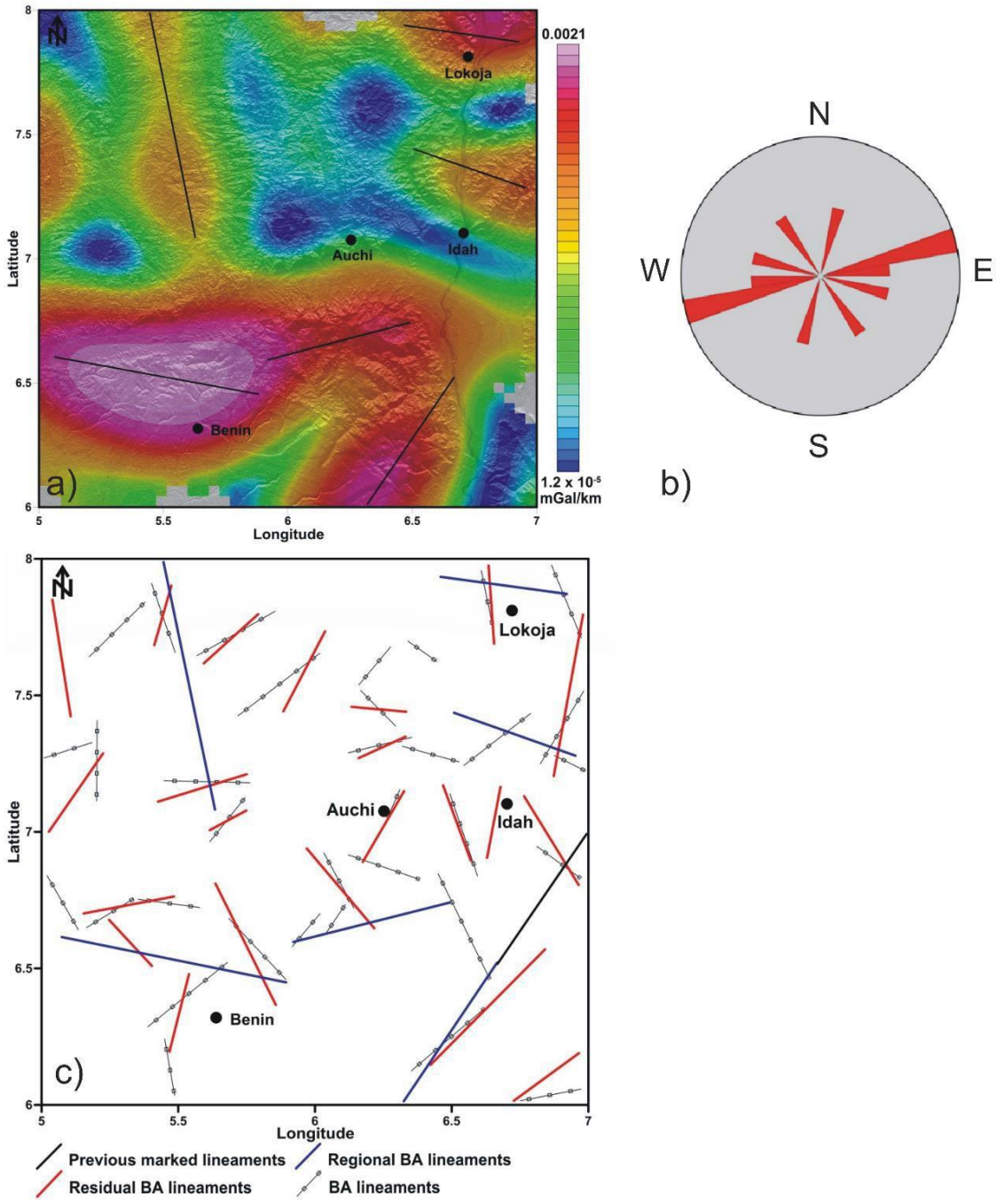

Figure 3.5. (a) Total horizontal derivative (THD) of the regional Bouguer anomaly over the Anambra Basin draped over the DEM. Black dots represent the major locations in the study area. Black lines represent the determined lineaments based on present result. (b) Rose diagram of the determined lineaments using THD of the regional Bouguer anomaly. (c) Revised tectonic map of the study area.

The faults that run across the western, eastern, northern and southern margins of the study area formed major and minor fractures with displacement (Benkhelil, 1982; Onuoha, 1999). The main structural systems that controlled the formation and the evolution of the basin affected all Cretaceous and Paleogene Formations. The predominant trends of the lineaments in the Cretaceous and Paleogene sediments are NW-SE and NE-SW, consistent with Onuoha's, (1999) trends for major faults in the Benue Trough and Anambra Basin. Other trends observed in the area such as NNE-SSW, ENE-WSW, NNW-SSE, E-W are of a lesser significance. In the lower Benue Trough, normal faults are found that cut across folds in the post-Santonian deposits (Benkhelil, 1982). They have been reported in outcrop sections within the Anambra Basin (Obi and Okogbue, 2004). Benkhelil et al. (1988) reported NNE-SSW and NE-SW directions as the main active structural trends in regions around Nsukka and Onitsha, which constitute the eastern margin of the basin. The Chain Fracture zone and Romanque Fracture zone characterize the lower Benue Trough and the Anambra Basin associated with the identified lineaments (Benkhelil, 1982; Onuoha, 1999).

The structural framework of the western Anambra Basin indicates the potential for a structural trapping framework for hydrocarbon accumulation in the Anambra Basin. The tectonic elements in the Anambra Basin can be attributed to the Santonian tectonic episode that affected the Cretaceous deposition (Burke et al., 1972; Agagu and Adighije, 1983) and is inferred as the possible explanation for the structural trends in the study area. Gravity anomalies and identified lineaments in the southwestern part of the Anambra Basin arising from high-resolution satellite data have been reported in this work.

Gravity modelling of profile AB reveals that the basement depth in the Lokoja region varies between 4 and 5 km. The power spectrum analysis and source parameter imaging of magnetic data depicts the basement depth in the region of Lokoja is approximately 5 km (Abbass and Mallam, 2013) , consistent with the present result. The gravity profile AB passes through the vicinity of the residual high Bouguer anomaly HR2, HR5 and HR6 (Fig. 3.2b). Basement depth values are 5 km, 4 km and 4 km over the zone of HR2, HR5 and HR6, respectively (Fig. 3.6a). The profile also passes through the zone of the low Bouguer anomaly HL4, where the basement depth is 6 km Fig. 3.6a.

Gravity modelling along profile CD passes through the high residual Bouguer anomaly HR3 and HR7, where basement depths of 3.5 and 4 km were identified (Fig. 3.2b). In the region of Idah,

basement depth ranges between 4 and 5 km, which is consistent with the results of Abbass and Mallam (2013). The basin's central and south eastern parts were reported to contain varying thicknesses ranging from 0.4 to 6km, with the basin's central part attaining the highest thickness value (Obasi et al., 2018). Also, Agagu and Adighije (1983) estimated sediment thicknesses of 5 to 10 km in the Onitsha Basin, the eastern margin of the Anambra Basin.

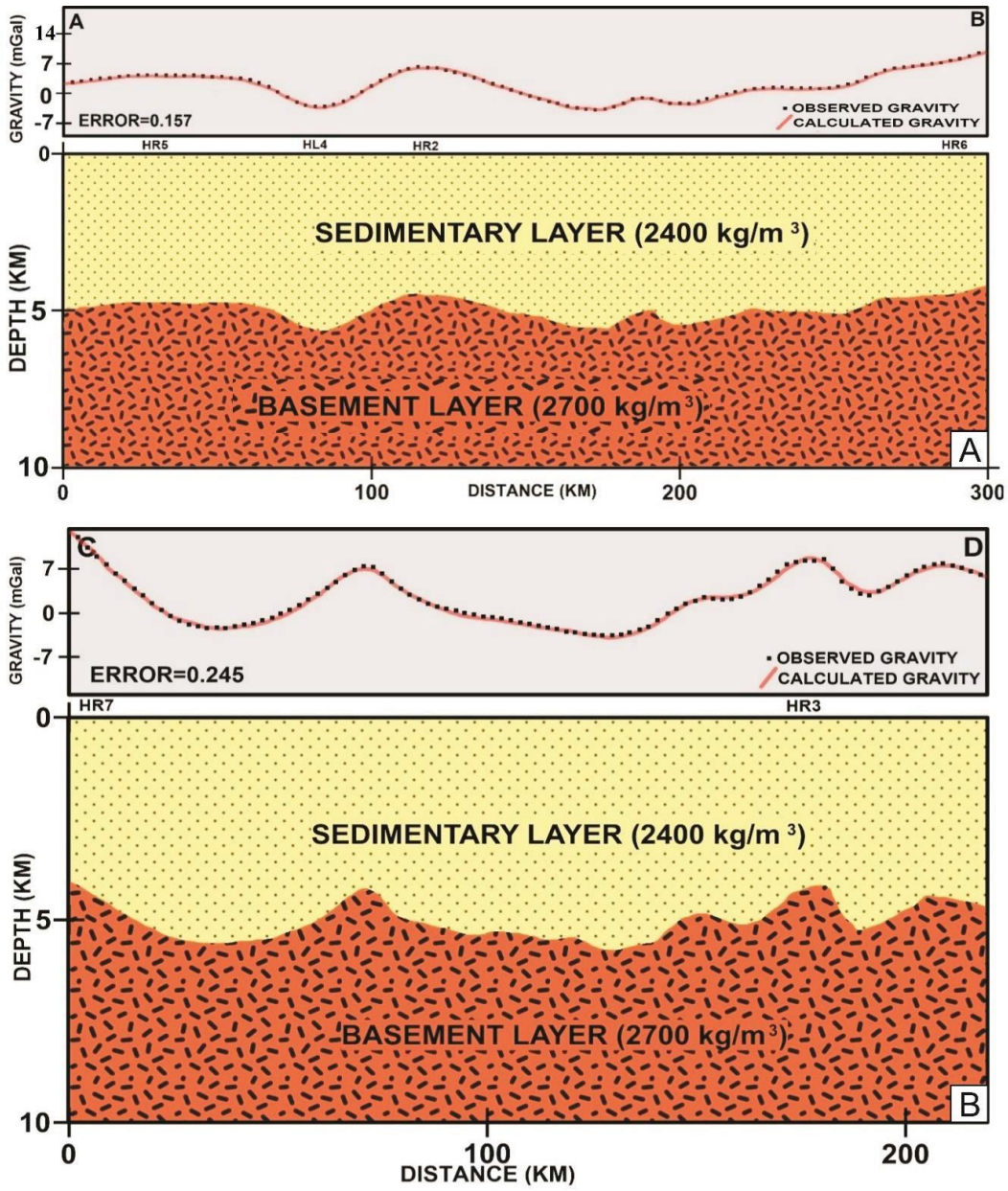

Figure 3.6. Gravity modelling along (a) AB profile, and (b) CD profile (Figure 3.2b). Density in the model is in kg/m^3.

The thickness of 5 km, calculated in this study, indicates that the basin was active during the Campanian – Maastrichtian tectonic event in the Cretaceous Period (Obi and Okogbue, 2004). The thick Cretaceous deposits indicate this in the western segment and overlying Paleogene sediments towards the southern Niger Delta complex. This study has shown that the sedimentary overburden is sufficient for the required minimum depth of 1 km for hydrocarbon accumulation with respect to the other elements of a petroleum system (Hunt, 1996). Exploration in the Cretaceous sections of the basin has not yielded much success, and this may be due to high geothermal gradients (20 - 35^{o}C/km; 25- 54°C/km) that may limit liquid hydrocarbon generation, and also the organic matter in the basin is more gas prone (Whiteman, 1982; Onwuemesi, 1997; Onuoha and Ekine, 1999; Obaje et al., 2004; Bello et al., 2017; Yakubu et al., 2020). Thus, exploration in the basin should

be focused on gas deposits within the matured sections of the basin with good organic richness, potential reservoir beds and a well-known structural framework. I can deduce that the subsidence and sedimentation rates in the Cretaceous and Paleogene evolution of the Anambra Basin and Niger delta complex can be hypothesized to have been influenced by the delineated faults and fractures (cf., Onuoha, 1999).

3.5. Conclusions

Analysis of high-resolution gravity data over the southwestern margin of the Anambra Basin of southern Nigeria and the interpretation of profiles reveal the following:

1. The Bouguer anomalies trend in E-W and NNE-SSW directions and five zones were identified in this study arising from amplitude pattern. The high gravity anomalies are associated with granites, granodiorites, and andesites. The intermediate gravity values represent the Middle to Upper Cretaceous sediments. The low gravity values occurring in the southern margin are interpreted as Paleogene sedimentary rocks.

2. The regional Bouguer anomaly in the present study reveals that Moho depths between 36.8 and 38.0 km and the low gravity anomaly recorded in the southern part result from the deeper Moho.

3. The residual Bouguer anomaly reveals seven high anomalies HR1-HR7 and four low residual anomalies HL1 - HL4.

4. Interpretation of the geophysical data indicated that two main structural trends control the Anambra Basin; NE-SW and NW-SE. The NW-SE, NE-SW lineaments may serve as possible migratory pathways for fluids (hydrocarbon and hydrothermal).

5. This study revealed that the sedimentary accumulation is sufficiently thick, reaching 5 km, and may serve as a good indication of hydrocarbon potential in the western segment. An integration of geochemical methods, well logs, and seismic data is recommended to validate these findings.

Chapter Four

Sedimentary geochemistry of Late Cretaceous-Paleocene deposits at the southwestern margin of the Anambra Basin (Nigeria): Implications for paleoenvironmental reconstructions

4.1. Introduction

During the last three decades, research in sedimentary geochemistry of siliciclastic deposits experienced significant progress (Nath et al., 1997; Barbera et al., 2006; Elliot et al., 2009; Fu et al., 2016; Zhang et al., 2020), and it is now used to decipher - among other factors - paleoclimatic and paleoenvironmental conditions, sediment recycling, biogenic silica inputs, hydrothermal influence, and paleo-hydrodynamic force (Jones and Manning, 1994; Barbera et al., 2006; Martinez-Ruiz et al., 2015; Fu et al., 2016; Li et al., 2018a; Wei and Algeo, 2020; Wei et al., 2021). The chemical composition of sedimentary rocks is strongly influenced by factors such as the chemical constituents of the source area, the energy of the transport medium and the increasing distance away from the source, marine and freshwater incursions, the water depth, the existence or absence of hydrothermal fluids, and the climatic, weathering and redox conditions during sedimentation (Moradi et al., 2016). Each of these factors leave their imprint in the resulting deposits that can be deciphered by analyzing their unique geochemical signature (Li et al., 2018b; Pehlivanli, 2019). Major elements (Al, Fe, Mn, and Ti), high field strength elements (U, Th, and Zr), large ion lithophile elements (Sr, Ba, and Rb), and transition elements (Co, Zn, Cr, V, Ni, and Cu) are all transported to the sedimentary basin without substantial fractionation and thereby retain the signature of the depositional environment (Tribovillard et al., 2006; Kahmann et al., 2008; Moradi et al., 2016). Furthermore, immobile (Zr, Fe, Al, Th) and mobile (Sr, Ba, Rb) chemical elements can be used to assess the paleoclimate, paleoredox and hydrothermal conditions, and the hydrodynamic pressure during sedimentation (Rimmer, 2004; Zhong et al., 2015; Goldberg and Humayun, 2016; Moradi et al., 2016; Tao et al., 2017; Li et al., 2018b; Pehlivanli, 2019; You et al., 2020). The research on these geochemical proxies is therefore of immense importance for the reconstruction of the changing environmental conditions during sedimentation in a (petroliferous) basin, which consequently also makes it an important tool for petroleum geologists. The Late Cretaceous and Paleocene epochs experienced extreme global temperature conditions (Hay and

Floegel, 2012; Scotese et al., 2021). In West Africa, warm temperature conditions typical of tropical climates were recorded in the geologic record (Chumakov et al., 1995; Scotese et al., 2021).

The Anambra Basin (Fig. 2.1), which is younger than the lower part of the Benue Trough, is a Cretaceous-Paleogene hydrocarbon-rich sedimentary basin in Nigeria, West Africa, with mainly gas prone hydrocarbon potential (Ene et al., 2019). Over the last two decades, several studies focusing on sedimentology (Tijani et al., 2010; Onyekuru and Iwuagwu, 2010; Dim et al., 2019) and stratigraphy (Uzoegbu et al., 2013), mineralogy (Akinyemi et al., 2013), palynology (Antolinez-Delgado and Oboh-Ikuenobe, 2007), reservoir characterization (Anakwuba and Onyekwelu, 2010), petroleum potential (Akaegbobi et al., 2000; Adebayo et al., 2018), aeromagnetics (Onwuemesi, 1997; Bello et al., 2017), and gravity modelling (Obasi et al., 2018; Omietimi et al., 2021) have been carried out on the basin. Most of the research focused on the basin's eastern and central margins (Tijani et al., 2010; Edegbai et al., 2019b). In contrast, little research has been carried out on its western margin (Ocheli et al., 2018; Edegbai et al., 2020).

The Imo, Mamu and Nkporo Formations (Fig. 2.2) are thought to have been deposited within estuarine, marginal to shallow-marine environments in a passive tectonic setting with their sediments largely derived from continental granitic rocks (Odunze and Obi, 2011; Odunze et al., 2013; Edegbai et al., 2019b). Nevertheless, there is still a plethora of open questions and a variety of unknown factors, particularly concerning the paleogeographic redox conditions, paleowater depth, hydrothermal influence, and paleohydrodynamic regime during deposition. The present study utilized drill core and ditch cuttings to provide a robust dataset in comparison to existing data on outcrop samples that are prone to alteration. Here, we use sedimentary geochemistry to constrain these parameters and reveal the major controlling factors during sedimentation. These findings will provide a better understanding of the sedimentation within the southwestern part of the basin. This study will also provide useful information for future research on siliciclastic systems, both locally and globally, as it takes a systematic approach to determine paleoredox conditions during deposition, hydrothermal impact, hydrodynamic strain, and ancient water depth using the example of the Late Cretaceous and Paleocene Nkporo, Mamu and Imo Formations.

4.2. Materials and methods

Two drill cores, the Owan-1 and the Ubiaja wells, that are stored and curated by the Nigerian Geologic Survey Agency in Kaduna, Nigeria, were studied. Both wells were drilled in the western segment of the Anambra Basin and reached a depth of 600 m and 970 m, respectively (Figs. 4.3 and 4.1), intersecting the Late Cretaceous Mamu, Nkporo, and Paleocene Imo Formations. The main lithofacies types (section 3.1) were sampled at regular intervals for geochemical analyses.

In total, 20 samples were used for geochemical analysis (Tables are included in Appendix 2). Circa 7-10 g of each sample were crushed to <75 μm in a Tungsten Carbide milling vessel, roasted at 1000°C to determine Loss On Ignition (LOI), and fused into a glass bead. Major element oxides were determined on the fused bead by X-ray fluorescence (XRF) using an ARL9400XP + Wavelength dispersive XRF Spectrometer with Rh tube, LiF220, GER, AXO6 and PET analyzing crystals. Another aliquot of the sample was pressed into a powder briquette to determine trace elements. Preparation of samples and analyses were carried out using standard methods after Loubser and Verryn (2008).

Analyses of trace elements and REE were conducted at the Earth Lab of the University of the Witwatersrand using a Thermo Scientific iCAP RQ for inductively coupled plasma mass spectrometry (ICP-MS). X-ray diffraction (XRD) was carried out at the Stoneman Lab of the University of Pretoria, using a PANalytical X'Pert Pro powder diffractometer with X'Celerator detector and Fe filtered Co-K radiation.

For this study, the weathering and paleoclimate indicators CIA (Chemical Index of alteration; Nesbitt and Young, 1982), PIA (Plagioclase lndex of Alteration; Fedo et al., 1995), CIW (Chemical Index of Weathering; Harnois, 1988) and C-value (Zhang et al., 2020) were computed and compared to PAAS (Post-Archean Australian Shale) and UCC (Upper Continental Crust) limits. The CIA, PIA, CIW and C-value are measured using the equations:

$$CIA=AL_2O_3/ (AL_2O_3+CaO^*+Na_2O+K_2O) \times 100 \quad (1)$$

$$PIA = [(Al_2O_3-K_2O)/ (Al_2O_3+CaO^*+Na_2O-K_2O)] \times 100 \quad (2)$$

$$CIW= [AL_2O_3/ (Al_2O_3+CaO^*+Na_2O)] \times 100 \quad (3)$$

$$C\text{-value} = [Fe + Mn + Cr + Ni + V + Co]/ [Ca + Mg + Sr + Ba + K + Na] \quad (4)$$

where CaO* measures the proportion of calcium oxide present in the siliciclastic sediments' silicate fraction. The technique proffered by McLennan et al. (1993) was adopted to determine the CaO* value in this work, where $CaO^*=CaO-(10/3*P_2O_5)$. The index of compositional variability (ICV,

Cox et al., 1995) is applied in this study to evaluate the chemical maturity of the Late Cretaceous-Paleocene units and also access sedimentation recycling. The ICV indicator was computed using the equation:

$$ICV = [Fe_2O_3 + K_2O + Na_2O + CaO + MgO + TiO_2]/ Al_2O_3 \quad (5)$$

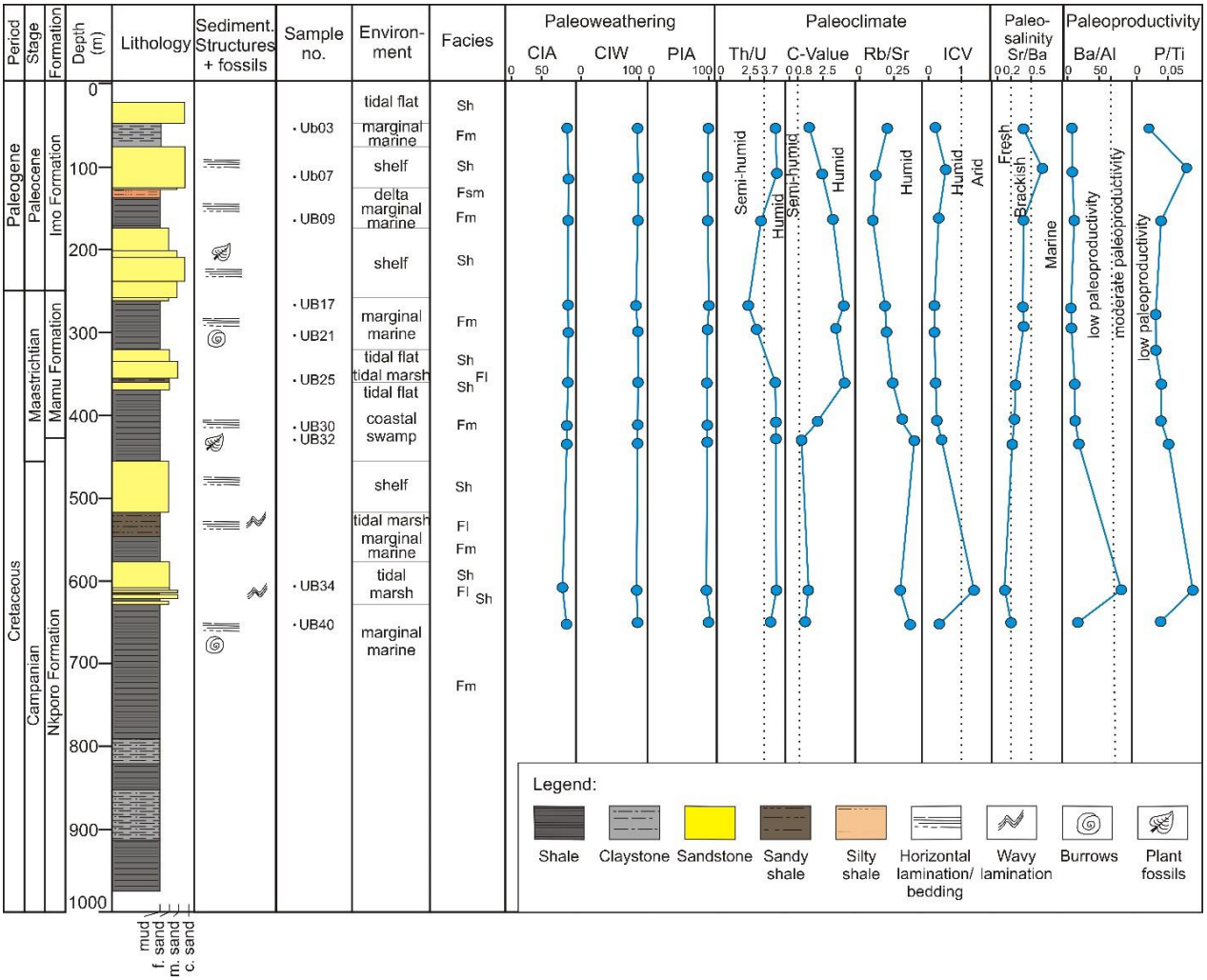

Figure 4.1. Lithostratigraphic section and paleoweathering, paleoclimatic proxies, paleosalinity and primary productivity indicators of the Nkporo, Mamu and Imo Formations within the Ubiaja well.

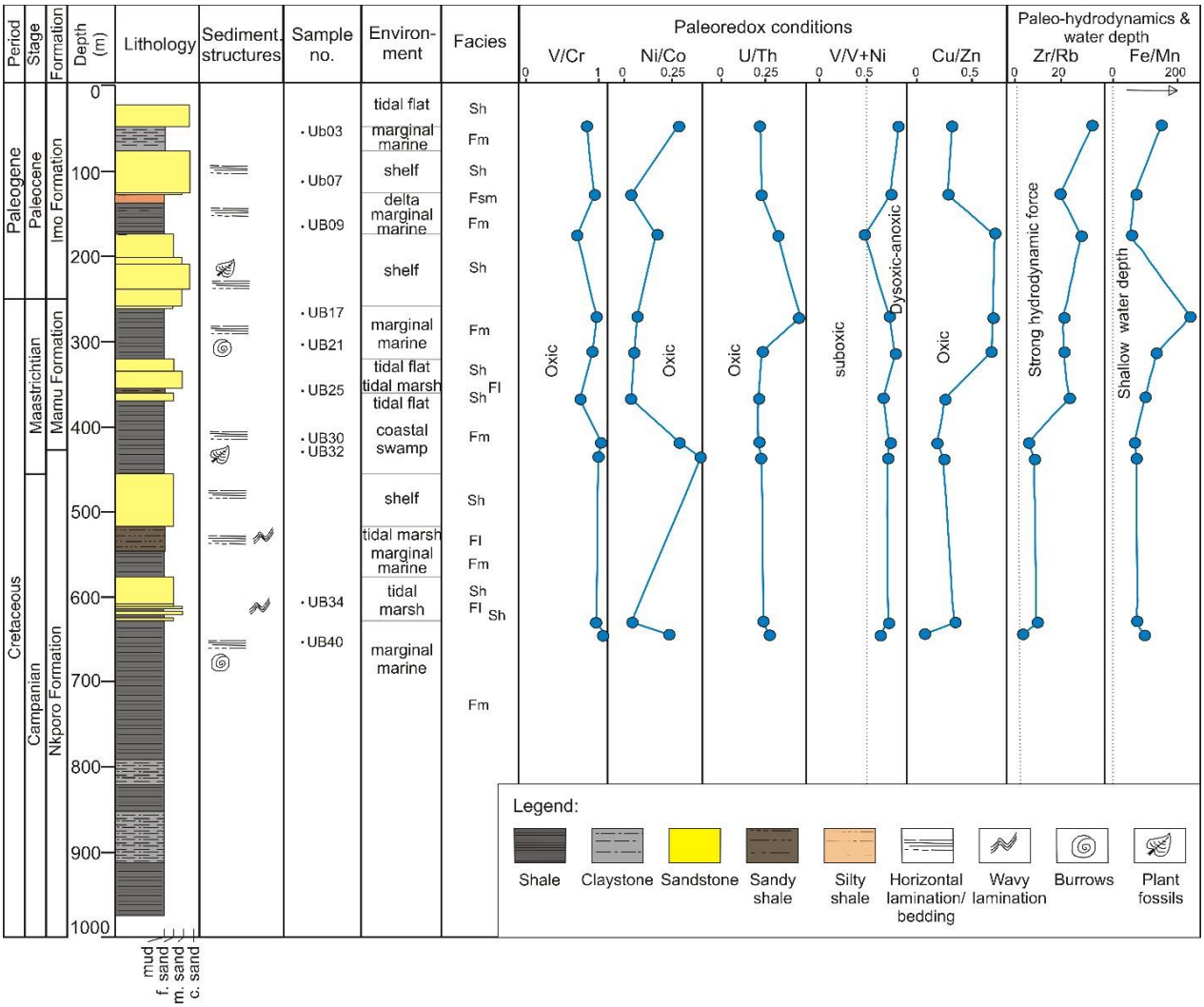

Figure 4.2. Stratigraphy and paleoredox proxies, hydrodynamic conditions and paleo-water depth of the Nkporo, Mamu and Imo Formations within the Ubiaja well.

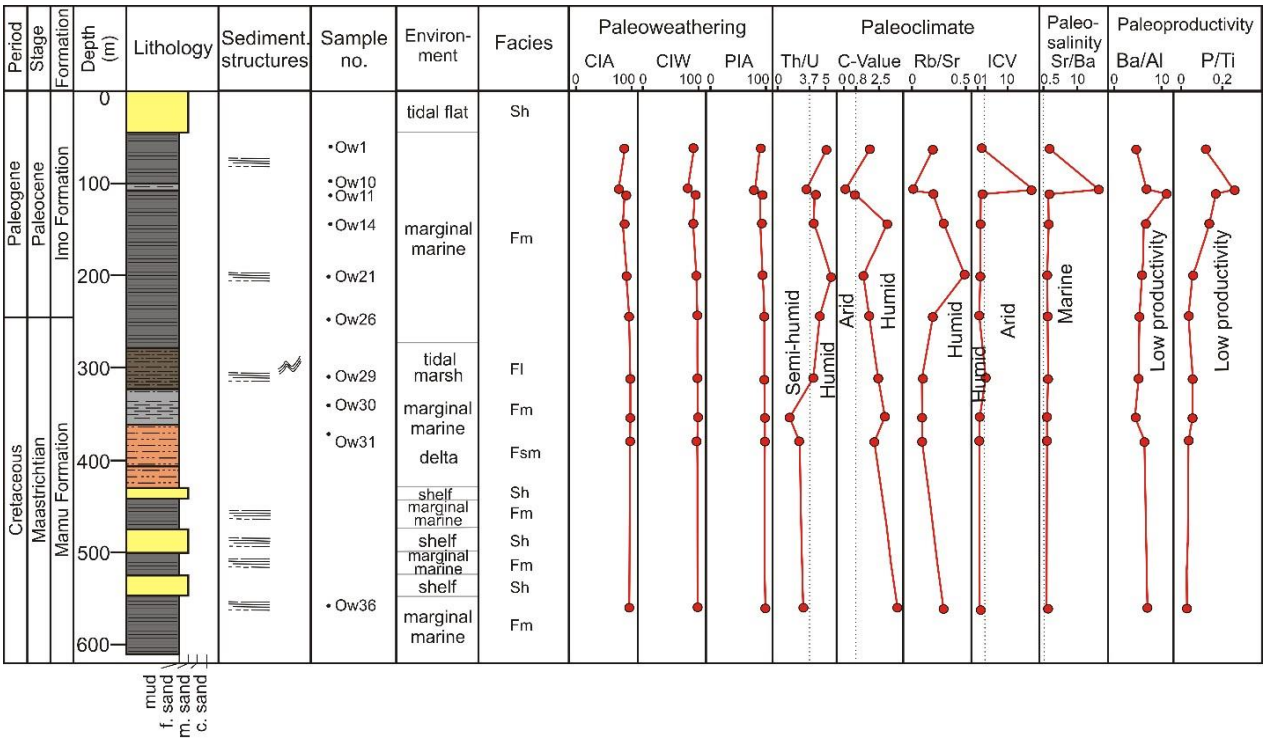

Figure 4.3. Lithostratigraphic section and paleoweathering, paleoclimatic proxies, paleosalinity and primary productivity indicators of the Mamu and Imo Formations within the Owan-1 well.

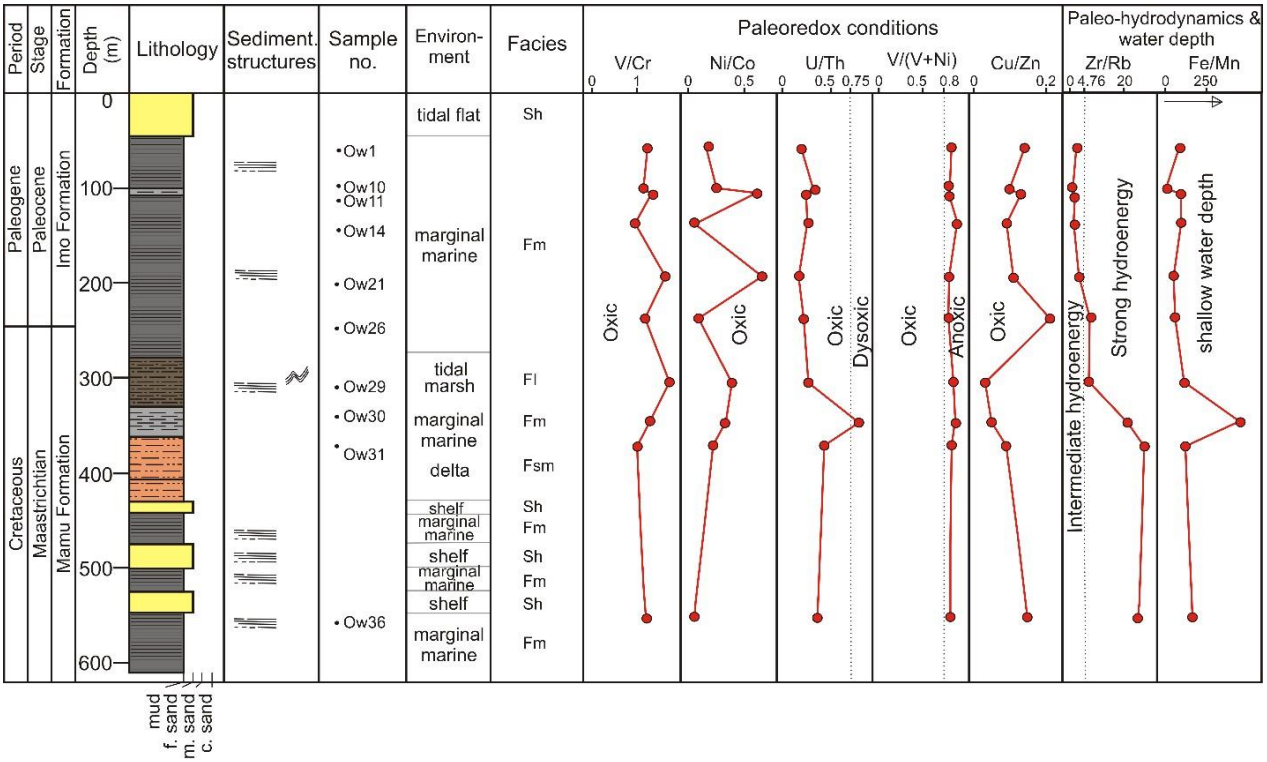

Figure 4.4. Stratigraphy and paleoredox proxies, hydrodynamic conditions and paleo-water depth of the Mamu and Imo Formations within the Owan-1 well.

4.2.1. Lithofacies types

Based on representative rock types, color, grain size, bedding pattern, mineral composition, and sedimentary structures, 4 lithofacies types have been identified within the two drill cores (Figs. 4.1 and 4.3). Lithofacies codes were adapted from Miall (1977, 2006).

4.2.1.1. Lithofacies I: Mudstone (Fm)

Lithofacies *Fm* is characterized by fine-grained clastic deposits that can be subdivided into laminated and non-laminated mudstones.

4. 2.1.1.1. Laminated mudstone (Fm 1)

The laminated mudstone was identified as the predominant lithofacies in the Mamu and Nkporo Formations (samples OW01-09, 11-28, 36, and UB09, 17, 22, 27-33, 36, 39-40, and 42-45). It is typically grey to dark grey, indurated, fissile, poorly to well laminated and carbonaceous. The cumulative thickness of this facies in the Owan-1 and Ubiaja wells is 208 m and 135 m, respectively. The bed thickness varies from 1.0 to >4.0 m. Sandstone, shaly sandstone, and sandy shale sequences are commonly overlain by the lithofacies. Few plant remains and burrows have

been found in the shale. The mineral content of this facies is primarily made up of palygorskite, kaolinite, smectite, ankerite, illite, anatase, gypsum, microcline, and minor quartz.

4.2.1.1.2. Non-laminated mudstone (Fm 2)

This subfacies is typically massive, light grey to milky brown, non-fissile, and non-carbonaceous. The cumulative thickness of this facies is 55 m in the Owan-1 well (samples OW 10, 30) and 72 m in the Ubiaja well (samples UB 03-06, 18-21). The bed thickness ranges from 2 to >7 m. The shale is dominated by kaolinite, quartz, calcite, anatase, jarosite, with minor pyrite and hematite.

4.2.1.2. Lithofacies II: Laminated sandy siltstone and mudrock (Fl)

This lithofacies type varies in color from grey to yellowish-brown with wavy lamination. The particle sizes range from fine sand to silt and clay. The rocks are slightly ferruginized and exhibit bed thicknesses of more than 2 m. The cumulative thicknesses of this facies, usually overlying the mudstone lithofacies, are 63 m and 10 m in the Owan-1 (samples OW 29 and 35) and Ubiaja wells (samples UB 25, 34, and 41), respectively. The mineralogy of this lithofacies is made up of quartz, kaolinite, siderite, and minor amounts of pyrite and hematite.

4.2.1.3. Lithofacies III: Silt- and mudstone (Fsm)

The colors of the *Fsm* lithofacies range from grey to dark brown. The dominant particle sizes are silt and clay-sized grains. Individual beds vary from 2 to 7 m in thickness. The cumulative thickness of this facies is 100 m and 44 m in the Owan-1 (samples OW 31-34) and Ubiaja wells (samples UB 08), respectively. The mineralogy of this lithofacies is dominated by quartz, kaolinite, and minor siderite and anatase.

4.2.1.4. Lithofacies IV: Sandstone (Sh)

This lithofacies type varies in color from milky white to brown and yellow. The grains are angular, sub-rounded to rounded, and poorly to moderately sorted. The major textural components are silt and fine-to-coarse sand grains. Individual bed thicknesses vary from 2 to 16 m. The sandstone facies is dominant in the Ubiaja well (samples UB 01,02,07,10-16,23-24,26,35,37 and 38), with a cumulative thickness of 161 m. Additionally, the aggregate thickness in the Owan-1 well is up to 40 m. A few plant remains could be identified within the samples. The sandstones are dominated by quartz and minor amounts of hematite and kaolinite.

4.2.2. Paleoclimate and paleoenvironmental proxies

The ratios Th/U, Rb/Sr, and the C-value are commonly used to reconstruct paleoclimatic variations and have been shown to be reliable (Figs. 4.1 and 4.3) (Chang et al., 2013; Li et al., 2021b; Zhang et al., 2021). Th/U increases with intense chemical weathering through oxidation and the reduction of U. Generally, values greater than PASS concentration indicate advanced chemical weathering (McLennan et al., 1993). In contrast, Rb/Sr ratios increase under arid conditions, i.e. low values reflect humid and warm climates whereas high values suggest arid, dry and hot climatic conditions (Chang et al., 2013; Martinez-Ruiz et al., 2015). Finally, the C-value is based on the fact that the elements Fe, Mn, Cr, Ni, V, and Co, are enhanced in humid settings, whereas Ca, Mg, Sr, Ba, K, and Na are concentrated in arid conditions due to precipitation of saline minerals (Hu et al., 2017; Krzeszowska, 2019). A humid paleoclimatic environment is indicated by a high C-value, with C-values > 0.8 indicating humid conditions, 0.6 - 0.8 suggesting semi-humid conditions, 0.4 - 0.6 indicating semi-humid–semiarid conditions, 0.2 - 0.4 indicating semiarid conditions, and C-values <0.2 indicating arid conditions (Figs. 4.1 and 4.3; Zhang et al., 2020).

The compositional maturity of sediments and sedimentary rocks is assessed by analyzing their geochemical signatures (Li et al., 2019; Huang et al., 2020; Overare et al., 2020). Commonly, the index of chemical variability (ICV) is utilized for this purpose (Cox et al., 1995).

The ternary plot of Fe_2O_3-K_2O-Al_2O_3 indicates Al_2O_3 enrichment, suggesting that clay mineralogy primarily controls the geochemistry of the lithofacies (Fig. 4.7a; Overare et al., 2020). Clay-rich sedimentary rocks contain high amounts of Al_2O_3 and low concentrations of K_2O, Na_2O and CaO compared to deposits that are poor in clay. Correspondingly, ICV values for clay-rich rocks are higher than for clay-poor rocks. The sedimentary facies with computed ICV values >1 reflect compositional immaturity within the first depositional cycle and active tectonic conditions (Fig. 4.7c). In contrast, ICV values <1 indicate compositionally matured sediments with high sediment recycling along tectonically inactive plate margins (Long et al., 2012). ICV values in clay minerals (such as montmorillonite and illite) are commonly less than 0.12, 0.13-5 in feldspars and biotite, 5-20 in amphibole and 20-300 in pyroxene due to diminishing Al_2O_3 concentrations (Li et al., 2019).

In the past, a variety of geochemical proxies have been used to assess paleoenvironmental parameters such as paleosalinity, paleoproductivity and the paleoredox conditions in sedimentary rocks (Wei and Algeo, 2020; Wang et al., 2021a; Zhang et al., 2021). Sr and Ba ratios in particular

can provide insights into changes in paleosalinity levels in sedimentary deposits (Moradi et al., 2016; Li et al., 2020b) as Sr enrichment is linked to rising paleo-water salinity and salinity rises with depth; thus, high Sr/Ba values indicate rising saltwater depth and salinity (Zhang et al., 2021). As a result, Sr/Ba geochemical signatures have increasingly been recognized as a proxy for paleo-water salinity (Zhang et al., 2021). The Sr/Ba ratio is proven to be a reliable proxy to estimate paleosalinity, except in carbonate rocks where Sr could be enriched and therefore affect the results (Wei and Algeo, 2020). Carbonate fractions typically have much higher Sr concentrations than clay fractions. Due to the low carbonate mineral content of the studied sections, however, carbonate-hosted Sr is insignificant for this study (Fig. 4.7b). As a result, the Sr/Ba ratio can be seen as a valid proxy for paleosalinity interpretation. Commonly, Sr/Ba ratios > 0.5 reflect deposition in a marine environment, 0.2-0.5 indicate brackish water and values < 0.2 point to a deposition within a terrestrial environment that is dominated by freshwater (Figs. 4.1 and 4.3; Wei and Algeo, 2020; Zhang et al., 2021). The paleosalinity is suggested to substantially affect the growth of organisms, accumulation, and conservation of organic matter (Li et al., 2020b).

The trace elemental ratios of Ba/Al and P/Ti provide valuable information on nutritional conditions and paleoproductivity, i.e. the uptake of dissolved inorganic carbon and its sequestration into organic compounds by primary marine producers (Tribovillard et al., 2006; Algeo et al., 2011; Li et al., 2020b; Zhang et al., 2020). Phosphorus is important for all kinds of life on Earth since it is a major component of skeletal material and is involved in a variety of metabolic activities (Li et al., 2020b; Zhang et al., 2021). The availability of organic matter is connected to the concentrations of P and Ba in sedimentary deposits, potentially resulting from high productivity (Tribovillard et al., 2006). Because Ti and Al are typically derived from terrigenous detrital matter, Ba/Al and P/Ti ratios are employed to estimate paleoproductivity (Li et al., 2020b). Lower productivity is indicated by a P/Ti value of less than 0.34, intermediate productivity is characterized by a P/Ti value of 0.34–0.79, and a P/Ti value of more than 0.79 indicates high productivity (Figs. 4.1 and 4.3; (Li et al., 2020b).

Redox sensitive elements, e.g. V, U, Fe, Mn, Co, Cr, and Ni, are known to indicate the depositional environment's redox characteristics because they do not move after deposition and burial. This fact makes these redox sensitive elements ideal and reliable proxies for interpreting paleoredox conditions of sedimentary rocks (Nath et al., 1997; Guo et al., 2011; Goldberg and Humayun, 2016; Li et al., 2018a; Xi and Tang, 2021). In this study, the trace element ratios V/Cr, Ni/Co,

U/Th, and V/(V+Ni) that are widely applied were utilized to assess the paleoredox setting. Hu et al. (2017) used Ni/Co, U/Th, V/Cr, and V/(V+Ni) as paleoredox indicators to investigate the sedimentary paleoredox conditions in the Zhanjin Formation of China's Qiangtang Basin. Furthermore, (Li et al., 2021b) used Ni/Co, V/Cr, and V/(V+Ni) as geochemical proxies to reconstruct the paleoredox conditions in the Ha'erjiawu Formation of China's Santanghu Basin. In addition, the proxies stated above have been successfully applied in the reconstruction of paleoenvironmental settings in other WCARS basins (Tan et al., 2017; Lai et al., 2018; Adeoye et al., 2020; Overare et al., 2020; Abubakar et al., 2021). Anoxic, dysoxic, and oxic environments were defined using reference standards for U/Th, V/Cr, Ni/Co, and V/(V + Ni) (Figs 4.2 and 4.4). Commonly, V/Cr ratios >4.25 signify an anoxic depositional environment, i.e., exhibit strong reducing conditions. Ratios between 2.0 - 4.25 indicate a dysoxic depositional setting, i.e. reducing conditions. Finally, ratios <2.0 point to an oxic depositional environment, i.e. oxidizing conditions (Li et al., 2018b). Similarly, Ni/Co values >7.0 show an anoxic depositional environment, 5.0 - 7.0 indicates dysoxic environment, and <5.0 suggests oxic conditions (Figs 4.2 and 4.4; (Jones and Manning, 1994; Guo et al., 2011). U/Th ratios >1.25 indicate anoxic conditions, 0.75 – 1.25 reflect dysoxic conditions, and <0.75 show oxic conditions (Jones and Manning, 1994). Finally, V/(V+Ni) ratios >0.84 indicate euxinic depositional conditions, i.e. anaerobic-reducing conditions, 0.54 – 0.82 indicates anoxic settings, and 0.46 – 0.60 indicates dysoxic depositional conditions (Figs. 4.2 and 4.4; (Hatch and Leventhal, 1992).

Zr is a common continental inert element that is preserved in continental, transitional and shallow marine environments (Pehlivanli, 2019). Rb is a common mobile element during a variety of different geological processes, and it is accumulated in deep water with low energy because of its active chemical properties (Li et al., 2018b). As a result, the Zr/Rb ratio can react to changes in water depth and therefore, it is considered a good indicator for paleo-hydrodynamics (Figs. 4.2 and 4.4; Teng, 2004; Teng et al., 2005; Zhao et al., 2016; Li et al., 2018b; Pehlivanli, 2019). The lower the Zr/Rb ratio, the greater the water depth and the weaker the hydrodynamic pressure (Li et al., 2018b; Pehlivanli, 2019). A higher Zr/Rb ratio indicates shallow water circulation and stronger hydrodynamic pressure. Teng (2004), Zhao et al. (2016), and Li et al. (2018b) applied the Zr/Rb indicator to determine the Zhuozishan, Shanxi and Yanchang Formations' hydrodynamic characteristics in the Ordos Basin of China, and their data revealed weak and comparatively strong paleo-hydrodynamic influences during the deposition of the mudrocks. The Zr/Rb ratio <0.92

shows a weak paleo-hydrodynamic regime, 1.25 - 4.76 means intermediate to strong hydrodynamic pressure, and > 4.76 indicates a strong paleo-hydrodynamic regime (Teng, 2004; Pehlivanli, 2019).

Fe and Mn major elements possess entirely different characteristics regarding the transportation and sedimentation processes in the sedimentary basin due to their chemical properties (Wang et al., 2020). Although the Fe element is easily oxidized and precipitated, the Mn is a major stable element that can be transferred to deep water regions far away from the seashore (Wang et al., 2020). Because the Fe/Mn ratio has a strong relationship with water depth, it can be used to classify paleowater depth, with higher ratios indicating shallower water conditions (Figs. 4.2 and 4.4; (Toyoda, 1993; Takamatsu et al., 2000; Wang et al., 2020).

4.3. Results

4.3.1. Sedimentary bulk-rock geochemistry

The major element oxides SiO_2 and Al_2O_3 constitute the dominant oxides, with contents ranging from 7.08 - 72.87 wt.% and 2.65 - 22.63 wt.%, in the Owan-1 well, and from 46.15 - 85.22 wt.% and 4.13 - 27.42 wt.% in the Ubiaja well (Appendix 2). The concentrations of Fe_2O_3, MgO and CaO in the Owan-1 well vary between 1.19 - 23.85 wt.%, 0.18 - 8.09 wt.% and 0.13 - 47.37 wt.%, respectively. In the Ubiaja well, they range from 0.70 - 10.77 wt.%, 0.08 - 0.54 wt.% and 0.04 - 0.49 wt.%, respectively. Na_2O, K_2O, P_2O_5, TiO_2 and MnO are available in small concentrations of less than 2%. The CIA values for the Owan-1 and Ubiaja samples (ranging from 78 to 99) are higher than the PAAS (70) and UCC (52). Similarly, the PIA values for the studied sections (ranging from 81 to 100) record higher values relative to the PAAS (79) and UCC (53). Except for sample OW 10, which exhibits a CIW of 81, the CIW for these samples ranges from 81 to 100, which is higher than PAAS (82) and higher relative to UCC (58). The C-values of the analyzed samples vary between 0.6-4.2 and 0.1-3.9 for the Ubiaja and Owan-1 rocks, respectively.

According to the classification scheme by Sprague et al. (2009), the samples from the Owan-1 well can be chemically classified as claystones (OW 1, 10, 11, 14, 21, 26, 29,30), and siltstones (OW 36, 31) (Fig. 4.5a). In contrast, the Ubiaja well samples are classified as claystones (UB 3, 17, 30, 32, 40), argillaceous sandstones (UB 21) and sandstones (UB 7, 9, 25, 34). The geochemical classification, therefore, agrees with the petrographical classification (see section 4.2.1). The

classification system by Herron (1988) shows that all samples can be classified as Fe-shales, Fe-rich sands, or shales, with most of the samples plotting in the Fe-shale field (Fig. 4.5b), which can probably be attributed to their pyrite, hematite, and siderite content.

The SiO_2 within the samples bears indications for detrital as well as biogenic contributions (Fig. 4.5c). The exact detrital influence was determined by the geochemical proxy D* = Al/(Al+Fe+Mn) (Boström, 1970; Barbera et al., 2006), that links Al_2O_3, which is found in the continental crust (i.e. D*=0.79; Taylor and McLennan, 1985; Barbera et al., 2006), with MnO and Fe_2O_3, as typified by the oceanic crust affinity (i.e. D*=0.68; Taylor and McLennan, 1985; Barbera et al., 2006). The detrital characteristics and continental crust source for the deposits in this study range from 0.43 to 0.95 D* (mean, 0.82 D*) for the Ubiaja well and from 0.32 to 0.88 D* (mean, 0.74 D*) for the Owan-1 well (Appendix 2), indicating a strong continental influence during the deposition of the sediments at the western margin of the Anambra Basin. The silica in our study is mainly sourced from terrigenous detrital quartz with minor biogenic input. The biogenic silica input is possibly from diatoms and other siliceous plankton, which are common sources of biochemically precipitated silica in marine environments, indicating an abridged period of comparatively shallow to deep depositional conditions remote from terrigenous input for mudrocks along the shore (Kidder and Erwin, 2001; Adeoye et al., 2020).

The major sources of trace elements in sedimentary basins are terrestrially weathered rocks, plankton remnants, and hydrothermal fluids (Tribovillard et al., 2006; Adeoye et al., 2020). The trace element geochemistry of sedimentary deposits have been proven to contain significant information on paleoenvironmental settings, and this has been utilized worldwide in interpreting depositional settings of ancient sedimentary rocks (Tribovillard et al., 2006; Wei and Algeo, 2020; Wang et al., 2021a; Xi and Tang, 2021; Zhang et al., 2021). In this contribution, the trace elemental concentrations were used to determine the paleoclimate, paleosedimentary environment, paleogeographic redox conditions, hydrodynamic pressure and paleowater depth of the studied formations. The stratigraphic variations of trace elemental ratios, and paleogeographic redox indicators in the Imo, Mamu and Nkporo Formations are shown in Figs. 4.1 to 4.3. Furthermore, I focused on the mudrocks since elemental geochemistry proxies and threshold limits have primarily been established and applied in marine-transitional shales and mudrocks and provide reliable interpretation (Zhang et al., 2021).

The enrichment factor (EF) is commonly used to assess the degree of element enrichment (Li et al., 2018b). It is calculated as the proportion of an element's concentration in the samples to the

equivalent value of UCC (Rudnick and Gao, 2003). REE and trace element patterns (Fig. 4.6) show enriched and depleted concentrations normalized to chondrite (Taylor and McLennan, 1985) and UCC (Rudnick and Gao, 2003).

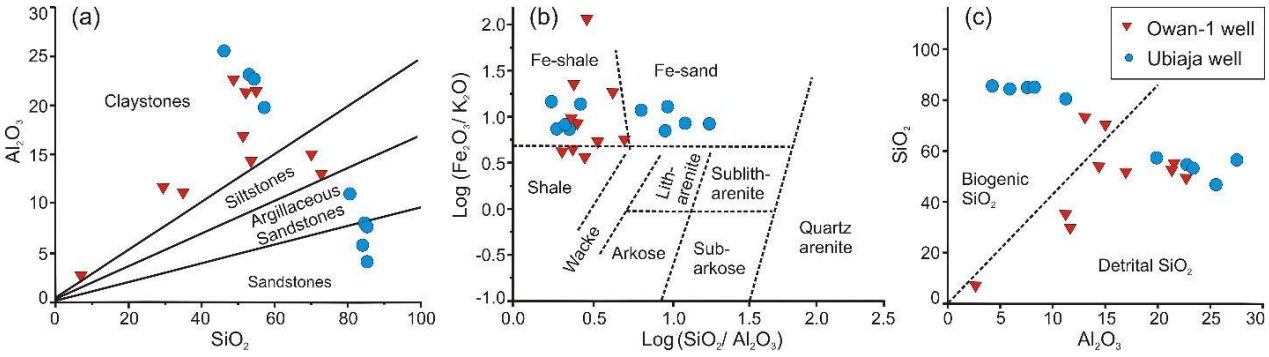

Figure 4.5. (a) Chemical classification of the sampled sedimentary rocks according to (Sprague et al., 2009) and (b) according to Herron (1988); c) Biogenic silica concentration in the Nkporo, Mamu and Imo Formations (Barbera et al., 2006).

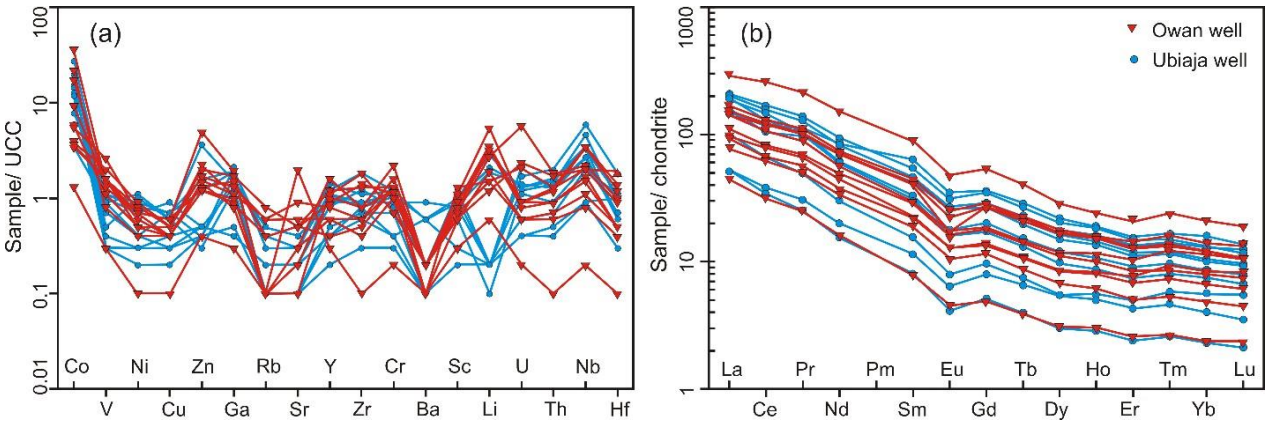

Figure 4.6. a) Trace element variation diagram with all samples normalized to UCC (Rudnick and Gao, 2003). b) Rare earth elements of all samples normalized to chondrite compositions (Taylor and McLennan, 1985).

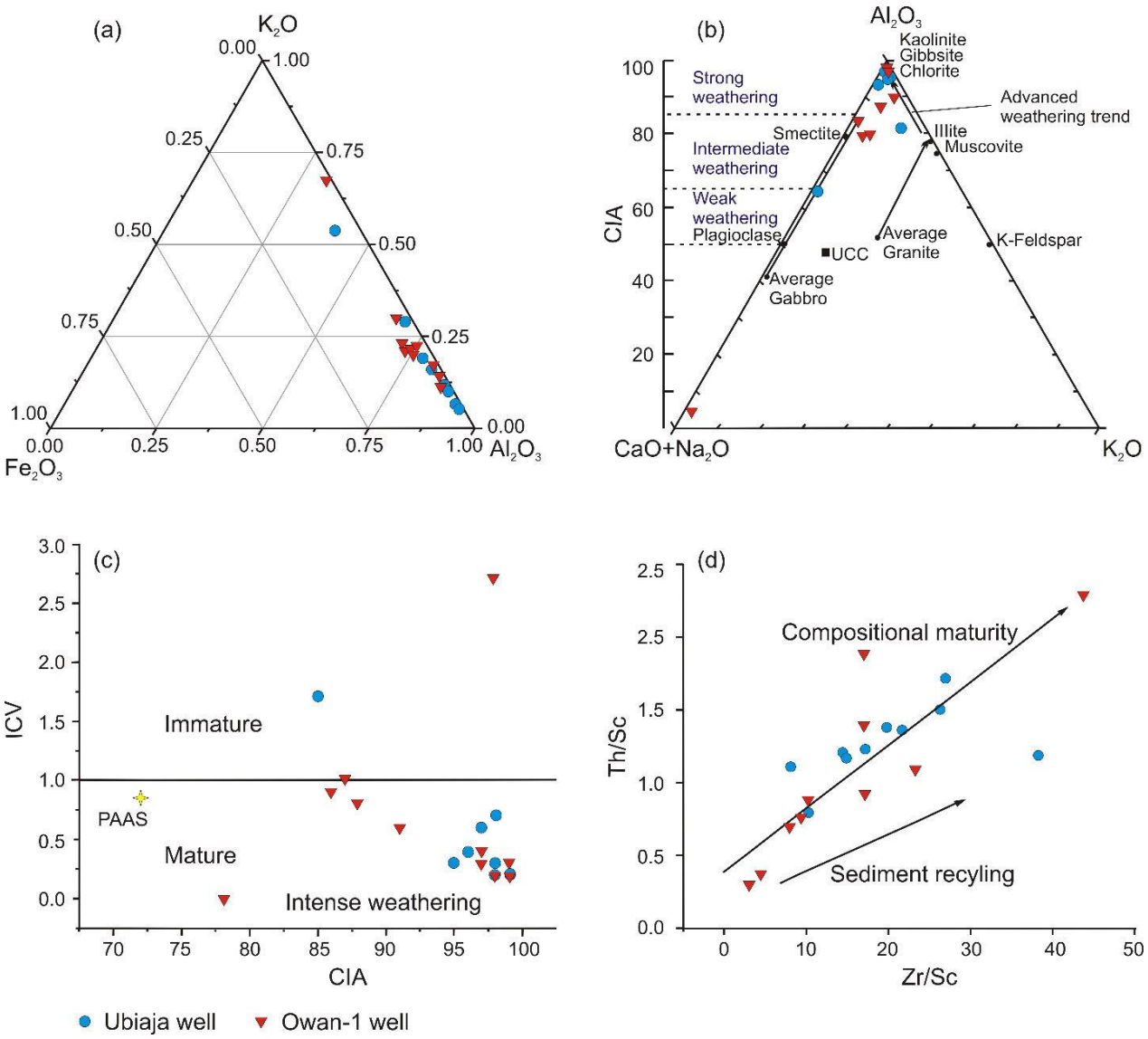

Figure 4.7. (a) Compositional domain of Fe_2O_3 *vs.* K_2O *vs.* Al_2O_3 indicating the distribution of major element oxides in the Nkporo, Mamu and Imo Formations (after Overare et al., 2020). (b) The A–CN–K (A=Al_2O_3; CN=(CaO* +Na_2O); K=K_2O) diagram depicts the chemical weathering pattern and sediment recycling (after Xu et al., 2011). (c) The ICV *vs.* CIA plot shows the maturity and severity of chemical weathering (Long et al., 2012). (d) The Th/Sc *vs.* Zr/Sc plot suggests intense sediment recycling and chemically matured rocks (Long et al., 2012).

4.4. Discussion

4.4.1. Paleoclimate and paleoenvironment

The geochemistry and mineralogy of clastic sedimentary deposits are strongly influenced by the existence and degree of chemical weathering (Liu et al., 2009; Krzeszowska, 2019; Bokanda et al., 2021), and a variety of different weathering indicators can be used to assess the degree of sedimentary rock weathering (Parker, 1970; Nesbitt and Young, 1982, 1984; Harnois, 1988; Fedo et al., 1995). Apart from a simple statement on the weathering conditions, these weathering indicators can also be used as parameters to understand the climatic conditions during deposition. Low degrees of weathering are usually considered to correspond to arid or cool and dry climatic conditions, whereas high degrees of weathering are generally interpreted as related to humid temperate to tropical conditions (Visser and Young, 1990; Chen et al., 2021b). All three weathering indicators that have been used for this study (CIA, PIA, CIW) are relatively high (higher than UCC and PASS) and are therefore an indication of high degrees of weathering as they can be found in humid tropical environments (Chen et al., 2021b). The high degree of weathering is also supported by the abundance of clay minerals such as kaolinite, smectite, and palygorskite (Liu et al., 2009). An exception is formed by sample OW10 with a CIA value of 78, which rather indicates a moderate degree of chemical weathering.

To support the evidence from these conventional parameters, a variety of other geochemical indicators of climate changes are applied to understand the Late Cretaceous-Paleogene paleoclimate of the Anambra Basin. Previous research has shown that paleoclimatic conditions at the time of deposition can be deduced from the relative concentration and distribution of trace elements in mudrocks (Hu et al., 2017; Zhang et al., 2020; Wei et al., 2021).

The Th/U, Rb/Sr and C-values used in this study corroborate with the CIA, PIA and CIW data; thus revealing deposition in a humid tropical environment (Chang et al., 2013; Chen et al., 2021b; Zhang et al., 2021). The Th/U ratios of most analyzed samples are higher than the average upper crustal value (avg. 4.0 and 3.7 for the Ubiaja and Owan-1 rocks, respectively), thus reflecting a high degree of chemical weathering in a humid tropical paleoclimate. Similarly, the Rb/Sr proxy and C-Values reveal a warm and humid environment (Figs. 4.1 and 4.3). The C-values are dominantly high, suggesting a warm and humid palaeoclimate. A few *Fm* lithofacies in this study reveal low C-values, i.e. 0.1-0.8 (OW 10 and 11) and from 0.6 - 0.8 (UB 32 and 40), reflecting

semi-humid to arid palaeoclimatic conditions. Based on subsurface data from the Amansiodo-1 well, Ejeh (2021) revealed a warm, humid, and hot arid paleoclimate in the basin's eastern segment. The Cretaceous period is known to have experienced extreme temperature conditions (Hay and Floegel, 2012). From the Early to Late Cretaceous, global temperature records show sustained high temperatures, preceded by cooling towards the end of the Cretaceous period (Ladant et al., 2020). Reconstruction of paleo-CO_2 levels in the Cretaceous reveals that CO_2 and temperatures peaked during the Cenomanian-Turonian before declining all across the Cretaceous; paleogeographic shifts and greater CO_2 amounts in the atmosphere were postulated as the main causes of warm Cretaceous temperatures (Ladant et al., 2020). There was abundance of rainfall throughout West Africa in the Cretaceous, which suggests the possibility of intense chemical weathering (Sellwood and Valdes, 2006). Data from Bolarinwa et al. (2019) recorded δ^2H (- 50.80 and - 66.40‰) and $\delta^{18}O$ (15.40 and 21.20‰) values that reveal high temperature conditions typical of warm tropical climates (25–40°C) for the Cretaceous Formations in the Benue Trough of Nigeria. Our present study corroborates the δ^2H and $\delta^{18}O$ values from the Maastrichtian deposits in the Lower Benue Trough with similar depositional conditions of the Anambra Basin, which formed under significantly warmer climatic conditions than the present (Bolarinwa et al., 2019; Edegbai et al., 2019b). Additionally, Chumakov et al. (1995) interpreted the Maastrichtian paleoclimate of West Africa to be predominantly warm and tropical, which supports our interpretations. According to recent calculations, tropical temperatures during the Cretaceous period ranged from 22-34°C (Scotese et al., 2021), with the highest temperatures recorded in the Cenomanian-Turonian period (~34°C).

The paleoenvironmental interpretation of the identified lithofacies as described in section 3.1 is given in Figs. 4.1 and 4.3. The fine particle size of the *Fm 1* lithofacies and the parallel lamination reflect deposition in a relatively quiet depositional setting with a low sedimentation rate. In our study, carbonaceous and non-carbonaceous mudrocks dominate this facies. The shales were transported and deposited in a low-to high-energy hydrodynamic setting, most probably in a deltaic and marginal marine depositional setting with incessant energy variations. According to Miall (2006), the described sediments reflect deposition in delta plain settings, comprising non-marine to brackish environments and in estuaries and tidal flats to interdistributary bays (Miall, 2006). This subfacies is therefore interpreted as marginal marine facies (Miall, 1977; Beukes, 1987; Dim et al., 2019).

Similar to the subfacies described before, the non-laminated mudstone facies (*Fm 2*) was deposited under low to medium transport energy conditions, either in a coastal swamp environment or a relatively distal marginal marine environment (Miall, 1988).

The *Fl* facies, characterized by laminated silt, shale, and very fine-grained sand with wavy lamination, is indicative of a variation in the depositional energy. Similar facies were interpreted as deposits accumulated in a tidal channel marsh to an intertidal environment with variation in depositional energy, resulting in the typical grain size variation (Walker and Cant, 1984; Onuigbo et al., 2012).

The particle distribution of the *Fsm* lithofacies suggests deposition under low to medium energy hydrodynamic conditions. Similar facies were interpreted to have accumulated either in a delta front setting or an open shelf environment (Miall, 1977, 2006; Dim et al., 2019).

The particle size of the *Sh* lithofacies is suggestive of medium to relatively high transport energy conditions. This lithofacies unit is therefore interpreted as being deposited within a tidal flat to shelf environment (Miall, 1997; Onuigbo et al., 2012).

4.4.2. Geochemical maturity

The analyzed samples from the Ubiaja and Owan-1 wells generally exhibit ICV values <1, suggesting a high influence of sediment recycling and probably long-distance transport under humid conditions (Figs. 4.7b and 4.7c). Only a few exceptions in the Owan-1 well (OW 10 and 29) show higher values than 1 and therefore imply the existence of immature sediments. All the lithofacies in our data show a similar maturity trend. The ICV values reflect the sediment recycling mechanism and paleosedimentary climate variations during deposition. The ICV values generally increase with increasing weathering intensity in a humid climate and can therefore be correlated to the weathering indices discussed in section 5.1 (Figs. 4.1 and 4.3).

The dominance of matured deposits at the western margin of the Anambra Basin suggests high sediment recycling; the provenance of the mudrocks indicates a passive plate tectonic setting (Long et al., 2012; Huang et al., 2020). Overare et al. (2020) recently assessed the Mamu Formation's geochemical maturity at the eastern margin of the Anambra Basin. Their data revealed similar results, thus pointing towards clay-rich, matured sediments in an inactive tectonic plate margin with active sediment recycling. The trace elemental composition of the Th/Sc *vs.* Zr/Sc

plot confirms this hypothesis, indicating a geochemical trend showing compositionally matured mudrocks (Fig. 4.7d).

4.4.3. Paleoproductivity and paleoredox conditions

Paleoproductivity indicates the quantity of organic matter that organisms can generate per unit area and time during the energy cycle (Chen et al., 2021a). Previous studies have shown that low Ba/Al and P/Ti ratios generally indicate low paleoproductivity and significant siliciclastic dilution in an oxic environment (Zhang et al., 2020; Li et al., 2020b).

Within the studied succession intersected by the Owan-1 and Ubiaja wells, the Ba/Al and P/Ti ratios for the Imo, Mamu, and Nkporo Formations are lower than typically laminated mudrocks (Zeng et al., 2015; Li et al., 2020b). The P/Ti values for all the lithofacies are below 0.34, indicating low primary productivity (Figs. 4.1 and 4.3). The Ba/Al ratio in the Ubiaja and Owan-1 rocks shows low values from the base to the top, indicating low paleoproductivity, except for sample UB 34 (Ba/Al value of 86.3), signifying moderate paleoproductivity. A humid climate can increase primary productivity because nutrient limitations in the marine environment are often drawn from the terrestrial environment (Xin et al., 2021a). However, despite providing adequate biological nutrition, influx can also dilute organic matter (Chen et al., 2021a). Nevertheless, our data show a low primary paleoproductivity for the studied sections, which is possibly due to a high detrital flux together with a turbulent water body and shallow water depth with a high energy, oxidizing environment that is unfavorable to high paleoproductivity (Yan et al., 2018; Zhang et al., 2019a; Wei et al., 2021). In addition, although humid climates with high weathering conditions can increase the nutrient supply in the marine environment, oxic conditions together with high amounts of terrigenous material can dilute the organic matter content in sediments, thus affecting the paleoproductivity during deposition of the mudrocks (Cheng et al., 2021; Chen et al., 2021a; Wei et al., 2021).

Trace elements in sedimentary environments react to redox fluctuations in relatively predictable patterns. Evaluating ambient paleoredox conditions requires a suite of trace elements rather than a single element index. The investigation of paleoredox conditions by the applied indicators of the two studied wells revealed comparable results: the lower Campanian Nkporo Formation, the Maastrichtian Mamu Formation, and the Paleocene Imo Formation reveal oxic environmental conditions (Figs. 4.2 and 4.4). The V/Cr values in the Campanian, Maastrichtian and Paleocene

lithofacies in the Ubiaja well increase gradually from the base to the top, with all the lithofacies showing low values, i.e. <2.0. The Maastrichtian Mamu and the Paleocene Imo units in the Owan-1 well record higher V/Cr values relative to the Ubiaja well. Similarly, the U/Th ratios for the Campanian Nkporo, the Maastrichtian Mamu and the Paleocene Imo Formations in the Ubiaja well record low values, i.e. on average 0.25, 0.27 and 0.25, respectively. Furthermore, the Ni/Co ratios in this study record low values, i.e. <1.0. Ejeh (2021) data revealed similar values from the Amansiodo-1 well. The V/Cr, U/Th and Ni/Co ratios consistently reveal strong oxic depositional conditions during the Late Cretaceous-Paleocene sedimentation period in the studied well sections except sample OW 30 (U/Th value of 0.79), signifying a dysoxic setting. However, the V/(V + Ni) ratios show prevailing lower oxygen concentrations (Hatch and Leventhal, 1992). The majority of lithofacies show V/(V + Ni) ratios above the threshold limit, i.e. V/(V+Ni) >0.6, except sample UB 09 (V/(V + Ni) ratio of 0.49), thus indicating dysoxic/anoxic conditions, which suggests that the water column was not entirely under oxic conditions throughout the formation of the Imo, Mamu and Nkporo Formations. The discrepancy between the V/(V+Ni) and other indicators can also be attributed to processes other than redox conditions, such as sediment recycling, sedimentation rates, depositional and subsequent diagenetic processes, all of which can affect the metal concentration (Wang et al., 2017b; Han et al., 2020). Therefore, paleoredox indicators should be applied with care when determining the redox conditions.

Low authigenic U enrichment suggests that the studied mudrocks were mostly deposited in oxic or suboxic environments (Tribovillard et al., 2006). The sedimentary facies of the Owan-1 and Ubiaja samples show enrichment in U and V, indicating euxinic depositional conditions in the water column (Fig. 4.6a) (Tribovillard et al., 2006). V and Cr concentrations are often depleted to UCC values, implying overall oxic bottom water conditions (Fig. 4.6a) (Kloss et al., 2015). Overare et al. (2020) postulated similar conditions at the eastern margin of the Anambra Basin. In a recent study, Ejeh (2021) reported an oxic paleo-redox environment for the Late Cretaceous Formations from the Amansiodo-1 well in the central-eastern segment of the Anambra Basin. The paleosedimentary redox proxies that were applied in this study show a similar trend and pattern in both wells. The paleoredox conditions determined from V/Cr, U/Th, and Ni/Co ratios show a good agreement. The paleoenvironmental conditions in the Imo, Mamu and Nkporo Formations are reconstructed as primarily oxic with minor dysoxic conditions, based on paleoredox index values.

In addition, the Cu/Zn ratio is used to further define the depositional environment. High Cu/Zn ratios in a sedimentary environment reflect reducing depositional conditions, whereas low Cu/Zn values indicate oxidizing depositional conditions (Hallberg, 1976). Consequently, the low Cu/Zn ratios recorded for the Ubiaja (averaging 0.38) and Owan-1 mudrocks (averaging 0.11) indicate that the different lithofacies of the three studied formations were all accumulated in an oxidizing depositional environment. Our data compare favorably with previous works in the Anambra Basin and thus support the interpretation of dominantly oxic conditions (Gebhardt, 1998; Adebayo et al., 2015; Edegbai et al., 2020; Overare et al., 2020; Ejeh, 2021).

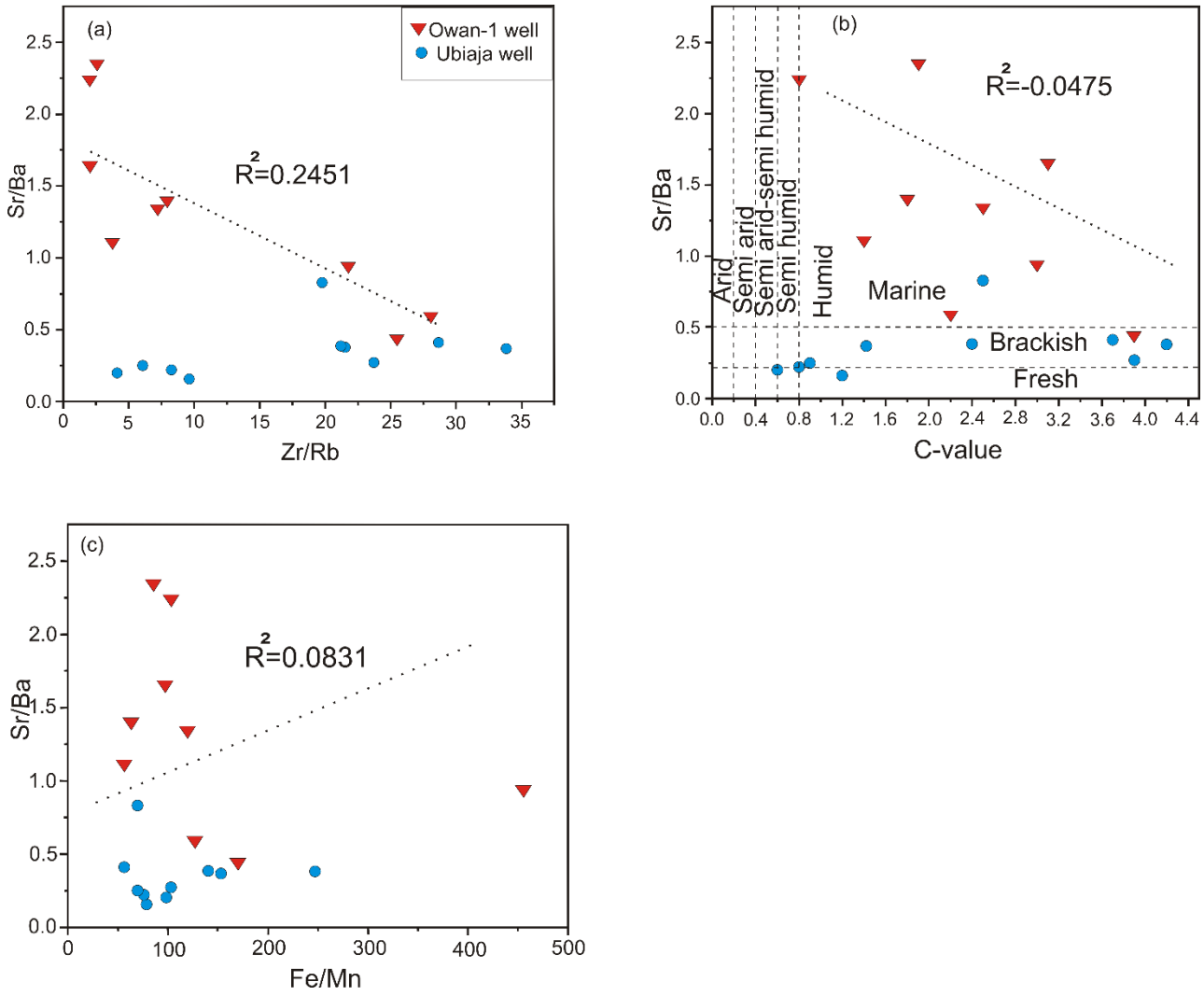

Figure. 4.8. Analysis of paleosalinity conditions, paleohydrodynamics and paleowater depth. a) A cross plot of Sr/Ba ratios vs the hydrodynamic proxy (Zr/Rb), b) cross plot of Sr/Ba vs C-value, c) paleosalinity vs paleowater depth graph

4.4.4. Paleohydrodynamics and paleowater depth/paleosalinity

Paleohydrodynamics describes the energy conditions of the water mass during the deposition of ancient sedimentary rocks in the aquatic environment (Pehlivanli, 2019). In this study, I utilized the Zr/Rb ratio to detect the paleohydrodynamic conditions during the deposition of Late Cretaceous-Paleocene Formations in the Anambra Basin (Figs. 4.2 and 4.4). The Zr/Rb ratio in the lower depth interval of the Ubiaja well, representing the Nkporo Formation, recorded lower values than the Mamu Formation. The Maastrichtian Mamu Formation in the Owan-1 well shows lower paleohydrodynamic values compared to the Ubiaja well, indicating a strong hydrodynamic regime for the basal units and a gradual transition to intermediate hydroenergy at the top, as shown from the Zr/Rb values (Li et al., 2018b). As a result, the data show a predominantly strong hydrodynamic regime and shallow sedimentary water circulation during the Mamu and Imo Formations' deposition. A cross plot of Sr/Ba ratios vs the hydrodynamic proxy (Zr/Rb) (Fig 4. 8a) shows a very weak and a negative correlation between paleosalinity and hydrodynamics, suggesting that there is no direct relationship between paleosalinity and paleohydrodynamics in the studied sections.

Overall, the Fe/Mn ratios show relatively high values in the Campanian Nkporo Formation in the Ubiaja well. The Maastrichtian Mamu Formation shows slightly higher values than the Nkporo and Imo Formations. The Mamu Formation in the Owan-1 well shows similar values. The Imo Formation reveals similar values except OW 10, which records a Fe/Mn ratio of 6, thus indicating a deep paleowater. Throughout the succession, the seawater became gradually shallower (Fig. 4.4), which is consistent with other data (Ubiaja well) from the Maastrichtian. The high Fe/Mn ratios recorded in this study suggest a prevailing shallow paleowater depth during the deposition of the Imo, Mamu, and Nkporo Formations. Edegbai et al. (2020) made similar estimates of paleowater depth in the Maastrichtian. The authors inferred shallow water depths for the Trans-Saharan Seaway in the Cretaceous during the deposition of the Mamu Formation in the Anambra Basin from palynofacies data, which is consistent with our present study. The paleowater depth corroborates the hydrodynamic influence detected in this study, indicating intense hydrodynamic pressure in a shallow water circulation.

Paleosalinity is an important indicator that is used to reflect the sedimentary environment of the water column in the geologic history (Cheng et al., 2021). In the Owan-1 and Ubiaja mudrocks, the Sr/Ba ratios fluctuate from the Campano-Maastrichtian to the Paleocene (Figs. 4.1 and 4.3).

The results show that the Campanian Nkporo Formation (average Sr/Ba values of 0.19) was formed in a brackish to freshwater environment. The *Fm* lithofacies in the Ubiaja well record the highest paleosalinity values. Upwards through the stratigraphy, the values gradually increase, thus depicting the transition from freshwater to brackish, then to marine, and finally back to brackish conditions, which can be seen as a shift towards deltaic deposition. The Mamu and Imo Formations in the Ubiaja well show relatively constant paleosalinity values throughout the Maastrichtian-Paleocene with average values of 0.32 and 0.5, indicating ongoing sedimentation in a brackish water environment.

In the Owan-1 well, the Mamu and Imo Formations generally exhibits higher Sr/Ba values than the Nkporo, Mamu and Imo Formations in the Ubiaja well (average of 4.71). The paleosalinity at the base of the Owan-1 well is low and gradually increases towards the top, as shown by the Sr/Ba values (Fig. 4.3), suggesting a lower sea level and more negligible seawater effect during sedimentation of the basal units. The Imo Formation formed in a marginal shallow-marine environment. The Mamu Formation was deposited in a proximal shallow-marine environment. Our data indicate comparatively high levels of salinities in the studied well sections. The Campanian Nkporo Formation formed in a brackish to freshwater environment, the Mamu Formation was deposited in a brackish to shallow-marine environment, and the Imo Formation formed in a marginal marine environment (Figs. 4.1 and 4.3), thus supporting the hypothesis that the Anambra Basin was formed in a deltaic setting (Nwajide and Reijers, 1996; Reijers et al., 1997; Odunze et al., 2013; Uzoegbu et al., 2013; Abubakar, 2014).

Water salinity is usually influenced by the environment. Hot and arid climates commonly have high evaporation rates, resulting in high salinity, whereas warm and humid climates have lower evaporation rates, resulting in lower salinity (Wei et al., 2021). I performed a cross plot of Sr/Ba *vs* C-value (Fig. 4.8b) and found no consistent salinity trend in the dataset of the Owan-1 and Ubiaja wells, indicating that the paleoclimate did not play a significant role in the marginal basin's salinity fluctuation. In addition, I observed a very weak correlation between paleosalinity and paleowater depth, suggesting that there is no direct relationship between salinity and water depth in the studied sections (Fig. 4.8c).

4.4.5. Paleoenvironmental implications

A critical part of the study was to understand the paleoenvironment of the Anambra Basin and the relationship with the Benue Trough development, the Western and Central African Rifts (WCARS) and the South Atlantic during the Cretaceous. The WCARS are related to extensive fracture structures that extend from Nigeria's Benue Trough, the Niger Graben Basin, and the grabens of Chad and Sudan. The Anambra Basin and Benue Trough are related structures that are part of the WCARS (Abubakar, 2014). The formation of the WCARS is strongly connected to the opening of the South Atlantic Ocean in the Early Cretaceous (130-119 Ma), with rifting spreading far into Africa through the Benue Trough (Fairhead, 1988). The Niger, Chad, Sudan and Nigeria WCARS basins are extensive and consist of Cretaceous marine siliciclastic sediments with minor volcanic rocks. The sedimentation period of the Cretaceous Mamu and Nkporo Formations in the Anambra Basin was less affected by biochemical deposition, as reflected by the high Fe_2O_3+Al_2O_3 values relative to the CaO+MgO contents, which supports the influx of terrigenous clastics into the Anambra Basin (Wei et al., 2021). During the Maastrichtian, the Trans-Saharan Seaway was re-established for the second time, and the connection line propagated westward over the Bida Basin, which connects the Anambra Basin and extends to the Atlantic Ocean (Edegbai et al., 2019a). The geochemistry of the Bida Basin and Benue Trough is similar to the results of this study and less affected by biochemical deposition, supporting our data. This study infers paleoclimate conditions from lithofacies revealing dominantly humid tropical environments except for a few *Fm* lithofacies that correspond to semi-humid-arid environments. For the Mamu and Nkporo Formations, it can be observed that the persistent humid tropical conditions matched the Campanian-Maastrichtian general climatic trend (Chumakov et al., 1995; Sellwood and Valdes, 2006; Hay and Floegel, 2012). The paleoclimate reconstructions of this study are similar to other WCARS basins. Palynological investigations of the Bida Basin revealed palm pollen as well as spores of *Acrostichum aureum* and pteridophytes, indicating a humid tropical climate, with predicted paleo- vegetation ranging from savanna to rainforest (Ojo and Akande, 2008; Onoduku et al., 2017). The Sekuliye shales in the Benue Trough also indicate deposition in a humid setting, in a brackish to shallow-marine environment with oxic conditions (Abubakar et al., 2021). The Aradeiba Formation in the Muglad Rift Basin (Sudan) formed under warm humid tropical environments where high precipitation occurred during the Early Cretaceous (Leyuan et al., 2021). Warm-humid tropical climate was also dominant in the Termit Basin (Niger-Chad region) in the Late Cretaceous during the sedimentation

of the Yogou Formation, as inferred from high ω(MgO)/ω(CaO) fractions, high CIA, and low Sr/Cu values (Lai et al., 2018). In addition, the Bongor Basin in Chad shows both warm, humid and hot arid paleoclimates as inferred from trace element geochemistry. The palynoflora similarly points to arid climatic conditions (Tan et al., 2017). Intense weathering and geochemically matured sediments are prevalent in the Anambra Basin, as inferred from elemental chemistry proxies (Ejeh, 2021). This is consistent with data presented by Sellwood and Valdes (2006) that reveal high amounts of rainfall during the Cretaceous period in West Africa. Abundant rainfall in a tropical environment favors chemical weathering of rocks, sediment recycling and thus reflects geochemical matured sediments (Cox et al., 1995). The lithofacies show deposition in a shallow-water environment with strong hydrodynamic conditions. The depth of the Trans-Saharan Seaway in the Cretaceous was determined to be shallow by Edegbai et al. (2020). The Trans-Saharan Seaway was a key supplier of sediments for the Anambra Basin. According to Ojo et al. (2021), the Maastrichtian Sea of the Bida Basin was shallow, short-term and disrupted by periodic river runoffs. This is consistent with our findings, which suggest that shallow water depths with considerable hydrodynamic effect existed in the Anambra Basin throughout the Campanian-Maastrichtian. The lithofacies show moderate to high paleosalinity, indicating that deposition took place in a brackish to shallow-marine environment. The primary reason for this environment is that the Mamu and Nkporo Formations were deposited due to the re-establishment of the Trans-Saharan Seaway and its link with the Tethys and the Atlantic Ocean during the Campanian-Maastrichtian (Edegbai et al., 2020). The geochemical proxies used to interpret the paleoproductivity all point to low primary productivity (P/Ti< 0.34), which can be linked to a strong hydrodynamic regime, shallow water depth, and input of terrestrial detritus, which negatively affected blooms of planktonic organisms (diatoms etc.), resulting in a decrease in primary productivity.

The mostly oxic conditions detected in this study reflect shallow-water environments in the Anambra Basin, where high oxygen levels persisted during deposition. Furthermore, the basin experienced slow sedimentation and intense sediment recycling during the deposition of the Mamu and Nkporo Formations. The variation in paleosalinity and depositional redox conditions might be linked to paleogeographic locations where detrital influx varies, resulting in variable redox hydrodynamic and water conditions (Edegbai and Schwark, 2020).

The Anambra Basin and the other WCARS basins share similarities in paleoweathering, paleoclimate, paleowater depth, paleosalinity, and paleoredox conditions despite differences in sediment provenance, paleogeographic locations, and the exposure of some WCARS basins to thermal fracture and crustal upheaval. Depositional settings varied during the Formation and sedimentation of these basins and are significantly more important than later alterations since there are only minor changes in the inorganic geochemical fingerprints of these WCARS basins.

4.5. Conclusions

Major oxides, trace elements, REE, mineralogy, and lithofacies data have been used to investigate paleoclimate, paleosalinity, as well as paleohydrodynamic and paleoenvironmental conditions of the hydrocarbon prospective Campano-Maastrichtian and Paleocene Formations of the southwestern Anambra Basin. The dominance of kaolinite and quartz minerals together with weathering and paleoclimate proxies, such as CIA, PIA, CIW, ICV, Th/U, Rb/Sr, and C-value, indicate that the Late Cretaceous-Paleogene Nkporo, Mamu, and Imo Formations were subjected to intense weathering throughout the Maastrichtian-Paleocene in a warm, humid, and tropical climate with only short-term semi-humid and semi-arid conditions in the Late Cretaceous. Compared to other WCARS basins, geochemical data from the Anambra Basin indicates that the basins dominantly formed under humid tropical climatic conditions.

The Sr/Ba, Ba/Al, and P/Ti ratios indicate that the Nkporo and Mamu mudrocks of the Anambra Basin were deposited under brackish to saline environments, and with low primary productivity due to the influx of terrestrial clastic materials and strong hydrodynamic conditions.

Despite the presence of dark grey carbonaceous *Fm* lithofacies, geochemical proxies indicate that anoxic conditions only occurred sporadically. This could have had an effect on organic matter accumulation in the studied succession, lowering the hydrocarbon potential at the basin's southwestern margin. Wavy laminations are found in *FI* lithofacies, indicating retreating seawater and significantly high hydrodynamic environments. Ultimately, the Imo, Mamu, and Nkporo Formations of the southwestern Anambra Basin represent deposits of a shallow Campano-Maastrichtian seaway, comparable with the Maastrichtian Patti Formation of the adjacent Bida Basin in the north.

Chapter Five

Organic geochemistry, palynofacies, maceral analysis, and petroleum potential of Campanian-Paleocene deposits of the western Anambra Basin (Nigeria)

5.1. Introduction

Insight into the organic matter constituents, their sources, and the thermal stress of a sedimentary basin fill is essential for the exploration and exploitation of hydrocarbons on a global scale (Lai et al., 2018; Cappuccio et al., 2021; Chen et al., 2021a; Li et al., 2021a; Wei et al., 2021). A hydrocarbon source bed can be described as a rock unit that contains adequate organic matter constituents which, under a specific thermal stress regime, can produce petroleum through the chemical breakdown of kerogen (Alalade and Tyson, 2010; Cappuccio et al., 2021). Organic matter composition is regarded as an essential control parameter in the ability of source rocks to produce and expel petroleum (Li et al., 2020a). The quantification of source rocks relies on elements such as volume, organic richness, and thermal maturity (Cappuccio et al., 2021; Mohammed et al., 2020). Petrographic data (macerals), palynofacies analysis (kerogen), and geochemical (i.e. TOC, Rock-Eval pyrolysis) interpretations have all been successfully used to provide accurate information on source rocks (Adeyilola et al., 2022; Alalade and Tyson, 2010; Chen et al., 2021a; Li et al., 2021a; Ma et al., 2022; Mohammed et al., 2020; Singh et al., 2017). In particular, organic-rich mudrocks have received much attention for many decades since they serve as the main source of conventional petroleum resources and unconventional shale oil/gas reservoirs in hydrocarbon systems (Adeyilola et al., 2022; Lai et al., 2018; Li et al., 2020a; Ma et al., 2022; Ndip et al., 2019; Williams et al., 2022). Additionally, these organic-rich rocks provide evidence of the interaction that links depositional environments and the biosphere recorded in the ancient sediments (Adeyilola et al., 2022; Cheng et al., 2021; Williams et al., 2022; Zhang et al., 2018).

The Nigerian Anambra Basin constitutes an inland basin, which is part of the greater Cretaceous-Paleogene West and Central African Rift System (WCARS) (Fig. 2.1; Obaje et al., 2004; Abubakar, 2014), and it is one of Nigeria's least-studied sedimentary basins (Anakwuba et al., 2018). The basin is considered next to the Niger Delta Basin in terms of hydrocarbon prospects,

and it serves as a structural link between the Benue Trough in the north and the Paleogene Niger Delta Basin in the south that accommodates a large portion of Nigeria's oil and gas deposits (Anakwuba et al., 2018). Currently, Nigeria is estimated to contain 34 billion barrels (Gbbl) of oil and 4 trillion cubic meters (m^3) of gas in its reserves (Obaje et al., 2004; Anakwuba et al., 2018), which originates primarily from the Niger Delta Basin. Oil and gas account for about 90% of Nigeria's foreign returns and has maintained significant structural support for the country's economy since its discovery and exploration of its commercial value from the 1950s to present (Anakwuba et al., 2018; Frynas, 1998; Monday and Salihu, 2017; Uwakonye et al., 2011). Internationally, hydrocarbon resources are expected to account for 56% of all energy consumption worldwide in 2030, dominating other energy resources i.e. renewable energy (Abubakar, 2014). Previous geochemical, seismic and sequence stratigraphic studies on the Anambra Basin have revealed potential source beds, reservoir units, cap and seal rocks, and an existing trapping framework (Adebayo et al., 2018; Akaegbobi et al., 2000; Anakwuba and Onyekwelu, 2010; Babatunde, 2010; Dim et al., 2020, 2019; Ejeh, 2021; Ekine and Onuoha, 2010; Obaje et al., 2004; Okwara et al., 2020), with the majority of these projects focusing on the eastern margin of the basin where complete outcrop sections are available. In contrast, so far, the western segment of the basin has received relatively little attention (Edegbai et al., 2019; Ogungbesan and Adedosu, 2020; Omietimi et al., 2021). Previous work classified the Anambra Basin as having mainly gas prone hydrocarbon potential. Ene et al. (2019) revealed that twenty-seven exploratory (wildcat) and two appraisal wells had been drilled in the basin, yielding three oil and gas discoveries and an estimated reserve of one billion barrels of oil and ca. 8.49 billion standard cubic meters (m^3) of gas (Dublin Green and Agha, 1999; Okagbue 2004). Recent work by Anyiam et al. (2015) suggested the eastern and central margins of the Anambra Basin as possibly the most prospective hydrocarbon exploration zone from a 'common risk segment' technique to play fairway analyses. Subsurface studies on the Nkporo and Mamu Formations from the Akukwa-2 well in central-eastern Anambra revealed fair to good hydrocarbon generation potential with TOC ranging from 0.27 to 3.02 wt. %, and with the prevalence of type III and III-II kerogen constituents that characterize thermally immature to early mature source beds (Adebayo et al., 2018). Edegbai et al. (2020) studied outcrop sections to access the organic matter composition that dominated during the sedimentation of the Mamu Formation in the western portion of the basin. Their data revealed terrestrial to mixed terrestrial-marine organic facies deposited under prevailing oxic depositional conditions. Omietimi et al. (2022)

came to similar conclusions through their studies on the Late Cretaceous-Paleocene Imo, Mamu and Nkporo Formations at the western margin of the basin. Their studies on lithofacies and sedimentary geochemistry showed that the formations formed in brackish to shallow-marine settings under primarily oxic conditions. Based on outcrop studies, Ogungbesan and Adedosu (2020) classified the organic matter content of the Mamu Formation on the western margin of the Anambra Basin. The mudrocks are derived from mixed terrestrial and marine organic material, suggesting dominantly type III kerogen with minor type II-III kerogen deposited in a deltaic to shallow-marine environment (Ogungbesan and Adedosu, 2020). Furthermore, the organic matter content in the studied formation revealed early thermal maturity. However, sedimentary organic matter (palynofacies and maceral data) and organic geochemistry (TOC and Rock-Eval) interpretations of the Campano-Maastrichtian to Paleocene deposits from subsurface data-based investigations from the Owan-1 and Ubiaja wells in the western segment of the basin are less documented and are reported here for the first time.

In this study, palynofacies, maceral and Rock-eval analyses have been performed for the deposits intersected by the Owan-1 and Ubiaja wells (Figs. 2.1-2.2, 5.1-5.5), consisting of the Nkporo, Mamu and Imo Formations of the southwestern segment of the Anambra Basin. The results of this contribution provide new insights into the paleoenvironment and sea-level changes from the Campanian to the Paleocene as well as important new information on the hydrocarbon potential of the Anambra Basin.

5.2. Materials and methods

Ditch cutting/core samples from two wells (Owan-1 and Ubiaja) in the western segment of the Anambra Basin, i.e., samples from the Cretaceous Mamu and Nkporo Formations, and the Paleocene Imo Formation are analysed. The investigated samples range in depth from 59.7 to 547.4 m and 22.9 to 647.7 m for the Owan-1 and Ubiaja wells, respectively (Figs. 5.1 and 5.5).

5.2.1. Palynofacies analysis

Palynofacies analysis was performed on 31 shale-mudrock samples from the Maastrichtian Mamu and Paleocene Imo Formations of the Owan-1 well. Preparation of the samples was carried out according to standard palynological preparation procedures, including washing the mudrocks and treating them with hydrochloric acid (HCl, 30%) and hydrofluoric acid (HF, 41%) to remove their carbonates and silicates. A nylon mesh size of 15 μm was used to sieve the residue and mounted with glycerine jelly. Slides were prepared and examined at various magnifications with a Leica

DM2500 transmitted light microscope. Using Tyson's (1993) classification, sedimentary organic matter was subdivided into three palynofacies groups: phytoclasts, palynomorphs, and amorphous organic matter (AOM). A minimum number of 300 particles is counted for each sample to determine the relative percentages of these components. Palynofacies data are plotted in the APP ternary diagram (Tyson, 1989; 1993; 1995) to determine the depositional environment, transgressive/regressive trends, and kerogen type.

5.2.2. Maceral analysis

Organic petrographic analysis was done on a total of 16 shale samples to determine the maceral composition and observable mineral matter following the ASTM (2014) and SANS 7404–3 (2016)/ ISO 7404-3 (2009) standards by using a Zeiss AxioImager m2M reflected light microscope. A total of 1000 counts were performed, including on mineral matter. The results were reported as a percentage by volume (vol. %). The organic petrography was done at the South African Bureau of Standards (SABS), CSIR Campus, Pretoria, South Africa.

5.2.3. Total organic carbon

The value of total organic carbon (TOC) is a measure of the amount of total organic carbon in a rock expressed as weight percent (wt. %). TOC analysis was done using a High-Frequency Infrared Absorption Carbon-Sulfur Analyzer (CS-902G; Beijing Wanliandaxinke Ltd., China) instrument. Forty mudrock samples from the Owan-1 and Ubiaja wells were selected for the analysis (Appendix 3). The analysis was performed at the Key Laboratory of Petroleum Resources Research, Northwest Institute of Eco-Environment and Resources, Chinese Academy of Sciences, Lanzhou, China.

2g of each sample was decarbonated with concentrated hydrochloric acid (HCl) to remove carbonates. This was done by treating the samples with concentrated HCl for a minimum of two hours. The samples were then rinsed and flushed through a filtration apparatus to remove the acid. The filter was then removed, placed into a LECO crucible, and dried in a low-temperature oven (110°C) for a minimum of 4 hours. This was completed by the combustion of these standards by heating them to 1200°C in the presence of oxygen. Both carbon monoxide and carbon dioxide were generated, and the carbon monoxide was converted to carbon dioxide by a catalyst. The carbon dioxide was measured by an IR cell. The combustion of unknowns was then completed,

and the response of unknowns per mass unit was compared to that of the calibration standard; thereby, the TOC was determined. A good source rock commonly contains a TOC range between 1-2% (Peters and Cassa, 1994). Shales and carbonates containing minimum values of 0.5% and 0.3% TOC, respectively, are considered as potential source rocks (Espitalie et al., 1977; Tissot and Welte, 1984).

5.2.4. Rock-Eval pyrolysis

Rock-Eval pyrolysis was carried out on 16 samples arising from TOC sufficiency to ascertain the kerogen types, source of organic matter (OM), and maturation of the organic matter. The Rock-Eval parameters S1, S2, S3, and Tmax were analyzed using a Rock-EVAL6 (Vinci Technology) instrument. The Rock-Eval pyrolysis was performed at Daqing Oil Field Co., Ltd., Experimental Center of the Institute of Exploration and Development, China.

The S1, S2 and S3 parameters were ascertained by heating 2g of each pulverized sample at a programmed temperature. The mudrocks were heated for 3 minutes at 300°C. Then the temperatures were further increased to 650°C at a heating rate of 25°C/min. S1 represents the free hydrocarbons that can be extracted at 300°C. S2 shows the remaining hydrocarbon potential produced by cracking of the organic matter during 300-650°C. Tmax is the temperature during which the maximum evolution of S2 hydrocarbons occurs. S3 is the organic carbon dioxide yield during pyrolysis. The Rock-Eval parameters were used to calculate the Hydrogen Index (HI = S2/TOC x 100), Oxygen Index (OI = S3/TOC x 100), Production Index (PI = S1/S1+S2), and the Hydrocarbon Type Index (HC type index = S2/S3), and oil saturation index OSI (S1/TOC x100).

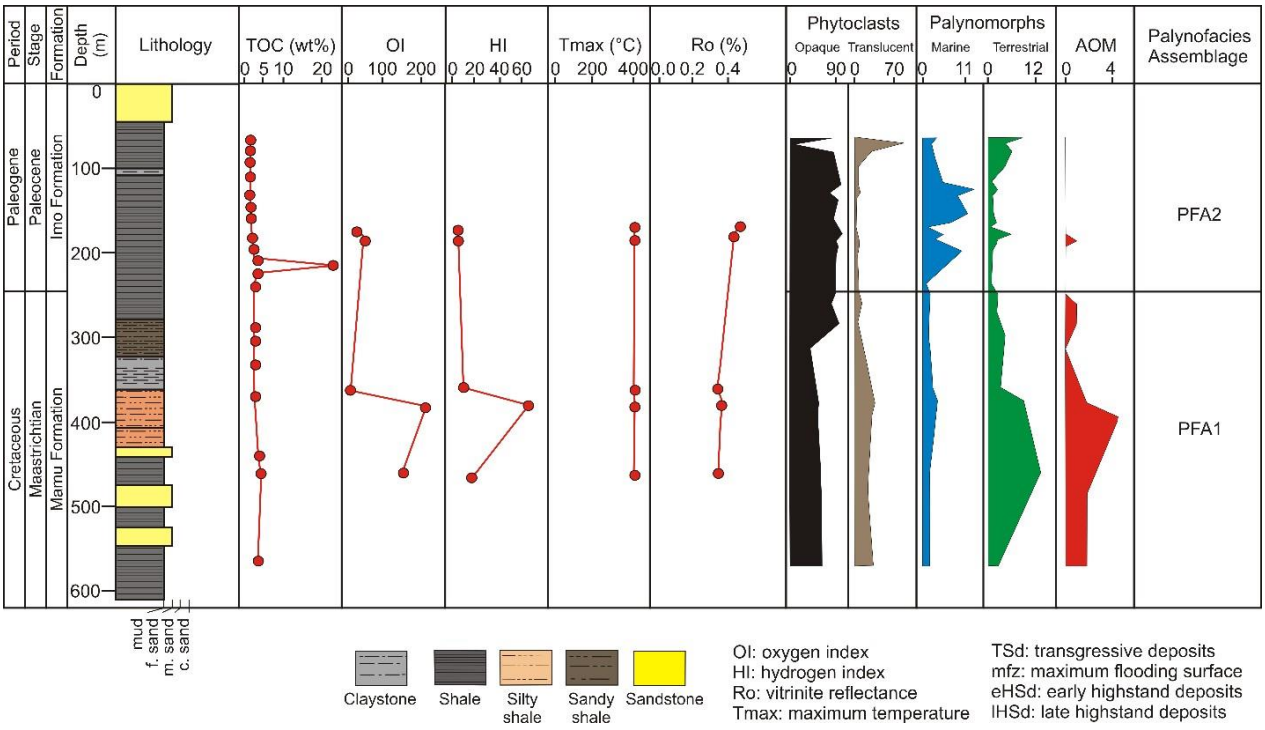

Figure 5.1. TOC, Rock-Eval parameters and palynofacies distribution in the Owan-1 well.

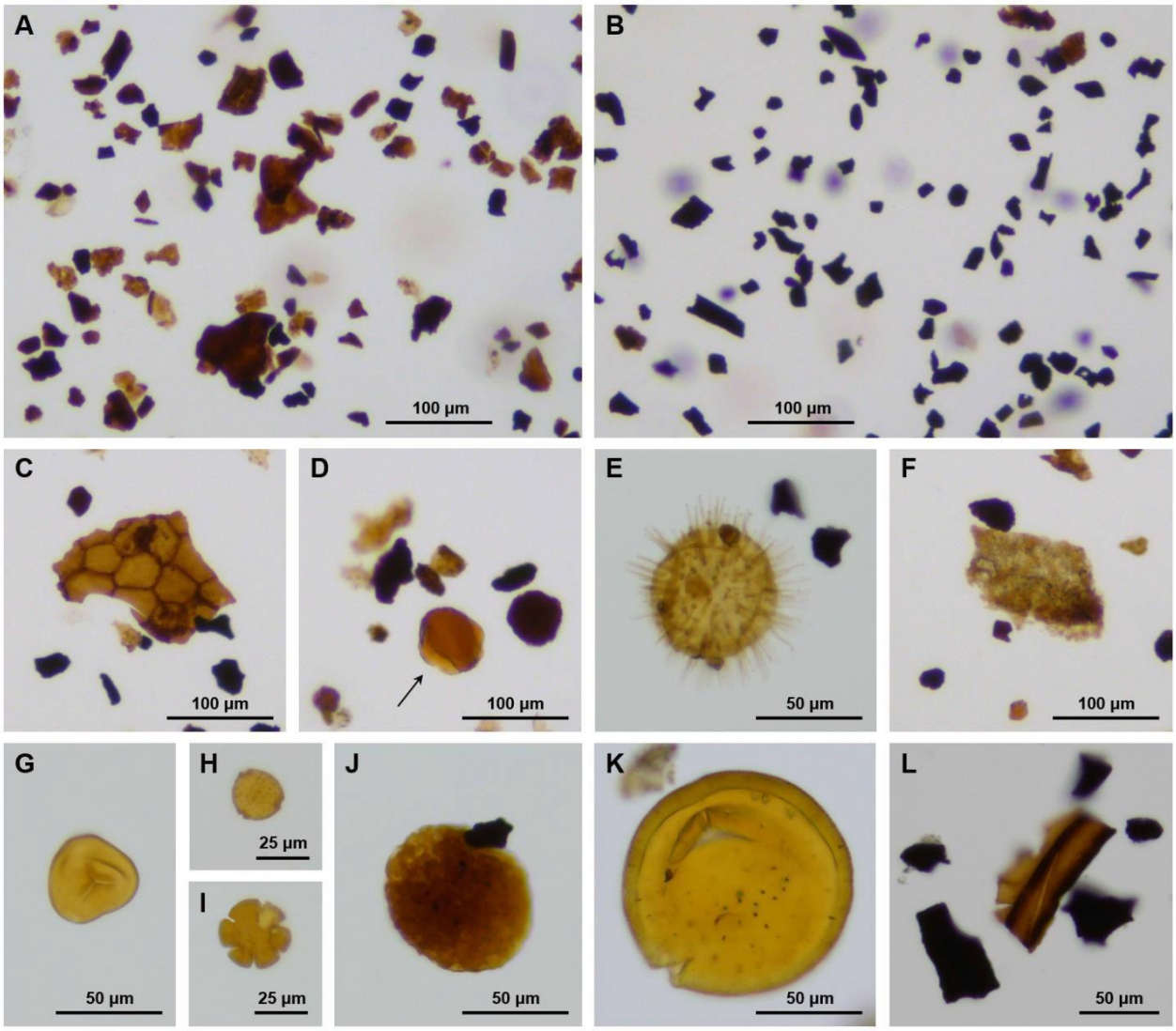

Figure 5.2. Palynofacies of the Mamu and Imo Formations intersected in the Owan-1 well is characterized by the general high amount of terrestrial phytoclasts. A) high amount of equidimensional and blade-shaped, translucent phytoclasts within the early transgressive and late highstand phase (OW9); B) opaque, mainly equidimensional phytoclasts characteristic of the maximum flooding and early highstand phase (OW12); C) well-preserved cuticles characteristic of the early transgressive phase with "fresh" plant debris (OW36); D) resin (highlighted by arrow) pointing to high terrestrial influx and degraded organic matter (DOM) during the early transgressive phase (OW34); E) peak abundance of marine phytoplankton (dinoflagellate cysts) and opaque, equidimensional phytoclasts during maximum flooding (OW15) in the Imo Formation; F) low amount of amorphous organic matter (AOM) in the lower Mamu Formation (OW31); G) trilete fern spores and pollen grains (H-I) documenting high terrestrial influx (OW1,

OW34); J) freshwater algae (*Botryococcus* sp.) pointing to periodic freshwater influx (OW30); K) prasinophytes (*Tasmanites* sp.) indicating fluctuation in salinity (OW36); L) terrestrial phytoclasts of different size and shape revealing a short distance from the source area (OW1).

Table 5.1. Palynofacies data (percentages) of the Owan-1 well, western Anambra Basin.

Well	Sample No	Depth (m)	Phytoclasts	Palynomorphs	AOM	Palynofacies type
Owan-1	OW1	93	87.9	12.1	0	PFA2
	OW9	99	93.5	6.5	0	
	OW11	107	92.3	7.7	0	
	OW12	122	92.0	8.0	0	
	OW14	139	94.8	5.2	0	
	OW15	147	86.4	13.6	0	
	OW16	153	91.4	8.6	0	
	OW18	172	88.9	11.1	0	
	OW19	182	92.5	7.5	0	
	OW20	187	98.5	1.5	0	
	OW22	194	89.4	10.0	0.6	
	OW24	199	95.1	4.9	0	
Owan-1	OW25	210	90.0	10.0	0	PFA1
	OW26	246	98.5	1.5	0	
	OW27	256	95.0	4.0	1.0	
	OW28	275	95.3	4.0	0.7	
	OW29	300	93.9	6.1	0	
	OW30	353	92.7	5.3	2.0	
	OW31	367	84.0	11.7	4.3	
	OW34	443	83.7	14.3	2.0	
	OW36	540	93.6	4.1	2.3	

5.3. Results

5.3.1. Lithology

The Imo, Mamu, and Nkporo Formations are mostly brown and grey to dark grey organic mudrocks containing significant amounts of clay minerals and quartz, as well as varying organic materials. In certain layers, plant remains and trace fossils were observed. In the preceding chapter, the sections of the Owan-1 and Ubiaja wells (Figs. 4.1 and 4.3) were grouped into laminated mudstone (Fm1), non-laminated mudstones (Fm2), laminated sandy siltstone and mudrock (FI), silt and mudstone (Fsm), and sandstone (Sh) units based on mineralogical, sedimentary geochemistry, and lithofacies analyses.

5.3.2. Palynofacies analysis

Phytoclasts, palynomorphs, and amorphous organic matter (AOM) are the three major groups of organic constituents identified within the Owan-1 well (Table 1, Figs. 5.1 and 5.3). In general, the preservation is very good and all samples yielded a rich palynofacies assemblage. In contrast, most of the samples from the Ubiaja well are characterized by a low amount of sedimentary organic matter, yielding AOM and phytoclasts, and only poorly preserved palynomorphs. The sandstones show reworked palynomorphs and a high content of equidimensional phytoclasts.

The Owan-1 well mudrocks are dominated by phytoclasts of different size and shape, and ratio of opaque vs translucent grains (Fig. 5.2). Plant tissues, cuticles and woody fragments make up the translucent phytoclasts (cf., Li et al., 2021a). Opaque phytoclasts derive from oxidised woody material during prolonged transport or post-depositional alteration. Partly, opaque material reflects charcoal, which indicates wildfires (Ma et al., 2022). Opaque phytoclasts represent 7.0 to 92.6% of the palynofacies, translucent particles range from 2.1 to 78.3%. Cuticles and larger plant debris contain up to 8.3% of the palynofacies, with sample OW36 showing the highest amount. The palynomorph group includes terrestrial particles such as pollen grains and spores, and freshwater algae such as *Botryococcus* sp., and marine particles such as dinoflagellate cysts, acritarchs, and prasinophytes. The percentage of pollen grains ranges from 0.62 to 10.92%, with the highest amount occurring in OW34. Spores are rare (up to 1.96%). Within the marine fraction, dinoflagellate cysts range between 0.63 to 10.53%, the maximum occurring in sample OW15. Prasinophytes reach up to 0.57%, while acritarchs present up to 0.62% of the palynofacies. Foraminiferal test linings are also present (up to 0.62%). Amorphous organic matter (AOM) and

degraded organic matter (DOM) represent semi-transparent to structureless kerogen particles derived from bacterial degradation of dinoflagellates and acritarchs (AOM) and biodegradation of higher plant materials (DOM), respectively (Fig. 5.2). The percentage of DOM ranges from 0.9 to 42%, with sample OW29 showing the highest content. The highest AOM value (4.2%) was recorded in sample OW31.

Two palynofacies associations (PFA1 and PFA2) (Figs. 5.1 and 5.3) are distinguished: PFA1 is detected in the Mamu Formation and lower Imo Formation. It is dominated by translucent and opaque phytoclasts. Terrestrial palynomorphs are dominated by pollen grains, showing maximum abundance in sample OW34. Fern spores are rare throughout the succession. *Botryococcus* sp., fungal remains and resin occur in the lower part of the Mamu Formation (samples OW30-OW36). The relative abundance of marine dinoflagellate cysts is increasing throughout in the Mamu Formation, and acritarchs occur only in very low abundances. AOM is characteristic of the lower part of the Mamu Formation, both AOM and DOM are most abundant in sample OW31. Terrestrial palynomorphs are light brown in color.

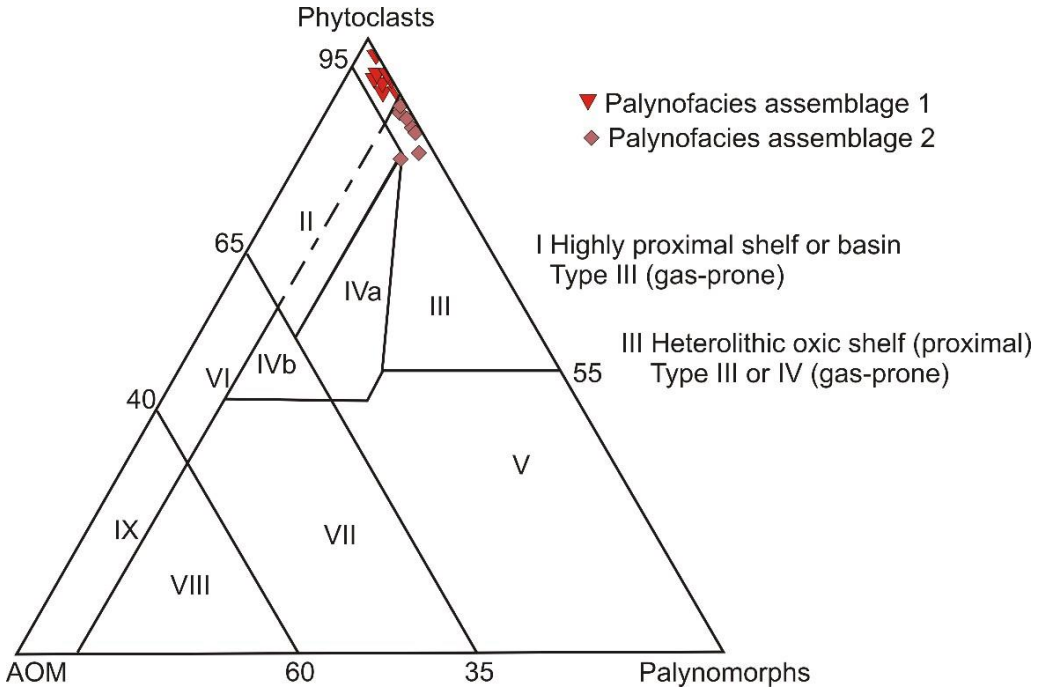

Figure. 5.3. Palynofacies data of the Owan-1 well plot in fields I and III of the APP ternary diagram introduced by Tyson (1989).

Table 5.2. Rock-evaluation data of the Owan-1 and Ubiaja wells Anambra Basin Nigeria

Well	Sample	Depth (m)	TOC	Tmax	S1	S2	S3	HI	OI	OSI	Hc type	PI	Ro
Owan-1	OW 22	194	21.9796	424	0.09	0.10	8.93	0.454	40.628	0.41	0.011	0.009	0.485
Owan-1	OW 24	199	1.36699	423	0.07	0.13	0.75	9.509	54.865	5.12	0.173	0.079	0.467
Owan-1	OW 30	353	1.88117	418	0.10	0.28	0.38	14.884	20.200	5.32	0.736	0.155	0.376
Owan-1	OW 31	367	2.40266	419	0.25	1.74	5.58	72.419	232.24	10.41	0.312	0.034	0.394
Owan-1	OW 34	443	1.40862	418	0.04	0.28	2.23	19.877	158.31	2.84	0.126	0.015	0.376
Ubiaja	UB 9	173	1.84256	424	0.19	3.66	0.32	198.64	17.367	10.31	11.44	0.047	0.485
Ubiaja	UB 17	265	4.07955	411	0.53	5.87	0.35	143.89	8.579	12.99	16.77	0.085	0.250
Ubiaja	UB 28	390	1.90958	421	0.28	1.75	8.09	87.684	423.65	14.66	0.216	0.028	0.430
Ubiaja	UB 29	397	1.3996	424	0.10	0.61	6.84	43.583	488.71	7.14	0.089	0.013	0.485
Ubiaja	UB 30	410	2.0074	429	0.11	1.14	2.33	56.789	116.07	5.48	0.489	0.031	0.575
Ubiaja	UB 32	425	2.74932	421	0.15	3.02	0.04	109.85	1.454	5.46	75.5	0.049	0.431
Ubiaja	UB 33	436	1.67161	415	0.16	0.37	34.90	22.134	2087	9.57	0.011	0.004	0.322
Ubiaja	UB 36	615	2.53447	433	0.09	1.52	0.43	59.973	16.96	3.55	3.534	0.046	0.647
Ubiaja	UB 39	623	1.38682	433	0.05	0.95	13.54	68.502	976	3.61	0.070	0.003	0.647

Ubiaja	UB 40	626	2.19686	417	0.21	1.41	5.58	64.182	253.99	9.56	0.252	0.03	0.358
Ubiaja	UB 43	629	2.27246	428	0.19	2.29	5.01	100.77	220.46	8.36	0.457	0.026	0.557

5.3.3. Maceral analysis

Maceral analysis showed that in all three studied formations (Nkporo, Mamu, and Imo Formations) contain relatively low amounts of macerals (i.e., lower than 10%) and a high percentage of mineral matter (MM) (i.e., 90% and above). The majority of the observed macerals are homogeneous organic matter fragments, which may be classified as solid bitumen (pyrobitumen) and vitrinite particles (Fig. 5.4).

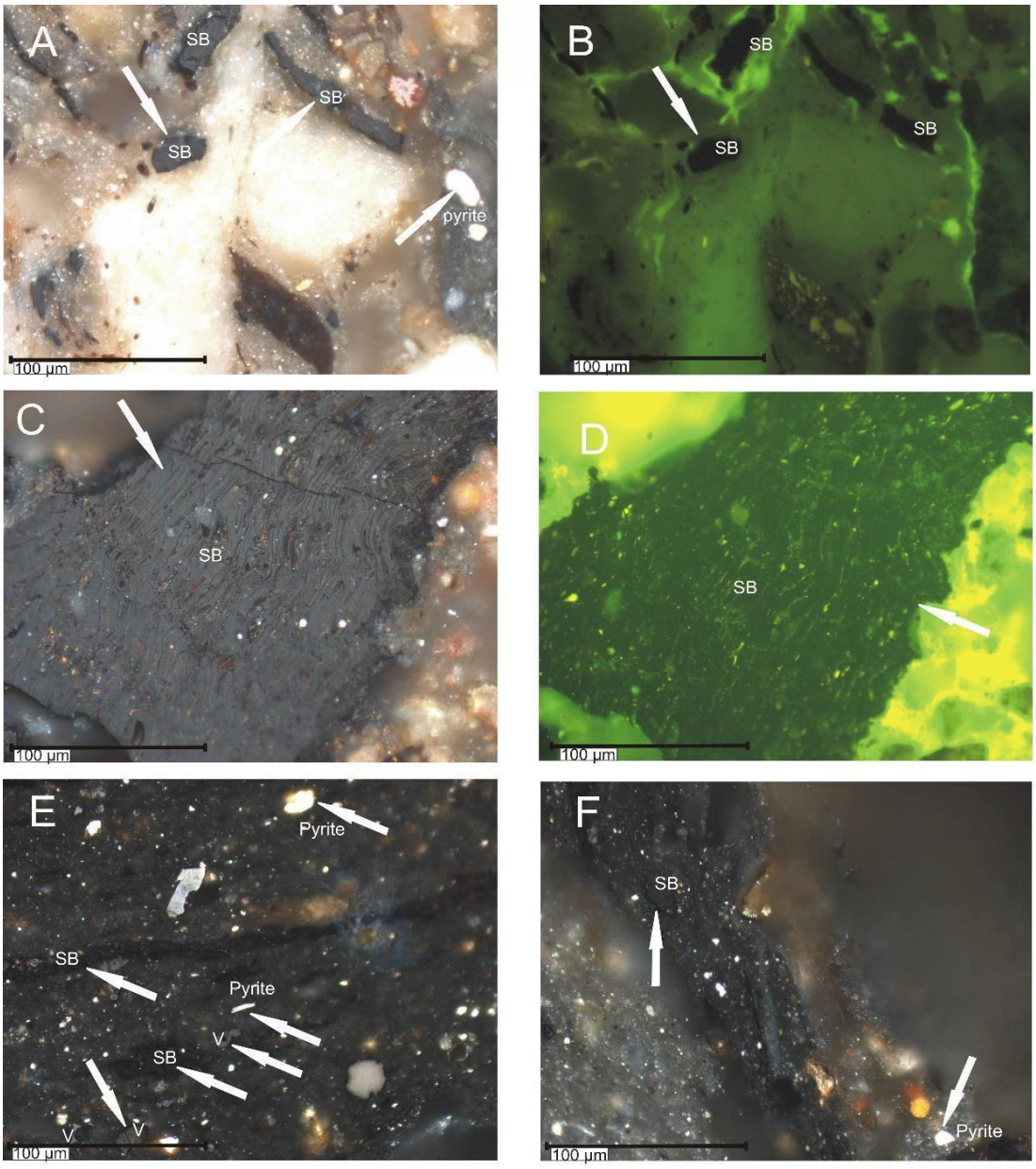

Figure 5.4. Photomicrographs of macerals and mineral matter in reflected white light (A,C,E &F) and reflected fluorescence light (B & D) within the Owan-1 and Ubiaja wells: A & B) made up of

solid bitumen, occurred at depth 623m (UB39); C & D) showing solid bitumen occurred at depth 625m (UB40); E) homogeneous organic matter fragments composed of vitrinite, solid bitumen particles at depth 353m (OW30); F) mudrock composed of solid bitumen at 353m depth (OW 30).

5.3.4. Geochemical evaluation of source rock potential

The TOC levels and Rock-Eval parameters are used internationally to classify organic-rich source beds (Adeyilola et al., 2022; Cappuccio et al., 2021; Chen et al., 2016; Li et al., 2021b; Ma et al., 2022). The results of the TOC and Rock-Eval pyrolysis of the studied section are shown in Table 5.2 and Figs. 5.1 and 5.5.

The TOC levels of the mudrocks vary from 0.2 to 21 wt.% (mean 1.6 wt.%) in the Owan-1 well and 0.1 to 4 wt.% (mean: 1.4 wt.%) in the Ubiaja well. Generally, greater depths recorded higher TOC values (Figs. 5.1 and 5.5). The highest TOC content in the Owan-1 well was measured in OW22, thus depicting a thin coal unit (Fig. 5.1). The S1 content of the mudrocks ranges from 0.04 to 0.25 mg HC/g rock (mean 0.11 mg HC/g rock) for the Owan-1 samples and 0.05 to 0.53 mg HC/g rock (mean 0.19 mg HC/g rock) for the Ubiaja samples. The S2 content ranges from 0.10 to 1.74 mg HC/g rock (mean 0.51 mg HC/g rock) for the Owan-1 samples and 0.61 to 5.87 mg HC/g rock (mean 2.14 mg HC/g rock) for the Ubiaja samples. The OI value ranges from 20 to 232 (mean 101.25) mg HC/g rock and 1.45 to 2087 (mean 419) mg HC/g rock, and the HI level ranges from 0.45 to 72.42 mg HC/g rock (mean 23.43), and 22.13 to 198.64 mg HC/g rock (mean 96.89) for the Owan and Ubiaja samples, respectively. The Tmax value for the Owan-1 well ranges from 418 to 424°C (mean 420.4°C). In contrast, the Tmax for the Ubiaja well ranges from 411 to 433°C (mean 423.3°C). The PI values are from 0.009 to 0.155 in the Owan-1 well and from 0.003 to 0.087 in the Ubiaja well. The OSI levels range from 0.41 to 10.41 mg HC/g TOC with a mean of 4.82 mg HC/g TOC and from 3.55 to 14.66 mg HC/g TOC with a mean of 8.24 mg HC/g TOC for the Owan-1 and Ubiaja mudrocks, respectively. The fraction of S2/S3 indicates the quality of the organic matter present. S2/S3 values <1 indicate the absence of generated petroleum (Singh et al., 2017). All the studied samples of the Owan-1 well show S2/S3 values lower than 1 (Table 5.2), indicating that the oil content of the samples did not vary significantly. The organic geochemistry values reflect marked upward variations (Figs. 5.1 and 5.5).

5.4. Discussion

5.4.1. Palynofacies and sea-level changes

Palynofacies analysis has been used on a global scale to reconstruct paleoenvironments, transgressive/regressive trends, as well as oxygenation conditions and transport of organic particles from potential source areas into a basin (Götz et al., 2008; Carvalho et al., 2013; El Beialy et al., 2016; Mahmoud et al., 2017; Achaegakwo and Atta-Peters, 2021; Li et al., 2021a).

The APP ternary plot (Tyson, 1989; 1993; 1995) is a well-established graphical tool for interpreting depositional environments and related kerogen types. The studied samples of the Owan-1 well fall into fields I (highly proximal shelf or basin; kerogen type III, gas prone) and III (heterolithic oxic shelf; kerogen type III or IV, gas prone), both characterized by the dominance of phytoclasts (Fig. 5.3). These shallow/marginal marine settings experience continuous high terrestrial input (mainly phytoclasts, but additionally pollen grains, spores, freshwater algae, and cuticles). These findings are similar to the interpretation made on the western flank of the Anambra Basin by Edegbai et al. (2020) from outcrop data. Palynofacies assemblage PFA1 plotting in field I suggests a deltaic, shallow-marine environment with high terrestrial input under oxidizing conditions (Li et al., 2021a). Palynofacies assemblage PFA2 plotting in field III suggests a marginal-marine and oxic shelf depositional setting (Tyson, 1993; Li et al., 2021a). The preservation of sedimentary organic matter is limited in marginal to shallow-marine environments due to continuous reworking and oxidation, which may be the main cause for the poor preservation of sedimentary organic matter in the Ubiaja well (Götz et al., 2008; Omietimi et al., 2022). Omietimi et al. (2022) reported fair to medium paleoproductivity in a dominantly oxic paleoredox environment with strong hydrodynamic conditions in a shallow seaway for the western margin of the basin. These factors possibly resulted in the poor preservation of sedimentary organic matter recorded in the Ubiaja well in the present study. Stratigraphic variations in the composition of the palynofacies reflect changes in coastline position in response to sea-level changes (Carvalho et al., 2013; Götz et al., 2008). In the studied Owan-1 well, I observed increasing marine phytoplankton (dinoflagellate cysts) in the Mamu Formation with peak abundance in sample OW15, also showing foraminiferal test linings. Higher percentages of dinoflagellate cysts and dominance of equidimensional, opaque phytoclasts within an interval spanning samples OW14 to OW19 are interpreted to document the maximum flooding phase (Fig. 5.1 and 5.2). The occurrence of cuticles, translucent phytoclasts and a high amount of DOM in the lower Mamu Formation within

an interval covered by samples OW30 to OW36 points to an early transgressive phase, followed by a continuous transgressive trend up-section as reflected by the increase of marine phytoplankton within the Imo Formation (samples OW20 to OW29). The lower part of the Mamu Formation, representing the early transgressive phase, was also affected by a periodic freshwater influx, as indicated by the occurrence of *Botryococcus* sp. and fungal remains. Palynofacies of the upper Imo Formation documents the early highstand phase with increasing translucent phytoclasts covered by samples OW11 and OW12. The late highstand phase is marked by a striking input of translucent phytoclasts, large cuticles, and spores as documented in samples OW1 and OW9 (Figs. 5.1 and 5.2).

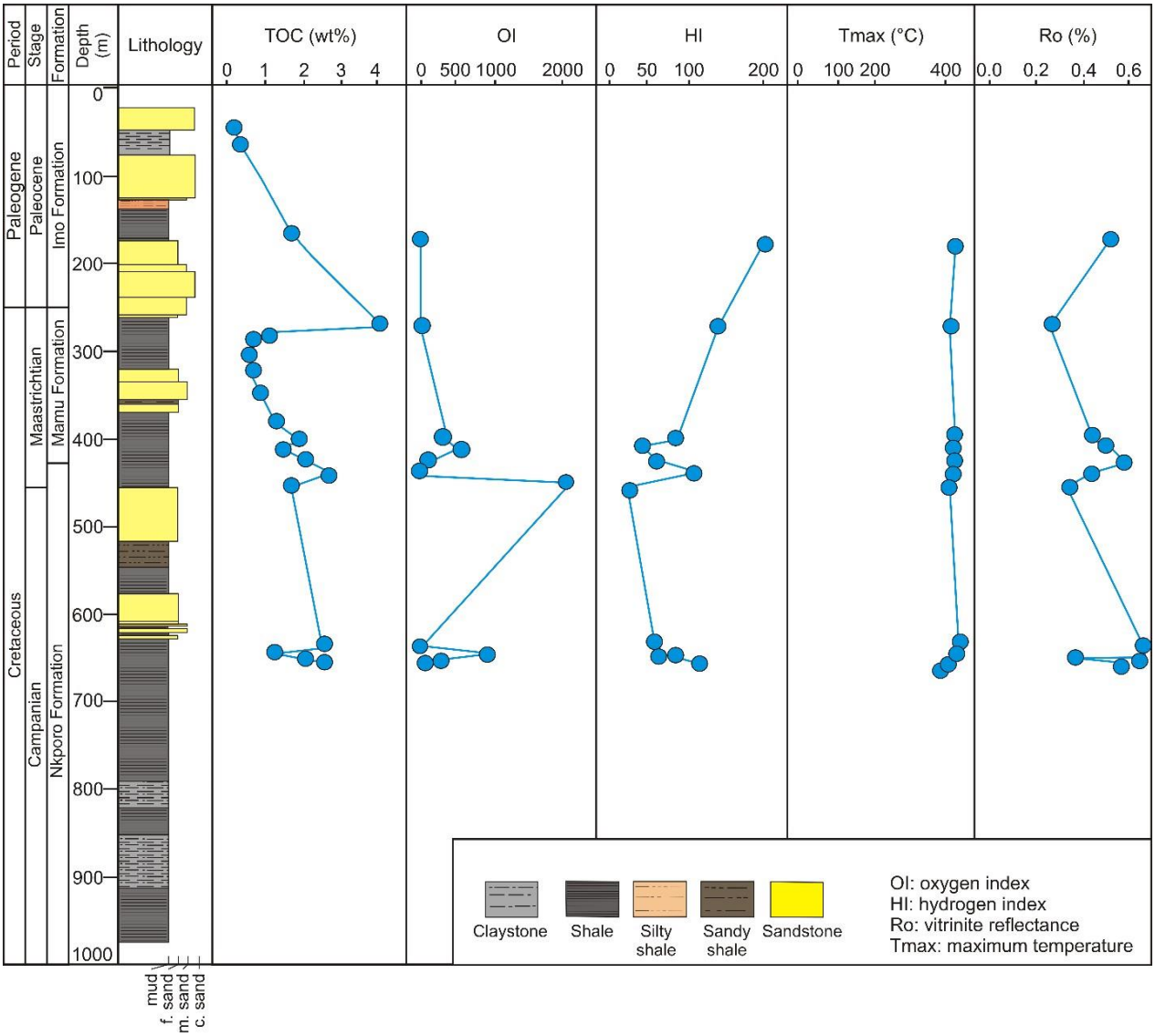

Figure. 5.5. TOC and Rock-Eval parameters in the Ubiaja well.

5.4.2. Organic richness of the source bed and hydrocarbon generation potential

The TOC log data (Figs. 5.1 and 5.5) indicates the studied formations' potential source and non-source sections. The broad variation of the TOC levels with depth ranges is possibly caused by poor preservation of organic matter due to a low sedimentation rate, paleoproductivity, high paleohydrodynamics, water depth, and high temperature and pressure conditions resulting from post-depositional diagenesis of the sediments (Huguet et al., 2008; Kumar et al., 2017; Lehmann et al., 2002; Loucks and Ruppel, 2007; Omietimi et al., 2022). The geochemical analysis of shale samples from the Akukwa-II well at the southeastern margin of the basin, carried out by Adebayo et al. (2018), revealed a TOC range of 0.78 to 2.57 wt.% for the Mamu Formation (mean 1.4 wt.%) and 0.27 to 3.02 wt.% (mean 1.5 wt.%) for the Nkporo Formation. The mean organic richness of the studied Mamu and Nkporo Formations on the western margin of the Anambra Basin is similar to that of the eastern margin (Adebayo et al., 2018). Our results are also consistent with those obtained from the Cretaceous basins of the Benue Trough, Bida, Muglad (Sudan), and Termit (Nigeria) (Akande et al., 2012; Harouna and Philp, 2012; Liu et al., 2015; Ojo et al., 2020; Qiao et al., 2016). A good source bed should contain TOC levels above 0.5 wt.%, signifying a petroleum source rock's lowest threshold (Chen et al., 2016; Ndip et al., 2019; Zhang et al., 2000).

Although the requirement for a good source bed is to have high TOC levels, it is not a standalone factor to determine petroleum generation potency (Dembicki Jr., 2009; Kumar et al., 2017). Thus, high TOC levels and sufficient HI levels are prerequisites for the mudrocks and shales to be an effective source rock (Espitalie et al., 1977; Kumar et al., 2017; Tissot and Welte, 1984). The studied sediments of the western margin of the Anambra Basin contain poor to very good organic content and poor to good potential to generate hydrocarbons at sufficient thermal maturity levels (Kumar et al., 2017; Langford and Blanc-Valleron, 1990; Zhang et al., 2018).

The source rock potentiality of clastic sedimentary rocks can be determined by applying the TOC-S2 cross-graph (Cappuccio et al., 2021). In the Ubiaja and Owan-1 wells, the Imo, Mamu, and Nkporo Formations are dominantly clustered in the good potential (GP) area (Fig. 5.6). However, sample OW 22 in the Owan well is spread into the rich potential area. Data from this study demonstrate that the total organic matter content (TOC, >1.0 wt%) is generally of acceptable quality.

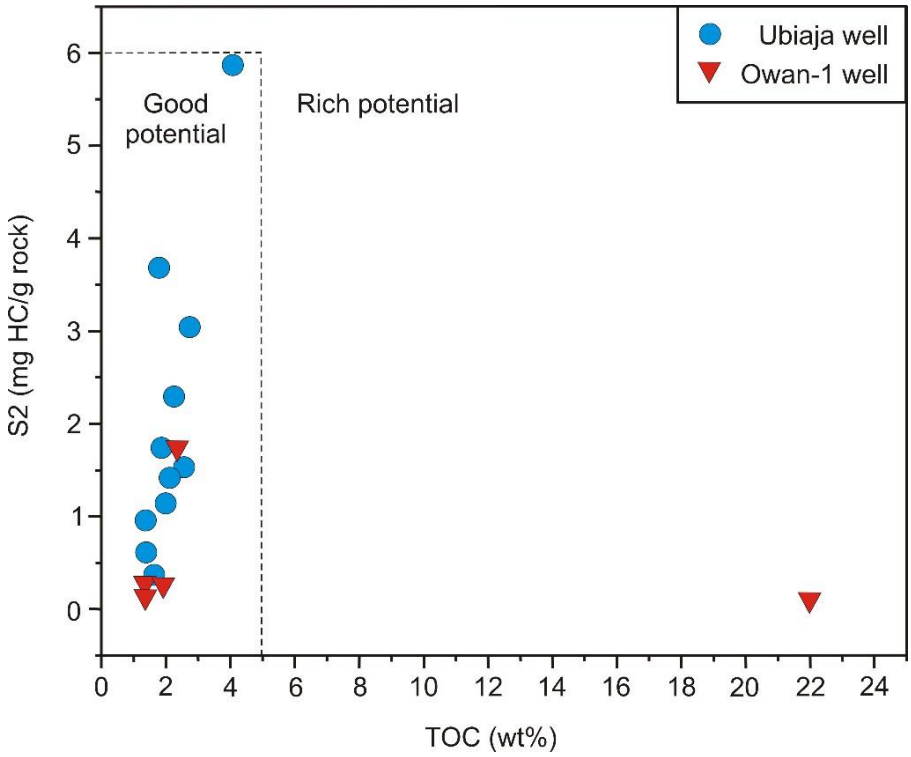

Figure 5.6. Graph of TOC vs. S2. The potentiality of a source rock is measured using this graph by plotting the organic carbon constituent (TOC in wt. percent) against S2 (mg HC/g Rock) geochemically measured in labs for the Owan-1 and Ubiaja wells.

5.4.3. Quality of organic matter (Kerogen type)

In this study, palynofacies, Rock-Eval parameters, and maceral data were used to determine the type and quality of OM. The hydrogen index (HI) indicates a general gas-prone type III kerogen type with a mean value of 67.07 mg HC/g TOC across all formations (Wei et al., 2021), except for sample UB 9, which indicates mixed oil-gas-prone Type II kerogen. The Nkporo, Mamu, and Imo Formations are located within gas-prone kerogen fields, as shown by the cross-graph of HI *vs* Tmax (Fig. 5.7) (Ndip et al., 2019; Cappuccio et al., 2021; Li et al., 2021b). Similarly, Adebayo et al. (2018) revealed type III and type II-III kerogen types from the Akukwa-II well for the Nkporo and Mamu Formations in the eastern part of the Anambra Basin. Generally, the mudrocks are characterized by low OI and HI values (Figs. 5.1 and 5.5), indicating that terrestrial materials influenced the Anambra Basin. The abundance of phytoclasts (mainly opaques), identified palynomorphs (pollen and spores, dinoflagellates), negligible zoomorphs (foraminiferal test linings) and minor AOM amounts indicate mainly kerogen type III (Figs. 5.1, 5.2 and 5.3). In earlier studies, maceral groups have been used to successfully characterize kerogen types

(Chalmers and Bustin, 2017; Cheng et al., 2022; Mastalerz et al., 2012; Ndip et al., 2019). The dominant maceral content in the Owan-1 and Ubiaja wells shows pyrobitumen > vitrinite (Fig. 5.4). The maceral data backs up the palynofacies and Rock-Eval findings, indicating that the studied sections are dominated by type III kerogen, which is gas-prone. The type III kerogen sourced from higher land plants can be related to the continuous terrestrial influx into deltaic to shallow marine settings. Our findings are consistent with inland Cretaceous basins in Nigeria that have similar depositional settings to the Anambra Basin. Akande et al. (2012) discovered that gas- prone type III OM predominated in the Cretaceous deposits of the Lower and Middle Benue Trough. Furthermore, Ojo et al. (2020) postulated that type III kerogen dominated in the Bida Basin.

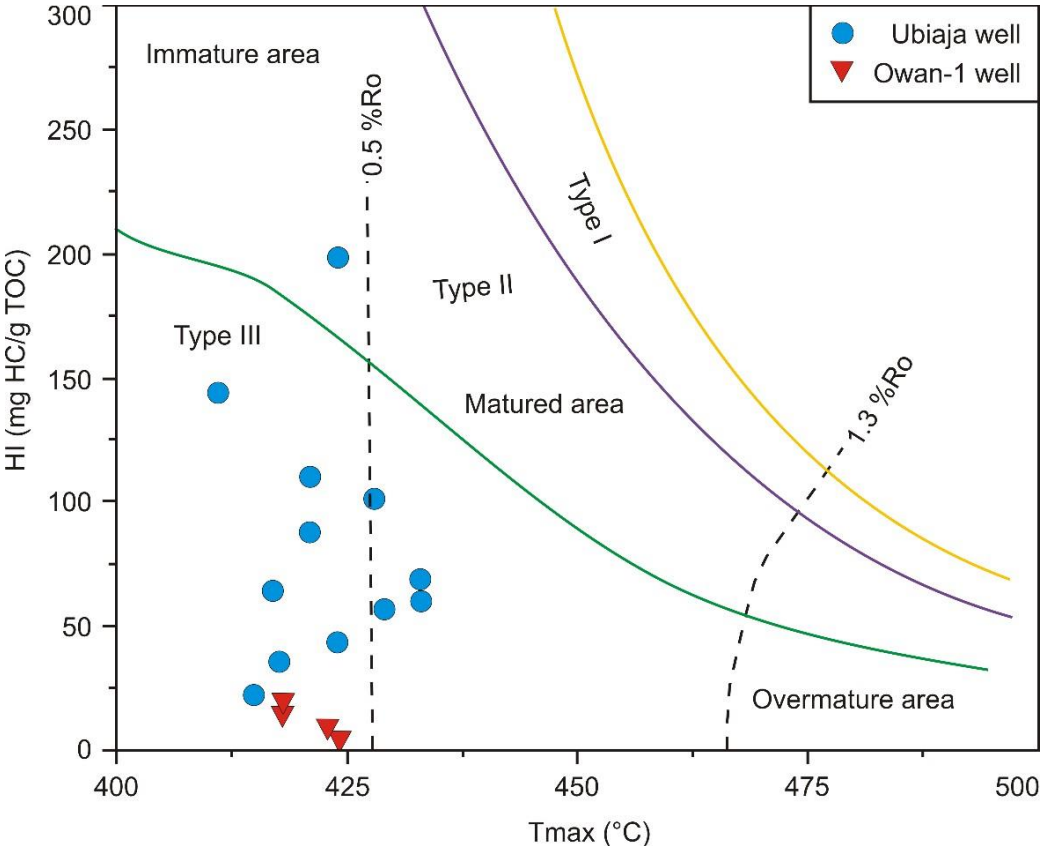

Figure 5.7. Tmax vs. HI graph (modified from Cappuccio et al., 2021). The range of HI values found in the studied wells (black lines) and the averaged value of a source rock's HI (mg HC/g TOC) are plotted against Tmax (°C) to determine the source rock's organic matter quality. Dashed black lines represent Ro maturity. The colored lines represent the boundaries between the different kerogen types.

5.4.4. Thermal maturity of organic matter

The thermal maturity of sedimentary organic matter, which is one of the key characteristics and significant parameters of hydrocarbon generation, determines the conversion of sedimentary organic matter to hydrocarbons (Ma et al., 2022; Wei et al., 2021). The Rock-Eval method was utilized to obtain maturity data for the two wells, such as Tmax, the calculated vitrinite reflectance (Ro), production index (PI) and Tmax vs HI graph (Fig 5.8a, b, c, and Table 2). Jarvie et al. (2001) used the calculated vitrinite ($R_{o)}$ formula in the Barnett shale to determine the thermal maturity of the shales. In this study, I applied the calculated vitrinite formula to determine the quality of the Late Cretaceous Formations in the Anambra Basin by using the formula:

$R_o = 0.0180 \times Tmax - 7.16$

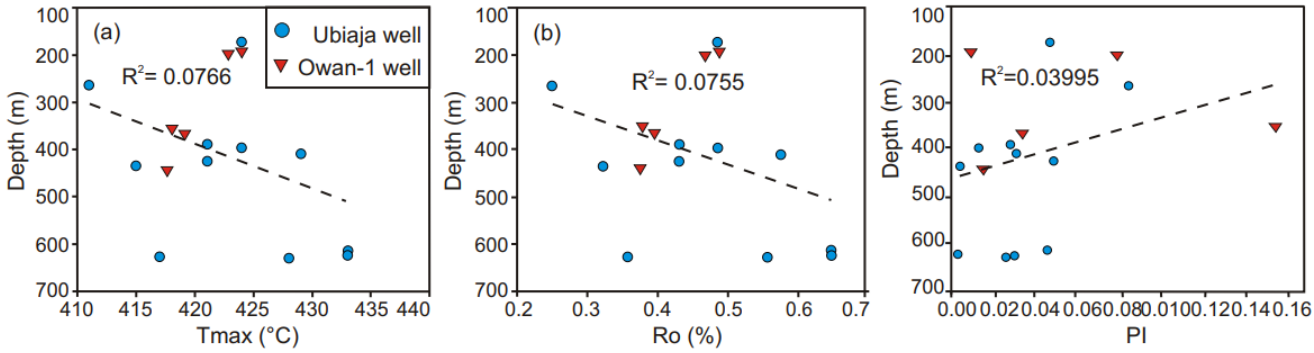

Figure 5.8. Thermal maturity vs depth graphs within the Owan-1 and Ubiaja wells. a) Tmax vs depth graph, b) Vitrinite reflectance vs depth plot, c) Production index vs depth plot.

The Tmax and R_o data were applied to identify the proper level of maturity (LOM) for the Campano-Maastrichtian to Paleogene source rocks. Maturity versus (*vs*) depth diagrams were created for the studied sections (Fig. 5.8a, b, c). The computed vitrinite reflectance values range from 0.36 to 0.47% for the Owan-1 samples and 0.24 to 0.63% for the Ubiaja samples, indicating thermal immaturity to moderately matured source beds for the basin (Fig. 5.8b). Accordingly, the measured Tmax values range between 418 to 424 and 411 to 433 for the Owan-1 and Ubiaja samples, respectively (Fig. 5.8a). The Tmax data also supports an immature to moderately mature oil window. In addition, the PI values range from 0.009 to 0.155 for the Owan-1 well and 0.003 to

0.085 for the Ubiaja well (Fig. 5.8c). The PI values show immature to marginally mature source

beds. The Tmax-HI graph displays the averaged HI data to show the link between hydrogen concentration and thermal maturity in order to evaluate the quality of the organic content and the proneness of the investigated source rocks (Cappuccio et al., 2021; Chen et al., 2017) (Fig. 5.9). As shown in Figure 5.9, all formations are immature to early-mature source rocks, putting them slightly below the oil window zone. I created maturity *vs* depth graphs (Fig. 5.8a, b) to understand the relationship between thermal maturity and depth in the Nkporo, Mamu, and Imo Formations. The data shows a very weak correlation, thus suggesting depth did not play a significant role in the maturity fluctuations in the study area.

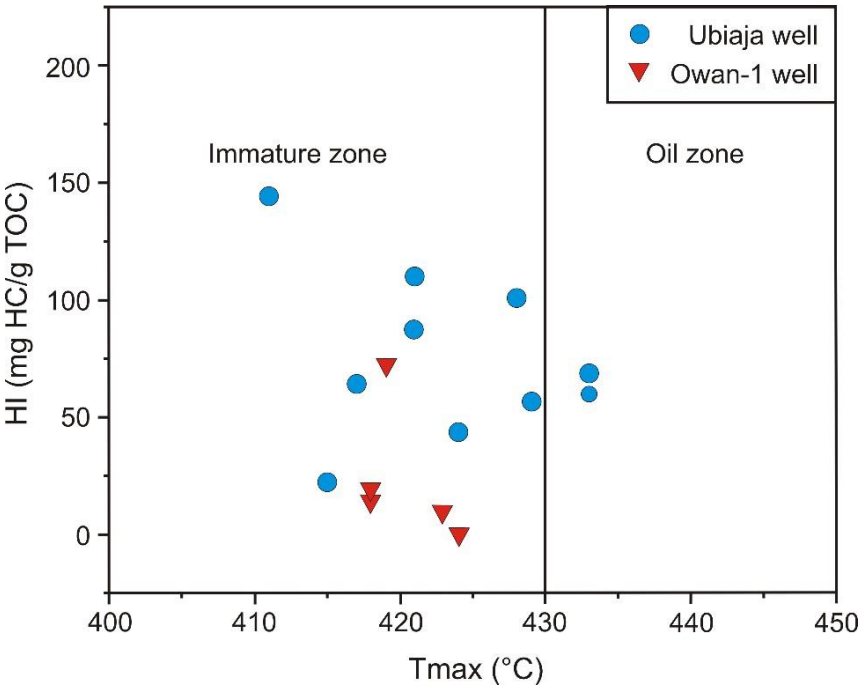

Figure 5.9. The thermal maturity of the studied samples within the Owan-1 and Ubiaja wells is expressed by the relationship between HI and Tmax in a Tmax Vs HI graph.

5.4.5. Potential for unconventional hydrocarbons

TOC and Rock-Eval data indicate that the studied Imo, Mamu, and Nkporo Formations have poor to good hydrocarbon potential for conventional oil sources (Figs. 5.6 and 5.9). Previous studies found commercial oil (1 billion barrels in reserve) and gas (8.49 billion m^3) in Anambra Basin reserve deposits from exploratory and appraisal wells (Abubakar, 2014; Ene et al., 2019). The current research also examined whether the organic-rich layers of the Campano-Maastrichtian Formations have a significant potential

for shale oil exploration based on organic geochemistry, macerals, mineralogy, and mineral matter. To estimate the shale oil potential, the oil saturation index OSI (S1/TOC100) was applied (Jarvie, 2012; Li et al., 2021b). According to Jarvie (2012), oil crossover occurs when the OSI is more than 100 mg HC/g TOC, indicating that shale oil is moveable. OSI levels ranging from 75–100 mg HC/g TOC have often been considered a viable shale oil prospect with a high concentration of absorbed hydrocarbons. The OSI values for the studied sections range between 0.41 and 10.41, with an average of 4.82 mg HC/g TOC for the Owan-1 samples. The Ubiaja samples vary from 3.55 to 14.66, with an average of 8.25 mg HC/g TOC. The OSI values of all the samples are below 100 mg HC/g TOC (Fig. 5.10a), thus revealing poor shale oil potential for the Anambra Basin's western segment. The S1 and OSI values for the Imo, Mamu, and Nkporo Formations are lower than those for the Lucaogou and Ha'erjiawu Formation's (Santanghu Basin) shale oil plays (Zhang et al., 2018; Li et al., 2021b), indicating a low shale oil potential for the studied samples. Oluwajana et al. (2021) reported low OSI values (i.e. lower than 10.0 mg HC/g TOC) for the organic shales and limestones of the Araromi Formation of the Dahomey Basin in south-western Nigeria, which are similar to the OSI values reported in this study, indicating poor shale oil potential for the Cretaceous Formations. The computed OSI values for the eastern (Akukwa-II well, values ranging from 2.72 to 59.26 mg HC/g TOC; Adebayo et al., 2018), central (Nzam -1 well, values ranging from 8.2 to 20.38 mg HC/g TOC; Adeleye et al., 2016), and northern margins of (ONP1 and ONP4 wells, values from 3.76 to 322.48 mg HC/g TOC; Faboya et al., 2019) the Anambra Basin from published data, and I discovered relatively low OSI values for the eastern, western, and central parts of the basin. The northern flank of the basin showed higher OSI values, suggesting good shale oil potential. Nonetheless, the organic chemistry, maceral data, and palynofacies interpretations show that the mudrocks have a poor to good potential for gas generation. Still, they are unsuitable for shale oil exploration and exploitation. The main reason for this could be that the low to moderate TOC values and high clay mineral content of the Campano-Maastrichtian to Paleocene Formations result in a high adsorption capacity of petroleum fluids, which is not suitable for shale hydraulic fracturing and the outflow of petroleum fluids (Faboya et al., 2020; Li et al., 2021b).

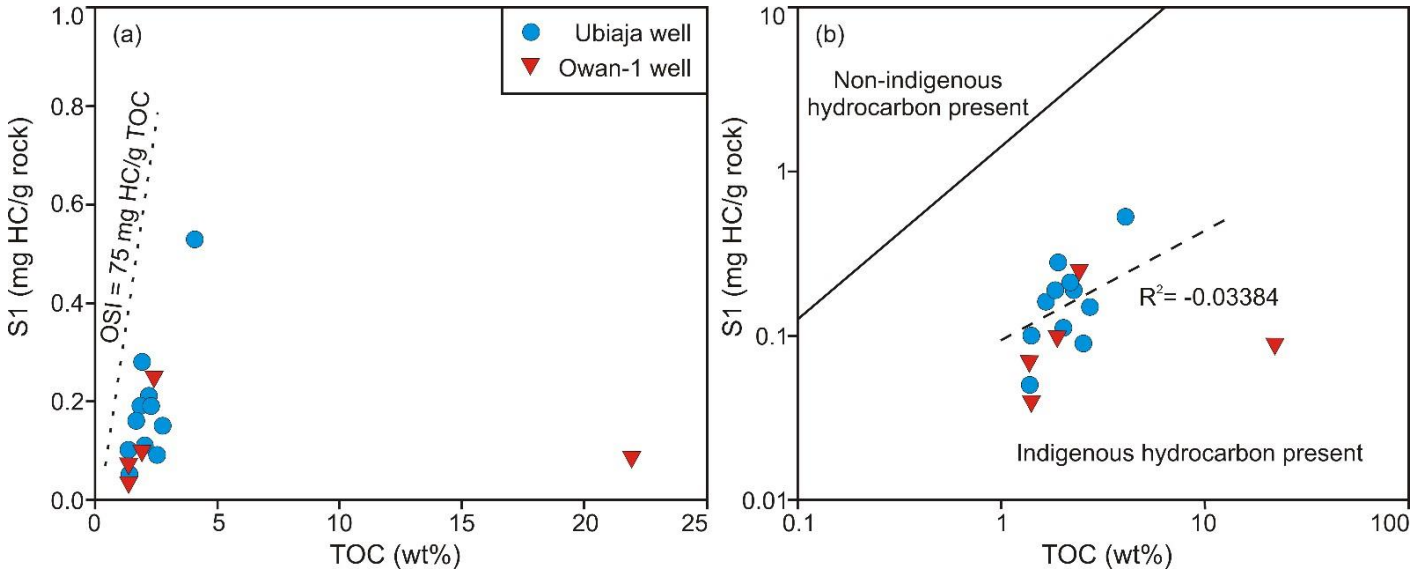

Figure 5.10. S1 Vs TOC graph (modified from Li et al 2021b) (a) showing movable oil content (b) showing indigenous hydrocarbon of the western segment deposits of the Anambra Basin.

5.4.6. *Economic potential of hydrocarbon sources and implication for petroleum prospecting*

The discovery of commercially viable petroleum deposits in the Cretaceous rift basins of Doba (Chad), Termit (Niger), and Muglad and Melut (Sudan) (Lai et al., 2018; Qiao et al., 2016; Wang et al., 2017a) has reignited interest in the rifts in Nigeria (Ene et al., 2019). Three petroleum systems occur in Nigeria's southern onshore and offshore sedimentary basins (Haack et al., 2000), consistent with the WCARS basins (Genik, 1993). The petroleum systems in the WCARS basins are Lower Cretaceous, Upper Cretaceous and Paleogene petroleum systems (Abubakar, 2014).

The Paleogene petroleum system is well developed in the Niger Delta Basin in southern Nigeria and the Termit Basin of the Niger Republic (Abubakar, 2014; Lai et al., 2018). The Lower Cretaceous Formations in the Anambra Basin occur at the northern and western margins of the basin (Ejeh, 2021; Ola-Buraimo and Akaegbobi, 2013). Thick sequences of marine shales may possibly serve as potential source beds, although reservoir beds are absent (Abubakar, 2014). The Upper Cretaceous petroleum system in the Anambra Basin is well developed. The lithological units of the Nkporo, Mamu and Ajali, Nsukka, and Imo Formations make up the petroleum system (Dim et al., 2018).

A petroleum system cannot function without the source rock horizons, which make up a critical part of any petroleum system (Dim et al., 2018; El Beialy et al., 2016). Thus, organic geochemistry (TOC, Rock-Eval pyrolysis), maceral, and palynofacies data was used to successfully characterize the source rock potential. The amount of sedimentary organic matter determines the potential of source beds, post-depositional alterations (diagenesis, metagenesis, and catagenetic processes) and thermal maturation (Lai et al., 2018; Singh et al., 2017). HI values are used as thresholds in defining source rock quality (Cappuccio et al., 2021). Type III kerogen is characterized by HI values below 200 mg HC/g TOC and would produce gas at appropriate thermal stress. Type II kerogen is typified by HI values greater than 200 mg HC/g and can generate oil and gas. Type I kerogen usually contains a HI amount of 600 mg HC/g TOC and above and can generate oil (Langford and Blanc-Valleron, 1990; Singh et al., 2017). The investigated samples from the Owan-1 and Ubiaja wells comprising the Nkporo, Mamu, and Imo Formations consist of low to moderate TOC values (av. 1.67 Owan-1 well; av. 1.53 Ubiaja well) and HI contents below 200 mg HC/g rock. The S2 and TOC contents from the Owan-1 and Ubiaja samples suggest fair to good potential source beds for gaseous hydrocarbons. A TOC-S2 cross-graph (Fig. 5.6) revealed dominantly good potential for the studied sections (Cappuccio et al., 2021). The S1 values indicate a negative correlation with TOC (Fig. 5.10b). The graph of S1 *vs* TOC shows the presence of indigenous petroleum in the studied section (Li et al., 2020a) (Fig. 5.10b). I performed a cross- graph of HI *vs* Tmax (Fig. 5.7), indicating gas prone type III kerogen (Cappuccio et al., 2021; Wei et al., 2021). The palynofacies data with dominantly phytoclasts reveals type III kerogen (Fig. 5.3), and the petrographic interpretations show mainly vitrinite and pyrobitumen (Fig. 5.4), thus suggesting gas-prone hydrocarbons (Li et al., 2021a). The Ubiaja samples show S2/S3 ratios lower than 1, indicating the absence of generated hydrocarbons in the studied sections. Samples UB 9, 32 and 36 revealed S2/S3 ratios >1, thus suggesting generated hydrocarbons (Singh et al., 2017). The thermal stress component of the rocks was evaluated from Tmax, Ro, PI and Tmax-HI cross plots. In this study, the Tmax interpretation, Ro values, and production index (PI: generally below 0.1) indicate an immature to marginally mature stage for hydrocarbon generation. The Tmax-HI graph (Figs. 5.7 and 5.9) shows early-marginal mature source beds below the oil window (Cappuccio et al., 2021; Wei et al., 2021). Thus, the overall characteristics suggest that the studied Campano-Maastrichtian to Paleocene Formations in the Anambra Basin's western segment are likely to generate gaseous hydrocarbons once mature.

The sandstone lithofacies of the Mamu, Ajali, and Nsukka Formations in the Anambra Basin could constitute reservoir beds (Dim et al., 2019, 2017). With porosities ranging from 25.5 to 32.8% and permeabilities ranging from 7.2 to 55 md, the Ajali Formation may be the best reservoir rock in the basin (Tijani and Nton, 2009). The shales in the Mamu and Imo Formations could serve as regional seals depending on the stratigraphic position of the reservoir beds. Dim et al. (2017) reported the presence of hanging wall, footwall, horst block and collapsed structures within the Anambra Basin from seismic sections and sequence stratigraphic interpretations. These structures have also been identified in outcrops in the eastern segment of the basin (Dim et al., 2020). The basin also possesses stratigraphic traps consisting of wedge/pinch-out structures, buried channels, hills, faulted sand lenses, and channel-fill/truncation. These structures are a result of multiple episodes of transgression and regression in the Campanian to Paleocene Formations of the basin (Abubakar, 2014; Dim et al., 2020) and could generally enhance migration and provide entrapment mechanisms for petroleum accumulation. Omietimi et al. (2021) also identified structural lineaments in the western segment of the Anambra Basin that could serve as possible migratory pathways for hydrocarbon migration and accumulation.

The Upper Cretaceous petroleum systems of the WCARS basins in West Africa, consisting of the Termit Basin in Niger and the Chad Republic, are well established. The source rocks are deltaic to shallow marine shales composed of type III organic matter (Harouna and Philp, 2012; Zanguina et al., 1998) with TOC ranges from 0.8 to 7.4 wt.%. The reservoir rocks are fluvial sandstones of Maastrichtian age with a thickness of 400m, an average porosity of 20% and an average permeability of 52 md (Genik, 1993).

The eastern, central, western, and northern margins of the Anambra basin indicate the dominance of type III organic matter (gas prone) with a minor presence of type II (oil-prone) organic matter (Abubakar, 2014; Adebayo et al., 2018; Faboya et al., 2020; Ogungbesan and Adedosu, 2020). The basin has the potential to generate gaseous hydrocarbons; thus, exploration in the basin should be focused on gas deposits within the matured sections of the basin with good sedimentary organic amounts, reservoir rocks, and an established structural framework (Omietimi et al., 2021). High geothermal gradients have been recorded in the basin, with ranges of 20–35^{o}C/km; 25–54^{o}C/km (Bello et al., 2017). Geothermal gradients of 2.16 - 5.26°C/100m, 2.6 - 2.9°C/100m, and 2.5 - 3.0°C/100m were reported for the Bornu sub-basin in Nigeria, Muglad basin of Sudan, Termit Basin of Niger and Chad republics, respectively (Nwaezeapu 1992; Avbovbo et al., 1986; Genik,

1993). Geothermal gradient modelling revealed depths of 2.3-5.0 km and 3.5–4.0 km for the oil window in the Termit and Muglad basins, respectively (Genik, 1993; Mohamed et al., 1999). Nwajide (2005) reported a depth range of 1.9 km for the oil window in the southern margins of the Anambra Basin with an inferred temperature of 60°C. The Anambra Basin has high geothermal gradients compared to the Bornu, Muglad, and Termit WCARS basins, and this has probably pushed the oil window in the basin to shallower depths.

5.5. Conclusions

A multi-proxy petroleum study comprising organic geochemistry, palynofacies, and maceral analysis has been applied to characterize subsurface deposits of the western segment of the inland Anambra Basin for the first time in this study. This is the first detailed petroleum study carried out for the Campanian to Paleogene, Nkporo, Mamu, and Imo Formations from the Owan-1 and Ubiaja wells. The organic matter richness varies from fair to good in the Imo, Mamu, and Nkporo Formations. These values compare favorably to other Cretaceous WCARS basins with similar depositional conditions. The S2 *vs* TOC graph used to assess the potential of the source beds shows predominantly good potential. The HI figures (<200 mg HC/g TOC) and a high abundance of phytoclasts and vitrinite macerals collectively reveal gas-prone type III kerogen. Tmax, *Ro* and depth diagrams indicate dominantly immature to early mature source beds, thus lowering the HC potential of the western segment of the basin. However, the organic-rich mudrocks reveal good potential for conventional gas in the western Anambra Basin. Furthermore, the northern segment of the basin indicates good potential for unconventional shale oil prospects.

Chapter Six

6.0 Conclusions and recommendation

6.1. Conclusions

A multi-disciplinary approach that comprises palynofacies, petrography, organic geochemistry, sedimentary geochemistry, and gravity modelling was applied for source rock characterization, paleoclimate deductions, hydrodynamic and water depth interpretations, redox conditions, bioproductivity, and structural interpretation for the subsurface deposits of the western segment of Nigeria's Anambra Basin. The assessments were carried out using a multi-proxy method, which provided a robust dataset for the basin and regional studies. This thesis makes significant deductions about the basin's southwestern Cretaceous to Paleogene sedimentary fill.

The paleosedimentary environment deductions have shown significant small-scale differences and variations in paleo-oxygen levels and contributions from marine ecosystems and terrestrial influx in the western basin segment. Data on the mineral composition of the mudrocks reveals they contain clay minerals, non-clay minerals, iron minerals, and minor carbonates. Sedimentary geochemistry data and proxies all point to a warm tropical climate with abundant rainfall and intense weathering. Thus, our data compares favorably to high global mean temperatures during the Cretaceous and early Paleogene periods. The enrichment of quartz and kaolinite also supports a high level of weathering. The reconstructed paleoredox conditions indicate dominantly oxic conditions and an occasional anoxic paleowater column during the Cretaceous to Paleogene succession deposition. The paleosalinity proxy adopted reveals predominantly brackish and marine paleosedimentary environments. The presence of gypsum in trace amounts suggests the possibility of an evaporated diagenetic paleosedimentary environment. The palynofacies data also supports a dominantly oxic basin. I hypothesize that the Cretaceous-Paleogene units in the western part of the Anambra Basin were deposited under high hydrodynamic conditions and derived from a shallow seaway, similar to those found in the northern Bida Basin.

Palynofacies investigations reveal high amounts of terrestrial organic matter components (phytoclasts and AOM) and marine sources (palynomorphs). In this research, basin topography, subsidence rates, hydrodynamic influence, and weathering control the distribution of terrestrial organic matter within the basin. In addition, sea-level fluctuations and water depth are the main controls of marine organic matter distribution within the basin. Furthermore, due to the impervious

nature of clay minerals in mudrocks, the adhesion of carbon compounds onto clay mineral walls and tectonic activity are crucial components responsible for the burial and conservation of sedimentary organic materials. The hydrocarbon potentiality of the Cretaceous to Paleogene units is determined based on integrated optical kerogen analyses in the investigated wells, and rock evaluation was performed to access the organic richness, kerogen quality, and thermal maturities in the Nkporo, Mamu, and Imo Formations. The integrated approach used in evaluating the organic-rich mudrocks shows that the studied sections have good potential to generate gaseous petroleum. The basin is dominated by type III organic matter, similar to other WCARS basins, which suggests the organic matter in the mudrocks originates from higher plant materials, linked to terrestrial upsurge into deltaic to shallow marine environments. The Cretaceous period experienced a high contribution of type III kerogen types, as evidenced from other WCARS basins. The Tmax, vitrinite reflectance, PI, and cross graphs of HI vs Tmax coherently point to marginally matured source beds, which places the studied sections relatively below the oil window zone. Our data revealed weak shale gas potential for the western segment. The identified structural lineaments could serve as potential traps for petroleum and hydrothermal fluids and a migratory pathway. The Cretaceous-Maastrichtian tectonic event contributed to the basin's sedimentary infill, as evidenced by the thickness of over 4.5 km in this study.

6.2 Recommendation

In Nigeria's Benue Trough, Bida Basin, and other inland basins, paleosedimentary conditions, primary productivity, paleohydrothermal interpretations, hydrodynamic conditions, water depth, and paleosalinity of the Cretaceous to Paleogene Formations are less well documented. Investigation of these parameters in other WCARS basins during the Cretaceous and Paleogene evolution of these basins will provide robust data for regional correlation. Furthermore, in the Anambra basin's central, eastern, and western segments, seismic data, well logs, biomarkers, and biostratigraphy data should be used to identify matured sections and characterize the structural framework, sequence boundaries, and reservoir units. This will boost exploration in the basin because research over the last decade has demonstrated the presence of a petroleum system in the basin.

Bibliography

Abarghani, A., Ostadhassan, M., Gentzis, T., Carvajal-Ortiz, H., Ocubalidet, S., Bubach, B., Mann, M., Hou, X., 2019. Correlating Rock-Eval^{TM} Tmax with bitumen reflectance from organic petrology in the Bakken Formation. International Journal of Coal Geology 205, 87–104.

Abbass, A.A., Mallam, A., 2013. Estimating the thickness of sedimentation within Lower Benue Basin and Upper Anambra Basin, Nigeria, using both spectral depth determination and source parameter imaging. International Scholarly Research Notices 2013.

Abdullahi, M., Singh, U.K., 2018. Basement geology derived from gravity anomalies beneath the Benue Trough of Nigeria. Arabian Journal of Geosciences 11, 1–8.

Abtout, A., Boukerbout, H., Bouyahiaoui, B., Gibert, D., 2014. Gravimetric evidences of active faults and underground structure of the Cheliff seismogenic basin (Algeria). Journal of African Earth Sciences 99, 363–373.

Abubakar, M.B., 2014. Petroleum potentials of the Nigerian Benue Trough and Anambra Basin: a regional synthesis. Natural Resources 2014.

Abubakar, U., Usman, M.B., Aliyuda, K., Dalha, A., Bello, A.M., Linus, L.N., 2021. Major and trace element geochemistry of the shales of Sekuliye Formation, Yola Sub-Basin, Northern Benue Trough, Nigeria: implications for provenance, weathering intensity, and tectonic setting. Journal of Sedimentary Environments 6, 473–484. https://doi.org/10.1007/s43217-021-00067-2

Achaegakwo, C.A., Atta-Peters, D., 2021. Palynofacies analysis and depositional environments of Upper Cretaceous sediments in the ST-9H well, offshore South Tano Basin, Western Ghana. Geological Journal.

Adebayo, O.F., Adegoke, A.K., Mustapha, K.A., Adeleye, M.A., Agbaji, A.O., Abidin, N.S.Z., 2018. Paleoenvironmental reconstruction and hydrocarbon potentials of Upper Cretaceous sediments in the Anambra Basin, southeastern Nigeria. International Journal of Coal Geology 192, 56–72.

Adebayo, O.F., Akinyemi, S.A., Ojo, A.O., 2015. Palaeoenvironmental studies of Odagbo coal mine sequence, Northern Anambra Basin, Nigeria: insight from palynomorph and geochemical analyses. Int J Curr Res 7, 20274–20286.

Adeleye, M.A., Daramola, D.A., 2018. Organic Source Input, Thermal Maturity and Paleodepositional Conditions of Imo Formation in the Anambra Basin, Nigeria. Conference of the Arabian Journal of Geosciences. Springer, 161–164.

Adeoye, J.A., Akande, S.O., Adekeye, O.A., Abikoye, V.T., 2020. Geochemistry and paleoecology of shales from the Cenomanian-Turonian Afowo formation Dahomey Basin, Nigeria: Implication for provenance and paleoenvironments. Journal of African Earth Sciences 169, 103887. https://doi.org/10.1016/j.jafrearsci.2020.103887

Adetona, A.A., Abu, M., 2013. Investigating the structures within the Lower Benue and Upper Anambra basins, Nigeria, using first Vertical Derivative, Analytical Signal and (CET) centre for exploration targeting plug-in.

Adeyilola, A., Zakharova, N., Liu, K., Gentzis, T., Carvajal-Ortiz, H., Ocubalidet, S., Harrison III, W.B., 2022. Hydrocarbon potential and Organofacies of the Devonian Antrim Shale, Michigan Basin. International Journal of Coal Geology 249, 103905.

Adighije, C.I., 1981. A gravity interpretation of the Benue Trough, Nigeria. Tectonophysics 79, 109–128.

Adighije, C.I., 1978. Studies of the gravity field of the Benue Trough of Nigeria. PhD Thesis. Ph. D. Thesis, Univ. Ibadan, Ibadan (unpubl.).

Agagu, O.K., Adighije, C.I., 1983. Tectonic and sedimentation framework of the lower Benue Trough, southeastern Nigeria. Journal of African Earth Sciences (1983) 1, 267–274.

Ahmed, A., Jahandad, S., Hakimi, M.H., Gharib, A.F., Mehmood, S., Kahal, A.Y., Khan, M.A., Munir, M.N., Lashin, A., 2022. Organic matter characteristics and conventional oil potentials of shales from the Early Jurassic Datta Formation in the Upper Indus Basin, Northern Pakistan. Journal of Asian Earth Sciences 224, 104975.

Akaegbobi, I.M., Nwachukwu, J.I., Schmitt, M., 2000. AAPG Memoir 73, Chapter 17: Aromatic Hydrocarbon Distribution and Calculation of Oil and Gas Volumes in Post-Santonian Shale and Coal, Anambra Basin, Nigeria.

Akande, S.O., Egenhoff, S.O., Obaje, N.G., Ojo, O.J., Adekeye, O.A., Erdtmann, B.D., 2012. Hydrocarbon potential of Cretaceous sediments in the Lower and Middle Benue Trough, Nigeria: Insights from new source rock facies evaluation. Journal of African Earth Sciences 64, 34–47.

Akande, S.O., Mücke, A., 1993. Depositional environment and diagenesis of carbonates at the Mamu/Nkporo formation, anambra basin, Southern Nigeria. Journal of African Earth Sciences (and the Middle East) 17, 445–456.

Akinyemi, S.A., Adebayo, O.F., Ojo, O.A., Fadipe, O.A., Gitari, W.M., 2013. Mineralogy and geochemical appraisal of paleo-redox indicators in Maastrichtian outcrop shales of Mamu formation, Anambra Basin, Nigeria. Journal of Natural Sciences Research 3, 48–64.

Alemu, T., Abdelsalam, M.G., Dawit, E.L., Atnafu, B., Mickus, K.L., 2018. The Paleozoic–Mesozoic Mekele sedimentary basin in Ethiopia: an example of an exhumed IntraCONtinental Sag (ICONS) basin. Journal of African Earth Sciences 143, 40–58.

Algeo, T.J., Kuwahara, K., Sano, H., Bates, S., Lyons, T., Elswick, E., Hinnov, L., Ellwood, B., Moser, J., Maynard, J.B., 2011. Spatial variation in sediment fluxes, redox conditions, and productivity in the Permian–Triassic Panthalassic Ocean. Palaeogeography, Palaeoclimatology, Palaeoecology 308, 65–83.

Alrefaee, H.A., 2017. Crustal modeling of the central part of the Northern Western Desert, Egypt using gravity data. Journal of African Earth Sciences 129, 72–81.

Altinoğlu, F.F., Sari, M., Aydin, A., 2015. Detection of lineaments in Denizli basin of western Anatolia region using Bouguer gravity data. Pure and Applied Geophysics 172, 415–425.

Anakwuba, E.K., Ajaegwu, N.E., Ejeke, C.F., Onyekwelu, C.U., Chinwuko, A.I., 2018. Sequence stratigraphic interpretation of parts of Anambra Basin, Nigeria using geophysical well logs and biostratigraphic data. Journal of African Earth Sciences 139, 330–340.

Anakwuba, K.E., Onyekwelu, C.U., 2010. Subsurface sequence stratigrphy and reservoir characterization of the Southern part of Anambra Basin, Nigeria. AAPG Search and Discovery.

Andersen, O.B., Knudsen, P., Berry, P.A., 2010. The DNSC08GRA global marine gravity field from double retracked satellite altimetry. Journal of Geodesy 84, 191–199.

Antolinez-Delgado, H., Oboh-Ikuenobe, F.E., 2007. New species of dinoflagellate cysts from the Paleocene of the Anambra basin, southeast Nigeria. Palynology 31, 53–62.

Anyiam, O.A., Onuoha, K.M., Jolly, B.A., 2015. Play fairway evaluation of the Anambra Basin, southeast Nigeria. Arabian Journal of Geosciences 8, 539–546.

ASTM, A., 2014. Standard Test Methods for Determination of Carbon, Hydrogen and Nitrogen in Analysis Samples of Coal and Carbon in Analysis Samples of Coal and Coke.

Avbovbo, A.A., Ayoola, E.O., Osahon, G.A., 1986. Depositional and structural styles in Chad Basin of northeastern Nigeria. AAPG Bulletin 70, 1787–1798.

Azevedo RLM., 2004. Paleoceanografia e a evolução do Atlântico Sul no Albiano. Bol Geoc PETROBRAS 12(2): 234-249

Babatunde, O.L., 2010. The main oil source formations of the Anambra Basin, Southeastern Nigeria. AAPG International Convention & Exhibition, September. 12–15.

Balmino, G., Vales, N., Bonvalot, S., Briais, A., 2012. Spherical harmonic modelling to ultra-high degree of Bouguer and isostatic anomalies. Journal of Geodesy 86, 499–520.

Barbera, G., Mazzoleni, P., Critelli, S., Pappalardo, A., Lo Giudice, A., Cirrincione, R., 2006. Provenance of shales and sedimentary history of the Monte Soro Unit, Sicily. Periodico Di Mineralogia 75, 313–330.

Batten, D.J., 1982. Palynofacies, palaeoenvironments and petroleum. Journal of Micropalaeontology 1, 107–114.

Bba, A.N., Boujamaoui, M., Amiri, A., Hejja, Y., Rezouki, I., Baidder, L., Inoubli, M.H., Manar, A., Jabour, H., 2019. Structural modeling of the hidden parts of a Paleozoic belt: Insights from gravity and aeromagnetic data (Tadla Basin and Phosphates Plateau, Morocco). Journal of African Earth Sciences 151, 506–522.

Bello, R., Ofoha, C.C., Wehiuzo, N., 2017. Geothermal gradient, Curie point depth and heat flow determination of some parts of lower Benue trough and Anambra basin, Nigeria, Using High Resolution Aeromagnetic Data. Physical Science International Journal 1–11.

Benkhelil, J., 1989. The origin and evolution of the Cretaceous Benue Trough (Nigeria). Journal of African Earth Sciences (and the Middle East) 8, 251–282. https://doi.org/10.1016/S0899-5362(89)80028-4

Benkhelil, J., 1982. Benue Trough and Benue Chain. Geological Magazine 119, 155–168. https://doi.org/10.1017/S001675680002584X

Benkhelil, J., Dainelli, P., Ponsard, J.F., Popoff, M., Saugy, L., 1988. The Benue Trough: wrench-fault related basin on the border of the equatorial Atlantic. Developments in Geotectonics. Elsevier, 787–819.

Beukes, N.J., 1987. Facies relations, depositional environments and diagenesis in a major early Proterozoic stromatolitic carbonate platform to basinal sequence, Campbellrand Subgroup, Transvaal Supergroup, Southern Africa. Sedimentary Geology 54, 1–46.

Binks, R.M., Fairhead, J.D., 1992. A plate tectonic setting for Mesozoic rifts of West and Central Africa. Tectonophysics 213, 141–151.

Blakely, R.J., 1996. Potential theory in gravity and magnetic applications. Cambridge university press.

Bokanda, E.E., Fralick, P., Ekomane, E., Bisse, S.B., Tata, C.N., Ashukem, E.N., Belinga, B.C., 2021. Geochemical constraints on the provenance, paleoweathering and maturity of the Mamfe black shales, West Africa. Journal of African Earth Sciences 175, 104078.

Bolarinwa, A.T., Idakwo, S.O., Bish, D.L., 2019. Rare-earth and trace elements and hydrogen and oxygen isotopic compositions of Cretaceous kaolinitic sediments from the Lower Benue Trough, Nigeria: provenance and paleoclimatic significance. Acta Geochimica 38, 350–363.

Boström, K., 1970. Submarine volcanism as a source for iron. Earth and Planetary Science Letters 9, 348–354.

Bryant, I., Levy, T., Neumaier, M., Tessen, N., 2012. A Novel Approach To Incorporate Full Petroleum System Analysis into Play Risk Assessments. EAGE Workshop on Petroleum Play Assessment. European Association of Geoscientists & Engineers, cp-277.

Burk, K., Dewey, J.F., 1974. Two plates in Africa during the Cretaceous? Nature 249, 313–316.

Burke, K., Whiteman, A.J., 1973. Uplift, rifting and the break-up of Africa. Implications of Continental Drift to the Earth Sciences 2, 735–755.

Burke, K.C., Dessauvagie, T.F.J., Whiteman, A.J., 1972. Geological history of the Benue Valley and adjacent areas. African Geology 1, 7–2.

Cappuccio, F., Porreca, M., Omosanya, K.O., Minelli, G., Harishidayat, D., 2021. Total organic carbon (TOC) enrichment and source rock evaluation of the Upper Jurassic-Lower Cretaceous rocks (Barents Sea) by means of geochemical and log data. International Journal of Earth Sciences 110, 115–126.

Carvalho, M. de A., Ramos, R.R.C., Crud, M.B., Witovisk, L., Kellner, A.W., Silva, H. de P., Grillo, O.N., Riff, D., Romano, P.S., 2013. Palynofacies as indicators of paleoenvironmental changes in a Cretaceous succession from the Larsen Basin, James Ross Island, Antarctica. Sedimentary Geology 295, 53–66.

Chalmers, G.R., Bustin, R.M., 2017. A multidisciplinary approach in determining the maceral (kerogen type) and mineralogical composition of Upper Cretaceous Eagle Ford Formation:

Impact on pore development and pore size distribution. International Journal of Coal Geology 171, 93–110.

Chang, H., An, Z., Wu, F., Jin, Z., Liu, W., Song, Y., 2013. A Rb/Sr record of the weathering response to environmental changes in westerly winds across the Tarim Basin in the late Miocene to the early Pleistocene. Palaeogeography, Palaeoclimatology, Palaeoecology 386, 364–373.

Chen, H., Tang, D., Chen, S., Tang, S., 2022. Geochemical characteristics of mudstones from the lower cretaceous strata of the Jixi Basin, NE China: Implications for organic matter enrichment. International Journal of Coal Geology 249, 103904.

Chen, L., Jiang, S., Chen, P., Chen, X., Zhang, B., Zhang, G., Lin, W., Lu, Y., 2021a. Relative sea-level changes and organic matter enrichment in the Upper Ordovician-Lower Silurian Wufeng-Longmaxi Formations in the Central Yangtze area, China. Marine and Petroleum Geology 124, 104809.

Chen, Q., Li, Z., Dong, S., Yu, Q., Zhang, C., Yu, X., 2021b. Applicability of chemical weathering indices of eolian sands from the deserts in northern China. CATENA 198, 105032.

Chen, Z., Jiang, C., Lavoie, D., Reyes, J., 2016. Model-assisted Rock-Eval data interpretation for source rock evaluation: Examples from producing and potential shale gas resource plays. International Journal of Coal Geology 165, 290–302.

Chen, Z., Liu, X., Guo, Q., Jiang, C., Mort, A., 2017. Inversion of source rock hydrocarbon generation kinetics from Rock-Eval data. Fuel 194, 91–101.

Cheng, Q., Chen, X., Zhang, J., Ji, Y., Zhang, D., He, F., Shi, Y., Zhang, C., 2022. Organic geochemical characteristics and shale oil geological significance of E1f4 in the GY1 well, Guanzhen subsag, Subei basin. Arabian Journal of Geosciences 15, 1–13.

Cheng, Y., Liu, W., Wu, W., Zhang, Y., Tang, G., Liu, C., Nie, Q., Wen, Y., Lu, P., Zhang, C., 2021. Geochemical characteristics of the lower Cambrian Qiongzhusi Formation in Huize area, east Yunnan: implications for paleo-ocean environment and the origin of black rock series. Arabian Journal of Geosciences 14, 1–16.

Chiadikobi, K.C., Chaghanam, O.I., Omyemesili, O.C., Omoboriowo, A.O., 2018. Palynological Study of the Campano-Maastrichtian Nkporo Group of Anambra Basin, Southeastern, Nigeria. World News of Natural Sciences 20.

Chouhan, A.K., 2020. Structural fabric over the seismically active Kachchh rift basin, India: insight from world gravity model 2012. Environmental Earth Sciences 79, 1–14.

Chouhan, A.K., Choudhury, P., Pal, S.K., 2020a. New evidence for a thin crust and magmatic underplating beneath the Cambay rift basin, Western India through modelling of EIGEN-6C4 gravity data. Journal of Earth System Science 129, 1–16.

Chouhan, A.K., Singh, D., Pal, S.K., Choudhury, P., 2020b. Delineation of subsurface geological fractures in the Cambay rift and surrounding regions of NW India: an integrated approach using satellite derived EIGEN-6C4 gravity data. Geocarto International 1–16.

Chumakov, N.M., Zharkov, M.A., Herman, A.B., Doludenko, M.P., Kalandadze, N.N., Lebedev, E.L., Ponomarenko, A.G., Rautian, A.S., 1995. Climatic belts of the mid-Cretaceous time. Stratigraphy and Geological Correlation 3, 42–63.

Cordell, L., Grauch, V.J.S., 1985. Mapping basement magnetization zones from aeromagnetic data in the San Juan Basin, New Mexico. The Utility of Regional Gravity and Magnetic Anomaly Maps. Society of Exploration Geophysicists, 181–197.

Cox, R., Lowe, D.R., Cullers, R.L., 1995. The influence of sediment recycling and basement composition on evolution of mudrock chemistry in the southwestern United States. Geochimica et Cosmochimica Acta 59, 2919–2940.

Cratchley, C.R., Louis, P., Ajakaiye, D.E., 1984. Geophysical and geological evidence for the Benue-Chad Basin Cretaceous rift valley system and its tectonic implications. Journal of African Earth Sciences (1983) 2, 141–150.

de Castro, D.L., Fuck, R.A., Phillips, J.D., Vidotti, R.M., Bezerra, F.H., Dantas, E.L., 2014. Crustal structure beneath the Paleozoic Parnaíba Basin revealed by airborne gravity and magnetic data, Brazil. Tectonophysics 614, 128–145.

Dembicki Jr, H., 2009. Three common source rock evaluation errors made by geologists during prospect or play appraisals. AAPG Bulletin 93, 341–356.

Dilalos, S., Alexopoulos, J.D., Lozios, S., 2019. New insights on subsurface geological and tectonic structure of the Athens basin (Greece), derived from urban gravity measurements. Journal of Applied Geophysics 167, 73–105.

Dim, C.I., Okonkwo, I.A., Anyiam, O.A., Okeugo, C.G., Maduewesi, C.O., Okeke, K.K., Umeadi, I.M., 2020. Structural, Stratigraphic and Combination Traps on Outcropping Lithostratigraphic Units of the Anambra Basin, Southeast Nigeria. Petroleum & Coal 62.

Dim, C.I., Onuoha, K.M., Anyiam, O.A., Okwara, I.C., Oha, I.A., Okonkwo, I.A., Okeugo, C.G., Nkitnam, E.E., Ozumba, B.M., 2018. ANALYSIS OF PETROLEUM SYSTEM FOR EXPLORATION AND RISK REDUCTION IN THE SOUTHEASTERN INLAND BASINS OF NIGERIA. Petroleum & Coal 60.

Dim, C.I.P., Onuoha, K.M., Okeugo, C.G., Ozumba, B.M., 2017. Petroleum system elements within the Late Cretaceous and Early Paleogene sediments of Nigeria's inland basins: An integrated sequence stratigraphic approach. Journal of African Earth Sciences 130, 76–86.

Dim, C.I.P., Onuoha, K.M., Okwara, I.C., Okonkwo, I.A., Ibemesi, P.O., 2019. Facies analysis and depositional environment of the Campano–Maastrichtian coal-bearing Mamu Formation in the Anambra Basin, Nigeria. Journal of African Earth Sciences 152, 69–83.

Ding, W., Hou, D., Gan, J., Jiang, L., Zhang, Z., George, S.C., 2022. Sedimentary geochemical records of late Miocene-early Pliocene palaeovegetation and palaeoclimate evolution in the Ying-Qiong Basin, South China Sea. Marine Geology 106750.

Djomani, Y.P., Nnange, J.M., Diament, M., Ebinger, C.J., Fairhead, J.D., 1995. Effective elastic thickness and crustal thickness variations in west central Africa inferred from gravity data. Journal of Geophysical Research: Solid Earth 100, 22047–22070.

Downey, M.W., 2004. Oil and Natural Gas Exploration. In: Cleveland, C.J. (Ed.), Encyclopedia of Energy. Elsevier, New York, 549–558. https://doi.org/10.1016/B0-12-176480-X/00252-7

Dublin-Green, W.P., Agha, G.U., 1999. Future Petroleum Potential of Nigeria. Department of Petroleum Resources, Nigeria—Open File Reports, 17pp.

Edegbai, A.J., Schwark, L., Oboh-Ikuenobe, F.E., 2020. Nature of dispersed organic matter and paleoxygenation of the Campano-Maastrichtian dark mudstone unit, Benin flank, western Anambra Basin: Implications for Maastrichtian Trans-Saharan seaway paleoceanographic conditions. Journal of African Earth Sciences 162, 103654.

Edegbai, A.J., Schwark, L., Oboh-Ikuenobe, F.E., 2019a. A review of the latest Cenomanian to Maastrichtian geological evolution of Nigeria and its stratigraphic and paleogeographic implications. Journal of African Earth Sciences 150, 823–837. https://doi.org/10.1016/j.jafrearsci.2018.10.007

Edegbai, A.J., Schwark, L., Oboh-Ikuenobe, F.E., 2019b. Campano-Maastrichtian paleoenvironment, paleotectonics and sediment provenance of western Anambra Basin,

Nigeria: Multi-proxy evidences from the Mamu Formation. Journal of African Earth Sciences 156, 203–239.

Edegbai and Schwark, 2020. Differentiation of Sediment Source Regions in the Southern Benue Trough and Anambra Basin, Nigeria: Insights from Geochemistry of Upper Cretaceous Strata. Geology, Earth & Marine Sciences 2, 1–37. https://doi.org/10.31038/GEMS.2020224

Ejeh, O.I., 2021. Geochemistry of rocks (Late Cretaceous) in the Anambra Basin, SE Nigeria: insights into provenance, tectonic setting, and other palaeo-conditions. Heliyon 7, e08110.

Ekine, A.S., Onuoha, K.M., 2010. Seismic geohistory and differential interformational velocity analysis in the Anambra Basin, Nigeria. Earth Sciences Research Journal 14, 88–99.

Ekwueme, O.U., Obiora, D.N., Igwe, E.A., Abangwu, J.U., 2018. Study of aeromagnetic anomalies of Idah and Angba areas, north central Nigeria, using high resolution aeromagnetic data. Modeling Earth Systems and Environment 4, 461–474.

El Beialy, S.Y., Zobaa, M.K., Taha, A.A., 2016. Depositional paleoenvironment and hydrocarbon source potential of the Oligocene Dabaa Formation, north Western Desert, Egypt: A palynofacies approach. Geosphere 12, 346–353.

Elliot, M., Welsh, K., Chilcott, C., McCulloch, M., Chappell, J., Ayling, B., 2009. Profiles of trace elements and stable isotopes derived from giant long-lived Tridacna gigas bivalves: potential applications in paleoclimate studies. Palaeogeography, Palaeoclimatology, Palaeoecology 280, 132–142.

Ene, G.E., Okogbue, C.O., Onuoha, K.M., 2019. Evaluating the impact of hydrodynamic flow on the hydrocarbon potentials of the Cretaceous Anambra basin, Southeastern Nigeria. Arabian Journal of Geosciences 12, 644. https://doi.org/10.1007/s12517-019-4810-5

Ennen, C., Hall, S., 2011. Structural mapping of the Vinton salt dome, Louisiana, using gravity gradiometry data. SEG Technical Program Expanded Abstracts 2011. Society of Exploration Geophysicists, 830–835.

Espitalié, J., Deroo, G., Marquis, F., 1985. La pyrolyse Rock-Eval et ses applications. Deuxième partie. Revue de l'Institut Français Du Pétrole 40, 755–784.

Espitalie, J., Madec, M., Tissot, B., Mennig, J.J., Leplat, P., 1977. Source rock characterization method for petroleum exploration. Offshore Technology Conference. Offshore Technology Conference.

Eyike, A., Werner, S.C., Ebbing, J., Dicoum, E.M., 2010. On the use of global potential field models for regional interpretation of the West and Central African Rift System. Tectonophysics 492, 25–39.

Fairhead, J.D., 2020. Regional tectonics and basin formation: the role of potential field studies–an application to the Mesozoic West and Central African Rift System. Regional Geology and Tectonics. Elsevier, 541–556.

Fairhead, J.D., 2012. Regional tectonics and basin formation: The role of potential field studies. Regional Geology and Tectonics: Principles of Geologic Analysis 1, 331.

Fairhead, J.D., 1988. Mesozoic plate tectonic reconstructions of the central South Atlantic Ocean: the role of the West and Central African rift system. Tectonophysics 155, 181–191.

Fedo, C.M., Wayne Nesbitt, H., Young, G.M., 1995. Unraveling the effects of potassium metasomatism in sedimentary rocks and paleosols, with implications for paleoweathering conditions and provenance. Geology 23, 921–924.

Flinders, A.F., Ito, G., Garcia, M.O., 2010. Gravity anomalies of the Northern Hawaiian Islands: Implications on the shield evolutions of Kauai and Niihau. Journal of Geophysical Research: Solid Earth 115.

Förste, C., Bruinsma, S.L., Abrikosov, O., Lemoine, J.M., Marty, J.-C., Flechtner, F., Balmino, G., Barthelmes, F., Biancale, R.E., 2014. 6C4 The latest combined global gravity field model including GOCE data up to degree and order 2190 of GFZ Potsdam and GRGS Toulouse. GFZ Data Services.

Frazão, A., Silva, H.R. da, Russo, C.A. de M., 2015. The Gondwana breakup and the history of the Atlantic and Indian oceans unveils two new clades for early neobatrachian diversification. PloS One 10, e0143926.

Frynas, J.G., 1998. Political instability and business: focus on Shell in Nigeria. Third World Quarterly 19, 457–478.

Fu, X., Wang, J., Chen, W., Feng, X., Wang, D., Song, C., Zeng, S., 2016. Elemental geochemistry of the early Jurassic black shales in the Qiangtang Basin, eastern Tethys: constraints for palaeoenvironment conditions. Geological Journal 51, 443–454.

Gebhardt, H., 1998. Benthic Foraminifera from the Maastrichtian lower Mamu Formation near Leru (southern Nigeria); paleoecology and paleogeographic significance. The Journal of Foraminiferal Research 28, 76–89.

Genik, G.J., 1993. Petroleum geology of cretaceous-tertiary rift basins in Niger, Chad, and Central African Republic. AAPG Bulletin 77, 1405–1434.

Genik, G.J., 1992. Regional framework, structural and petroleum aspects of rift basins in Niger, Chad and the Central African Republic (CAR). Tectonophysics 213, 169–185.

Goldberg, K., Humayun, M., 2016. Geochemical paleoredox indicators in organic-rich shales of the Irati Formation, Permian of the Paraná Basin, southern Brazil. Brazilian Journal of Geology 46, 377–393.

Götz, A.E., Feist-Burkhardt, S., Ruckwied, K., 2008. Palynofacies and sea-level changes in the Upper Cretaceous of the Vocontian Basin, southeast France. Cretaceous Research 29, 1047–1057.

Grauch, V.J.S., Cordell, L., 1987. Limitations of determining density or magnetic boundaries from the horizontal gradient of gravity or pseudogravity data. Geophysics 52, 118–121.

Guo, L., Gao, R., 2018. Potential-field evidence for the tectonic boundaries of the central and western Jiangnan belt in South China. Precambrian Research 309, 45–55.

Guo, L., Jiang, Z., Zhang, J., Li, Y., 2011. Paleoenvironment of Lower Silurian black shale and its significance to the potential of shale gas, southeast of Chongqing, China. Energy Exploration & Exploitation 29, 597–616.

Haack, R.C., Sundararaman, P., Diedjomahor, J.O., Xiao, H., Gant, N.J., May, E.D., Kelsch, K., 2000. AAPG Memoir 73, Chapter 16: Niger Delta Petroleum Systems, Nigeria.

Hallberg, R.O., 1976. A geochemical method for investigation of palaeoredox conditions in sediments. Ambio Special Report 4, 139–147.

Han, S., Zhang, Y., Huang, J., Rui, Y., Tang, Z., 2020. Elemental Geochemical Characterization of Sedimentary Conditions and Organic Matter Enrichment for Lower Cambrian Shale Formations in Northern Guizhou, South China. Minerals 10, 793.

Harnois, L., 1988. The CIW index: a new chemical index of weathering. Sedimentary Geology 55, 319–322.

Harouna, M., Philp, R.P., 2012. Potential petroleum source rocks in the Termit Basin, Niger. Journal of Petroleum Geology 35, 165–185.

Hatch, J.R., Leventhal, J.S., 1992. Relationship between inferred redox potential of the depositional environment and geochemistry of the Upper Pennsylvanian (Missourian)

Stark Shale Member of the Dennis Limestone, Wabaunsee County, Kansas, USA. Chemical Geology 99, 65–82.

Hay, W.W., Floegel, S., 2012. New thoughts about the Cretaceous climate and oceans. Earth-Science Reviews 115, 262–272.

Herron, M.M., 1988. Geochemical classification of terrigenous sands and shales from core or log data. Journal of Sedimentary Research 58, 820–829.

Hope, J., Eaton, D., 2002. Crustal structure beneath the Western Canada Sedimentary Basin: constraints from gravity and magnetic modelling. Canadian Journal of Earth Sciences 39, 291–312.

Hu, J., Li, Q., Song, C., Wang, S., Shen, B., 2017. Geochemical characteristics of the Permian sedimentary rocks from Qiangtang Basin: constraints for paleoenvironment and paleoclimate. Terrestrial, Atmospheric and Oceanic Sciences 28, 271–282.

Hu, W., Hao, T., Jiang, W., Xu, Y., Zhao, B., Jiang, D., 2015. An integrated geophysical study on the Mesozoic strata distribution and hydrocarbon potential in the South China Sea. Journal of Asian Earth Sciences 111, 31–43.

Huang, H., He, D., Li, D., Li, Y., Zhang, W., Chen, J., 2020. Geochemical characteristics of organic-rich shale, Upper Yangtze Basin: Implications for the Late Ordovician–Early Silurian orogeny in South China. Palaeogeography, Palaeoclimatology, Palaeoecology 554, 109822.

Huguet, C., de Lange, G.J., Gustafsson, Ö., Middelburg, J.J., Damsté, J.S.S., Schouten, S., 2008. Selective preservation of soil organic matter in oxidized marine sediments (Madeira Abyssal Plain). Geochimica et Cosmochimica Acta 72, 6061–6068.

Hunt, J.M., 1996. Petroleum geology and geochemistry.

Ilevbare, M., Omodolor, H.E., 2020. Ancient deposition environment, mechanism of deposition and textural attributes of Ajali Formation, western flank of the Anambra Basin, Nigeria. Case Studies in Chemical and Environmental Engineering 2, 100022.

Isyaku, A.A., 2018. Lithostratigraphy and tectonic evolution of the north-eastern Bornu basin, from integrated surface and subsurface interpretation. PhD Thesis. University of Portsmouth United Kingdom.

Jacobsen, B.H., 1987. A case for upward continuation as a standard separation filter for potential-field maps. Geophysics 52, 1138–1148.

Jarvie, D.M., 2012. Shale resource systems for oil and gas: Part 2—Shale-oil resource systems.

Jarvie, D.M., Morelos, A., Han, Z., 2001. Detection of pay zones and pay quality, Gulf of Mexico: Application of geochemical techniques.

Jones, B., Manning, D.A., 1994. Comparison of geochemical indices used for the interpretation of palaeoredox conditions in ancient mudstones. Chemical Geology 111, 111–129.

Kahmann, J.A., Seaman III, J., Driese III, S.G., 2008. Evaluating trace elements as paleoclimate indicators: multivariate statistical analysis of late Mississippian Pennington Formation paleosols, Kentucky, USA. The Journal of Geology 116, 254–268.

Kahveci, M., Çırmık, A., Doğru, F., Pamukçu, O., Gönenç, T., 2019. Subdividing the tectonic elements of Aegean and Eastern Mediterranean with gravity and GPS data. Acta Geophysica 67, 491–500.

Kamguia, J., Manguelle-Dicoum, E., Tabod, C.T., Tadjou, J.M., 2005. Geological models deduced from gravity data in the Garoua basin, Cameroon. Journal of Geophysics and Engineering 2, 147–152.

Karcol, R., Mikuška, J., Marušiak, I., 2017. Normal earth gravity field versus gravity effect of layered ellipsoidal model. Understanding the Bouguer Anomaly. Elsevier, 63–77.

Khazri, D., Gabtni, H., 2018. Geophysical methods integration for deep aquifer reservoir characterization and modeling (Sidi Bouzid basin, central Tunisia). Journal of African Earth Sciences 138, 289–308.

Kidder, D.L., Erwin, D.H., 2001. Secular distribution of biogenic silica through the Phanerozoic: comparison of silica-replaced fossils and bedded cherts at the series level. The Journal of Geology 109, 509–522.

Kloss, T.J., Dornbos, S.Q., Chen, J.-Y., McHenry, L.J., Marenco, P.J., 2015. High-resolution geochemical evidence for oxic bottom waters in three Cambrian Burgess Shale-type deposits. Palaeogeography, Palaeoclimatology, Palaeoecology 440, 90–95.

Krzeszowska, E., 2019. Geochemistry of the Lublin Formation from the Lublin Coal Basin: Implications for weathering intensity, palaeoclimate and provenance. International Journal of Coal Geology 216, 103306.

Kumar, S., Ojha, K., Bastia, R., Garg, K., Das, S., Mohanty, D., 2017. Evaluation of Eocene source rock for potential shale oil and gas generation in north Cambay Basin, India. Marine and Petroleum Geology 88, 141–154.

Kumar, U., Narayan, S., Pal, S.K., 2020. Structural and tectonic interpretation of EGM2008 gravity data around the Laccadive ridge in the Western Indian Ocean: an implication to continental crust. Geocarto International 1–20.

Kumar, U., Narayan, S., Pal, S.K., 2019. New insights on structure and tectonics over the Laxmi Ridge using EIGEN6C4 modelled gravity data.

Ladant, J.-B., Poulsen, C.J., Fluteau, F., Tabor, C.R., MacLeod, K.G., Martin, E.E., Haynes, S.J., Rostami, M.A., 2020. Paleogeographic controls on the evolution of Late Cretaceous ocean circulation. Climate of the Past 16, 973–1006.

Lai, H., Li, M., Liu, J., Mao, F., Xiao, H., He, W., Yang, L., 2018. Organic geochemical characteristics and depositional models of Upper Cretaceous marine source rocks in the Termit Basin, Niger. Palaeogeography, Palaeoclimatology, Palaeoecology 495, 292–308. https://doi.org/10.1016/j.palaeo.2018.01.024

Langford, F.F., Blanc-Valleron, M.-M., 1990. Interpreting Rock-Eval pyrolysis data using graphs of pyrolizable hydrocarbons vs. total organic carbon. AAPG Bulletin 74, 799–804.

Lehmann, M.F., Bernasconi, S.M., Barbieri, A., McKenzie, J.A., 2002. Preservation of organic matter and alteration of its carbon and nitrogen isotope composition during simulated and in situ early sedimentary diagenesis. Geochimica et Cosmochimica Acta 66, 3573–3584.

Leyuan, F., Jiapeng, W., Wan, D., Yang, L.I., 2021. Sedimentary characteristics of the shallow water delta in rifted lacustrine basin: A case study in the Aradeiba Formation, Unity Sag, Muglad Basin. Earth Science Frontiers 28, 155.

Li, D., Li, R., Zhu, Z., Wu, X., Liu, F., Zhao, B., Cheng, J., Wang, B., 2018a. Elemental characteristics and paleoenvironment reconstruction: a case study of the Triassic lacustrine Zhangjiatan oil shale, southern Ordos Basin, China. Acta Geochimica 37, 134–150.

Li, D., Li, R., Zhu, Z., Xu, F., 2018b. Elemental characteristics of lacustrine oil shale and its controlling factors of palaeo-sedimentary environment on oil yield: a case from Chang 7 oil layer of Triassic Yanchang Formation in southern Ordos Basin. Acta Geochimica 37, 228–243.

Li, H., Liu, B., Liu, X., Meng, L., Cheng, L., Wang, H., 2019. Mineralogy and inorganic geochemistry of the Es4 shales of the Damintun Sag, northeast of the Bohai Bay Basin: Implication for depositional environment. Marine and Petroleum Geology 110, 886–900.

Li, L.-Q., Wang, Y.-D., Vajda, V., 2021a. Palynofacies analysis for interpreting paleoenvironment and hydrocarbon potential of Triassic–Jurassic strata in the Sichuan Basin, China. Palaeoworld 30, 126–137.

Li, Q., Wu, S., Xia, D., You, X., Zhang, H., Lu, H., 2020a. Major and trace element geochemistry of the lacustrine organic-rich shales from the Upper Triassic Chang 7 Member in the southwestern Ordos Basin, China: Implications for paleoenvironment and organic matter accumulation. Marine and Petroleum Geology 111, 852–867. https://doi.org/10.1016/j.marpetgeo.2019.09.003

Li, T.-J., Huang, Z.-L., Chen, X., Li, X.-N., Liu, J.-T., 2021b. Paleoenvironment and organic matter enrichment of the Carboniferous volcanic-related source rocks in the Malang Sag, Santanghu Basin, NW China. Petroleum Science 18, 29–53.

Li, X., Gang, W., Yao, J., Gao, G., Wang, C., Li, J., Liu, Y., Guo, Y., Yang, S., 2020b. Major and trace elements as indicators for organic matter enrichment of marine carbonate rocks: A case study of Ordovician subsalt marine formations in the central-eastern Ordos Basin, North China. Marine and Petroleum Geology 111, 461–475.

Liu, B., Wan, L., Mao, F., Liu, J., Lü, M., Wang, Y., 2015. Hydrocarbon potential of Upper Cretaceous marine source rocks in the Termit Basin, Niger. Journal of Petroleum Geology 38, 157–175.

Liu, Z., Zhao, Y., Colin, C., Siringan, F.P., Wu, Q., 2009. Chemical weathering in Luzon, Philippines from clay mineralogy and major-element geochemistry of river sediments. Applied Geochemistry 24, 2195–2205.

Long, X., Yuan, C., Sun, M., Xiao, W., Wang, Y., Cai, K., Jiang, Y., 2012. Geochemistry and Nd isotopic composition of the Early Paleozoic flysch sequence in the Chinese Altai, Central Asia: evidence for a northward-derived mafic source and insight into Nd model ages in accretionary orogen. Gondwana Research 22, 554–566.

Loubser, M., Verryn, S., 2008. Combining XRF and XRD analyses and sample preparation to solve mineralogical problems. South African Journal of Geology 111, 229–238. https://doi.org/10.2113/gssajg.111.2-3.229

Loucks, R.G., Ruppel, S.C., 2007. Mississippian Barnett Shale: Lithofacies and depositional setting of a deep-water shale-gas succession in the Fort Worth Basin, Texas. AAPG Bulletin 91, 579–601.

Lowrie, W., 2007. Fundamentals of Geophysics. Published in the United States of America by Cambridge University Press. New York 393.

Ma, B., Ji, L., Jin, P., Zhang, M., Yuan, B., Long, L., 2022. Geochemical characteristics and depositional paleoenvironment of source rocks from the Lower Cretaceous Chijinbao Formation in Jiuxi Basin, China. Journal of Petroleum Science and Engineering 210, 109968.

Macgregor, D.S., 1995. Hydrocarbon habitat and classification of inverted rift basins. Geological Society, London, Special Publications 88, 83–93.

Mahmoud, M.S., Deaf, A.S., Tamam, M.A., Khalaf, M.M., 2017. Palynofacies analysis and palaeoenvironmental reconstruction of the Upper Cretaceous sequence drilled by the Salam-60 well, Shushan Basin: implications on the regional depositional environments and hydrocarbon exploration potential of north-western Egypt. Revue de Micropaléontologie 60, 449–467.

Martinez-Ruiz, F., Kastner, M., Gallego-Torres, D., Rodrigo-Gámiz, M., Nieto-Moreno, V., Ortega-Huertas, M., 2015. Paleoclimate and paleoceanography over the past 20,000 yr in the Mediterranean Sea Basins as indicated by sediment elemental proxies. Quaternary Science Reviews 107, 25–46.

Mastalerz, M., Schimmelmann, A., Lis, G.P., Drobniak, A., Stankiewicz, A., 2012. Influence of maceral composition on geochemical characteristics of immature shale kerogen: Insight from density fraction analysis. International Journal of Coal Geology 103, 60–69.

Mauri, G., Husein, A., Mazzini, A., Irawan, D., Sohrabi, R., Hadi, S., Prasetyo, H., Miller, S.A., 2018. Insights on the structure of Lusi mud edifice from land gravity data. Marine and Petroleum Geology 90, 104–115.

McLennan, S.M., Hemming, S., McDaniel, D.K., Hanson, G.N., 1993. Geochemical approaches to sedimentation, provenance, and tectonics. Special Papers-Geological Society of America 21–21.

Miall, A.D., 2013. Principles of sedimentary basin analysis. Springer Science & Business Media.

Miall, A.D., 2006. Reconstructing the architecture and sequence stratigraphy of the preserved fluvial record as a tool for reservoir development: A reality check. AAPG Bulletin 90, 989–1002.

Miall, A.D., 1988. Architectural elements and bounding surfaces in fluvial deposits: anatomy of the Kayenta Formation (Lower Jurassic), southwest Colorado. Sedimentary Geology 55, 233–262.

Miall, A.D., 1977. Lithofacies types and vertical profile models in braided river deposits: a summary.

Mode, A.W., Anyiam, O.A., Anigbogu, E.C., 2016. The effect of diagenesis on reservoir quality of Mamu Sandstone, Anambra Basin, Nigeria. Journal of the Geological Society of India 87, 583–590.

Mohamed, A.Y., Pearson, M.J., Ashcroft, W.A., Iliffe, J.E., Whiteman, A.J., 1999. Modeling petroleum generation in the Southern Muglad rift basin, Sudan. AAPG Bulletin 83, 1943–1964.

Mohammed, S., 2020. Geochemical evaluation of source rock potential and characterization of hydrocarbon occurrences in the Eastern Dahomey Basin, Nigeria.

Mohammed, S., Opuwari, M., Titinchi, S., 2020. Source rock evaluation of Afowo clay type from the Eastern Dahomey Basin, Nigeria: insights from different measurements. Scientific Reports 10, 1–13.

Mohammed, S., Opuwari, M., Titinchi, S., Bata, T., Abubakar, M.B., 2019. Evaluation of source rock potential and hydrocarbon composition of oil sand and associated clay deposits from the Eastern Dahomey Basin, Nigeria. Journal of African Earth Sciences 160, 103603.

Monday, T.U., Salihu, M., 2017. Crude oil and the politics of Nigerian foreign policy: Issues and explanations. Res Human Soc Sci 7, 38.

Moradi, A.V., Sarı, A., Akkaya, P., 2016. Geochemistry of the Miocene oil shale (Hançili Formation) in the Çankırı-Çorum Basin, Central Turkey: Implications for Paleoclimate conditions, source–area weathering, provenance and tectonic setting. Sedimentary Geology 341, 289–303.

Nath, B.N., Bau, M., Rao, B.R., Rao, C.M., 1997. Trace and rare earth elemental variation in Arabian Sea sediments through a transect across the oxygen minimum zone. Geochimica et Cosmochimica Acta 61, 2375–2388.

Ndip, E.A., Agyingi, C.M., Nton, M.E., Hower, J.C., Oladunjoye, M.A., 2019. Organic petrography and petroleum source rock evaluation of the Cretaceous Mamfe Formation, Mamfe basin, southwest Cameroon. International Journal of Coal Geology 202, 27–37.

Nesbitt, H.W., Young, G.M., 1984. Prediction of some weathering trends of plutonic and volcanic rocks based on thermodynamic and kinetic considerations. Geochimica et Cosmochimica Acta 48, 1523–1534.

Nesbitt, Hw., Young, G.M., 1982. Early Proterozoic climates and plate motions inferred from major element chemistry of lutites. Nature 299, 715–717.

Njeudjang, K., Essi, J.M.A., Kana, J.D., Teikeu, W.A., Nouck, P.N., Djongyang, N., Tchinda, R., 2020. Gravity investigation of the Cameroon Volcanic Line in Adamawa region: Geothermal features and structural control. Journal of African Earth Sciences 165, 103809.

Nwachukwu, S.O., 1972. The tectonic evolution of the the southern portion of the Benue Trough, Nigeria. Geological Magazine 109, 411–419.

Nwajide, C.S., 2013. Geology of Nigeria's sedimentary basins. CSS Bookshop Limited.

Nwajide, C.S., 2005. Anambra Basin of Nigeria: synoptic basin analysis as a basis for evaluating its hydrocarbon prospectivity. Hydrocarbon Potentials of the Anambra Basin, PTDF Chair 2–46.

Nwajide, C.S., 1990. Cretaceous sedimentation and paleogeography of the central Benue Trough. The Benue. Tough Structure and Evolution International Monograph Series, Braunschweig 19–38.

Nwajide, C.S., 1980. Eocene tidal sedimentation in the Anambra Basin, southern Nigeria. Sedimentary Geology 25, 189–207.

Nwajide, C.S., Reijers, T.J.A., 1996. Geology of the southern Anambra Basin. Selected Chapters on Geology, SPDC, Warri 133–148.

Obaje, N.G., 2009. Geology and mineral resources of Nigeria. Springer.

Obaje, N.G., Wehner, H., Scheeder, G., Abubakar, M.B., Jauro, A., 2004. Hydrocarbon prospectivity of Nigeria's inland basins: From the viewpoint of organic geochemistry and organic petrology. AAPG Bulletin 88, 325–353.

Obasi, A.I., Selemo, A.O.I., Nomeh, J.S., 2018. Gravity models as tool for basin boundary demarcation: A case study of Anambra Basin, Southeastern Nigeria. Journal of Applied Geophysics 156, 31–43.

Obi, G.C., Okogbue, C.O., 2004. Sedimentary response to tectonism in the Campanian–Maastrichtian succession, Anambra Basin, southeastern Nigeria. Journal of African Earth Sciences 38, 99–108.

Obi, G.C., Okogbue, C.O., Nwajide, C.S., 2001. Evolution of the Enugu Cuesta: a tectonically driven erosional process. Global Journal of Pure and Applied Sciences 7, 321–330.

Obiora, D.N., Ossai, M.N., Okwoli, E., 2015. A case study of aeromagnetic data interpretation of Nsukka area, Enugu State, Nigeria, for hydrocarbon exploration. International Journal of Physical Sciences 10, 503–519.

Oboh-Ikuenobe, F.E., Obi, C.G., Jaramillo, C.A., 2005. Lithofacies, palynofacies, and sequence stratigraphy of Palaeogene strata in Southeastern Nigeria. Journal of African Earth Sciences 41, 79–101. https://doi.org/10.1016/j.jafrearsci.2005.02.002

Ocheli, A., Okoro, A.U., Ogbe, O.B., Aigbadon, G.O., 2018. Granulometric and pebble morphometric applications to Benin Flank sediments in western Anambra Basin, Nigeria: proxies for paleoenvironmental reconstruction. Environmental Monitoring and Assessment 190, 1–17.

Odunze, O.S., Obi, S.G.C., 2011. Sequence stratigraphic framework of the Imo Formation in the Southern Benue Trough. Journal of Mining and Geology 47, 135–146.

Odunze, S.O., Obi, G.C., Yuan, W., Min, L., 2013. Sedimentology and sequence stratigraphy of the Nkporo Group (Campanian–Maastrichtian), Anambra Basin, Nigeria. Journal of Palaeogeography 2, 192–208.

Ofoegbu, C.O., 1985. A review of the geology of the Benue Trough, Nigeria. Journal of African Earth Sciences (1983) 3, 283–291.

Ogala, J.E., 2011. Hydrocarbon potential of the Upper Cretaceous coal and shale units in the Anambra Basin, Southeastern Nigeria. Petroleum and Coal 53, 35–44.

Oguama, B.E., Okeke, F.N., Obiora, D.N., 2021. Mapping of subsurface structural features in some parts of Anambra Basin, Nigeria, using aeromagnetic data. Modeling Earth Systems and Environment 7, 1623–1637.

Ogungbesan, G.O., Adedosu, T.A., 2020. Geochemical record for the depositional condition and petroleum potential of the Late Cretaceous Mamu Formation in the western flank of Anambra Basin, Nigeria. Green Energy & Environment 5, 83–96.

Ojo, O.J., Akande, S.O., 2008. Microfloral assemblage, age and paleoenvironment of the upper Cretaceous Patti Formation, southeastern Bida Basin, Nigeria. Journal of Mining and Geology 44, 71–81.

Ojo, O.J., Bamidele, T.E., Adepoju, S.A., Akande, S.O., 2021. Genesis and paleoenvironmental analysis of the ironstone facies of the Maastrichtian Patti Formation, Bida Basin, Nigeria. Journal of African Earth Sciences 174, 104058. https://doi.org/10.1016/j.jafrearsci.2020.104058

Ojo, O.J., Jimoh, A.Y., Umelo, J.C., Akande, S.O., 2020. Organic geochemical and palynological studies of the Maastrichtian source rock intervals in Bida Basin, Nigeria: implications for hydrocarbon prospectivity. Journal of Petroleum Exploration and Production Technology 10, 3191–3206.

Okorie, A.C., Obiora, D.N., Igwe, E., 2019. Geophysical study of Ubiaja and Illushi area in northern Anambra basin, Nigeria, using combined interpretation methods of aeromagnetic data. Modeling Earth Systems and Environment 5, 1071–1082.

Okwara, I.C., Dim, C.I.P., Anyiam, O.A., 2020. Reservoir evaluation within the sequence stratigraphic framework of the Upper Cretaceous Anambra Basin, Nigeria. Journal of African Earth Sciences 162, 103708.

Olabode, S.O., 2014. Soft sediment deformation structures in the maastrichtian ajali formation western flank of anambra basin, Southern Nigeria. Journal of African Earth Sciences 89, 16–30.

Ola-Buraimo, A.O., Akaegbobi, I.M., 2013. Palynological evidence of the oldest (Albian) sediment in the Anambra Basin, southeastern Nigeria. Journal of Biological and Chemical Research 30, 387–408.

Olade, M.A., 1975. Evolution of Nigeria's Benue Trough (Aulacogen): a tectonic model. Geological Magazine 112, 575–583.

Omietimi, E.J., Chouhan, A.K., Lenhardt, N., Yang, R., Bumby, A.J., 2021. Structural interpretation of the south-western flank of the Anambra Basin (Nigeria) using satellite-derived WGM 2012 gravity data. Journal of African Earth Sciences 104290.

Omietimi, E.J., Lenhardt, N., Yang, R., Götz, A.E., Bumby, A.J., 2022. Sedimentary geochemistry of Late Cretaceous-Paleocene deposits at the south-western margin of the Anambra Basin (Nigeria): Implications for paleoenvironmental reconstructions. Palaeogeogr. Palaeoclimatol. Palaeoecol. 600,111059. https://doi.org/10.1016/j.palaeo.2022.111059

Onoduku, U., Okosun, E., Obaje, N., Goro, I., Salihu, H., Chukwuma-Orji, J., 2017. Palynological Evidence of a Campanian-Maastrichtian Age of the Central Bida Basin, Nigeria: Implication for Paleoenvironment, Paleoclimate and Hydrocarbon Prospectivity. Minna Journal of Geosciences 1, 165–178.

Onuigbo, E.N., Etu-Efeotor, J.O., Okoro, A.U., 2012. Palynology, paleoenvironment and sequence stratigraphy of the campanian-maastrichtian deposits in the anambra basin, Southeastern Nigeria. European Journal of Scientific Research 78, 333–348.

Onuoha, K.M., 1999. Structural features of Nigeria's coastal margin: an assessment based on age data from wells. Journal of African Earth Sciences 29, 485–499.

Onuoha, K.M., Ekine, A.S., 1999. Subsurface temperature variations and heat flow in the Anambra Basin, Nigeria. Journal of African Earth Sciences 28, 641–652.

Onwuemesi, A.G., 1997. One-dimensional spectral analysis of aeromagnetic anomalies and Curie depth isotherm in the Anambra Basin of Nigeria. Journal of Geodynamics 23, 95–107.

Overare, B., Osokpor, J., Ekeh, P.C., Azmy, K., 2020. Demystifying provenance signatures and paleo-depositional environment of mudrocks in parts of south-eastern Nigeria: Constraints from geochemistry. Journal of African Earth Sciences 172, 103954.

Parker, A., 1970. An index of weathering for silicate rocks. Geological Magazine 107, 501–504.

Parmera, T.C., Gallo, V., SILVA, H. and FIGUEIREDO, F.J., 2017. Distributional patterns of Aptian-Albian paleoichthyofauna of Brazil and Africa based on Track Analysis. Anais da Academia Brasileira de Ciências, 91(suppl2), 1-12.

Parthasarathy, P., Madhavaraju, J., Montoya, E.R., Ramasamy, S., 2020. Geochemistry of estuarine sediments from Marakkanam area, Tamil Nadu, India: source area weathering and provenance implications. Arabian Journal of Geosciences 13, 1–13.

Pavlis, N.K., Holmes, S.A., Kenyon, S.C., Factor, J.K., 2012. The development and evaluation of the Earth Gravitational Model 2008 (EGM2008). Journal of Geophysical Research: Solid Earth 117.

Pehlivanli, B.Y., 2019. Factors controlling the paleo-sedimentary conditions of Çeltek oil shale, Sorgun-Yozgat/Turkey. Maden Tetkik ve Arama Dergisi 158, 251–263.

Perner, M.J., 2018. Evolution of palaeoenvironment, kerogen composition and thermal history in the Cenozoic of the northern Upper Rhine Graben, SW-Germany. PhD Thesis. Universität Heidelberg.

Peters, K.E., Cassa, M.R., 1994. Applied source rock geochemistry: Chapter 5: Part II. Essential elements.

Petit, C., Déverchère, J., Calais, E., San'kov, V., Fairhead, D., 2002. Deep structure and mechanical behavior of the lithosphere in the Hangai–Hövsgöl region, Mongolia: new constraints from gravity modeling. Earth and Planetary Science Letters 197, 133–149.

Pilkington, M., Keating, P., 2004. Contact mapping from gridded magnetic data? A comparison of techniques. Exploration Geophysics 35, 306–311.

Qiao, J., Liu, L., An, F., Xiao, F., Wang, Y., Wu, K., Zhao, Y., 2016. Hydrocarbon potential evaluation of the source rocks from the Abu Gabra Formation in the Sufyan Sag, Muglad Basin, Sudan. Journal of African Earth Sciences 118, 301–312.

Rani, K., Guha, A., Mondal, S., Pal, S.K., Kumar, K.V., 2019. ASTER multispectral bands, ground magnetic data, ground spectroscopy and space-based EIGEN6C4 gravity data model for identifying potential zones for gold sulphide mineralization in Bhukia, Rajasthan, India. Journal of Applied Geophysics 160, 28–46.

Reijers, T.J.A., Petters, S.W., Nwajide, C.S., 1997. Chapter 7 The niger delta basin. In: Selley, R.C. (Ed.), Sedimentary Basins of the World, African Basins. Elsevier, 151–172. https://doi.org/10.1016/S1874-5997(97)80010-X

Riad, S., 1977. Shear zones in north Egypt interpreted from gravity data. Geophysics 42, 1207–1214.

Rimmer, S.M., 2004. Geochemical paleoredox indicators in Devonian–Mississippian black shales, Central Appalachian Basin (USA). Chemical Geology, Geochemistry of Organic-Rich Shales: New Perspectives 206, 373–391. https://doi.org/10.1016/j.chemgeo.2003.12.029

Rudnick, R.L., Gao, S., 2003. 3.01 - Composition of the Continental Crust. In: Holland, H.D., Turekian, K.K. (Eds.), Treatise on Geochemistry. Pergamon, Oxford, 1–64. https://doi.org/10.1016/B0-08-043751-6/03016-4

Sahoo, S.D., Pal, S.K., 2021. Crustal structure and Moho topography of the southern part (18° S–25° S) of Central Indian Ridge using high-resolution EIGEN6C4 global gravity model data. Geo-Marine Letters 41, 1–20.

Sahoo, S.D., Pal, S.K., 2019. Mapping of Structural Lineaments and Fracture Zones around the Central Indian Ridge (10° S–21° S) using EIGEN 6C4 Bouguer Gravity Data. Journal of the Geological Society of India 94, 359–366.

Saibi, H., Amrouche, M., Fowler, A.-R., 2019. Deep cavity systems detection in Al-Ain City, UAE, based on gravity surveys inversion. Journal of Asian Earth Sciences 182, 103937.

SANS 7404–3 (2016)/ISO 7404-3, 2009. Methods for the Petrographic Analysis of Bituminous Coal and Anthracite. Part 3: Method of Determining Maceral Group Composition. [WWW Document], ISO. URL https://www.iso.org/cms/render/live/en/sites/isoorg/contents/data/standard/01/41/14129.html (accessed 10.4.21).

Schoenborn, W.A., Fedo, C.M., 2011. Provenance and paleoweathering reconstruction of the Neoproterozoic Johnnie Formation, southeastern California. Chemical Geology 285, 231–255.

Scotese, C.R., Song, H., Mills, B.J., van der Meer, D.G., 2021. Phanerozoic paleotemperatures: The earth's changing climate during the last 540 million years. Earth-Science Reviews 103503.

Selley, R.C., 1997. Sedimentary basins of africa introduction and acknowledgements. Sedimentary Basins of the World. Elsevier, IX–XI.

Sellwood, B.W., Valdes, P.J., 2006. Mesozoic climates: General circulation models and the rock record. Sedimentary Geology 190, 269–287.

Simpson, A., 1954. The geology of parts of Onitsha, Owerri and Benue Provinces. Bull Geol Survey Nigeria 24, 1–85.

Singh, V.P., Singh, B.D., Singh, A., Singh, M.P., Mathews, R.P., Dutta, S., Mendhe, V.A., Mahesh, S., Mishra, S., 2017. Depositional palaeoenvironment and economic potential of Khadsaliya lignite deposits (Saurashtra Basin), western India: based on petrographic, palynofacies and geochemical characteristics. International Journal of Coal Geology 171, 223–242.

Sprague, R.A., Melvin, J.A., Conradi, F.G., Pearce, T.J., Dix, M.A., Hill, S.D., Canham, H., 2009. Integration of core-based chemostratigraphy and petrography of the Devonian Jauf Sandstones, Uthmaniya area, Ghawar field, eastern Saudi Arabia. Search and Discovery Article 20065, 34.

Takamatsu, T., Kawai, T., Nishikawa, M., 2000. Elemental composition of short sediment cores and ferromanganese concretions from Lake Baikal. Lake Baikal. Elsevier, 155–164.

Talwani, M., Heirtzler, J.R., 1964. Computation of magnetic anomalies caused by two-dimensional structures of arbitrary shape: Stanford University Publications of the Geological Sciences. Computers in the Mineral Industries.

Talwani, M., Worzel, J.L., Landisman, M., 1959. Rapid gravity computations for two-dimensional bodies with application to the Mendocino submarine fracture zone. Journal of Geophysical Research 64, 49–59.

Tan, M., Zhu, X., Geng, M., Zhu, S., Liu, W., 2017. The occurrence and transformation of lacustrine sediment gravity flow related to depositional variation and paleoclimate in the Lower Cretaceous Prosopis Formation of the Bongor Basin, Chad. Journal of African Earth Sciences 134, 134–148. https://doi.org/10.1016/j.jafrearsci.2017.06.003

Tao, S., Xu, Y., Tang, D., Xu, H., Li, S., Chen, S., Liu, W., Cui, Y., Gou, M., 2017. Geochemistry of the Shitoumei oil shale in the Santanghu Basin, Northwest China: Implications for paleoclimate conditions, weathering, provenance and tectonic setting. International Journal of Coal Geology 184, 42–56.

Taylor, S.R., McLennan, S.M., 1985. The continental crust: its composition and evolution.

Teng, G.E., 2004. The Distribution of elements, carbon and oxygen isotopes on Marine Strata and environmental correlation between they and hydrocarbon source rocks formation an example from Ordovician Basin, China. Graduate School of Chinese Academy of Sciences (Lanzhou Institute of Geology), Lanzhou.

Teng, G.E., Liu, W.H., Xu, Y.C., Chen, J.F., 2005. Correlative study on parameters of inorganic geochemistry and hydrocarbon source rocks formative environment. Advances in Earth Sciences 20, 193–200.

Tijani, M.N., Nton, M.E., 2009. Hydraulic, textural and geochemical characteristics of the Ajali Formation, Anambra Basin, Nigeria: implication for groundwater quality. Environmental Geology 56, 935–951.

Tijani, M.N., Nton, M.E., Kitagawa, R., 2010. Textural and geochemical characteristics of the Ajali Sandstone, Anambra Basin, SE Nigeria: implication for its provenance. Comptes Rendus Geoscience 342, 136–150.

Tissot, B.P., Welte, D.H., 1984. From kerogen to petroleum. Petroleum Formation and Occurrence. Springer, 160–198.

Titi, Y.L.A., Minarto, E., 2017. The subsurface three-dimensional modeling of volcano arc of Flores island based on gravity data analysis. AIP Conference Proceedings. AIP Publishing LLC, 030106.

Toyoda, K., 1993. Geochemical history of ancient Lake Biwa in Japan—chemical indicators of sedimentary paleo-environments in a drilled core. Palaeogeography, Palaeoclimatology, Palaeoecology 101, 169–184.

Tribovillard, N., Algeo, T.J., Lyons, T., Riboulleau, A., 2006. Trace metals as paleoredox and paleoproductivity proxies: an update. Chemical Geology 232, 12–32.

Trurnit, P., 1988. Growth and breakup of supercontinents and evolution of oceans and continental margins during the global tectonic megacycles. GeoJournal 17, 37–73.

Tuttle, M.L., Charpentier, R.R., Brownfield, M.E., 1999. The Niger Delta Petroleum System: Niger Delta Province, Nigeria, Cameroon, and Equatorial Guinea, Africa. US Department of the Interior, US Geological Survey.

Tyson, R.V., 2001. Sedimentation rate, dilution, preservation and total organic carbon: some results of a modelling study. Organic Geochemistry 32, 333–339.

Tyson, R.V., 1995. Abundance of organic matter in sediments: TOC, hydrodynamic equivalence, dilution and flux effects. Sedimentary Organic Matter. Springer, 81–118.

Tyson, R.V., 1993. Palynofacies analysis. Applied Micropalaeontology. Springer, 153–191.

Uwakonye, M.N., Osho, G.S., Anucha, H., 2011. The Impact Of Oil And Gas Production On The Nigerian Economy: A Rural Sector Econometric Model. International Business & Economics Research Journal (IBER) 5. https://doi.org/10.19030/iber.v5i2.3458

Uzoegbu, U.M., Uchebo, U.A., Okafor, I., 2013. Lithostratigraphy of the Maastrictian Nsukka Formation in the Anambra Basin, SE Nigeria. IOSR Journal Of Environmental Science, Toxicology, and Food Technology 5, 96–102.

Visser, J.N., Young, G.M., 1990. Major element geochemistry and paleoclimatology of the Permo-Carboniferous glacigene Dwyka Formation and postglacial mudrocks in southern Africa. Palaeogeography, Palaeoclimatology, Palaeoecology 81, 49–57.

Walker, R.G., Cant, D.J., 1984. Sandy fluvial systems. Facies Models 1, 71–89.

Wang, A., Wang, Z., Liu, J., Xu, N., Li, H., 2021a. The Sr/Ba ratio response to salinity in clastic sediments of the Yangtze River Delta. Chemical Geology 559, 119923.

Wang, Q., Jiang, F., Ji, H., Jiang, S., Liu, X., Zhao, Z., Wu, Y., Xiong, H., Li, Y., Wang, Z., 2020. Effects of paleosedimentary environment on organic matter enrichment in a saline lacustrine rift basin - A case study of Paleogene source rock in the Dongpu Depression, Bohai Bay Basin. Journal of Petroleum Science and Engineering 195, 107658. https://doi.org/10.1016/j.petrol.2020.107658

Wang, X., Wan, L., Jiang, Z., Liu, R., Wang, Xiabin, Tang, W., Gao, Y., Liu, S., Xu, W., 2017a. Controlling factors and accumulation model of hydrocarbon reservoirs in the Upper Cretaceous Yogou formation, Koulele area, Termit basin, Niger. Journal of Earth Science 28, 1126–1134.

Wang, Y., Chen, L., Yang, G., Wu, L., Xiao, A., Zhou, Y., Sun, L., Zhang, C., Yang, S., Chen, H., 2021b. The late Paleoproterozoic to Mesoproterozoic rift system in the Ordos Basin and its tectonic implications: Insight from analyses of Bouguer gravity anomalies. Precambrian Research 352, 105964.

Wang, Z., Fu, X., Feng, X., Song, C., Wang, D., Chen, W., Zeng, S., 2017b. Geochemical features of the black shales from the Wuyu Basin, southern Tibet: Implications for palaeoenvironment and palaeoclimate. Geological Journal 52, 282–297.

Wang, Z., Wang, J., Yu, F., Fu, X., Chen, W., Zhan, W., Song, C., 2021c. Geochemical characteristics of the Upper Triassic black mudstones in the eastern Qiangtang Basin, Tibet: Implications for petroleum potential and depositional environment. Journal of Petroleum Science and Engineering 207, 109180.

Wei, W., Algeo, T.J., 2020. Elemental proxies for paleosalinity analysis of ancient shales and mudrocks. Geochimica et Cosmochimica Acta 287, 341–366.

Wei, Y., Li, Xiaoyan, Zhang, R., Li, Xiaodong, Lu, S., Qiu, Y., Jiang, T., Gao, Y., Zhao, T., Song, Z., 2021. Influence of a Paleosedimentary Environment on Shale Oil Enrichment: A Case Study on the Shahejie Formation of Raoyang Sag, Bohai Bay Basin, China. Frontiers in Earth Science 732.

Whiteman, A., 1982. Nigeria: Its Petroleum Geology, Resources and Potential. I and II. Graham and Trotman Ltd., London.

Williams, T.S., Bhattacharya, S., Song, L., Agrawal, V., Sharma, S., 2022. Petrophysical analysis and mudstone lithofacies classification of the HRZ shale, North Slope, Alaska. Journal of Petroleum Science and Engineering 208, 109454.

Wu, Y., Liu, C., Liu, Y., Gong, H., Awan, R.S., Li, G., Zang, Q., 2022. Geochemical characteristics and the organic matter enrichment of the Upper Ordovician Tanjianshan Group, Qaidam Basin, China. Journal of Petroleum Science and Engineering 208, 109383.

Wu, Y., Tian, H., Gong, D., Li, T., Zhou, Q., 2020. Paleo-environmental variation and its control on organic matter enrichment of black shales from shallow shelf to slope regions on the Upper Yangtze Platform during Cambrian Stage 3. Palaeogeography, Palaeoclimatology, Palaeoecology 545, 109653.

Xi, Z., Tang, S., 2021. Geochemical characteristics and organic matter accumulation of Late Ordovician shale in the Upper Yangtze Platform, South China. Energy Reports 7, 667–682.

Xin, B., Hao, F., Han, W., Xu, Q., Zhang, B., Tian, J., 2021a. Paleoenvironment evolution of the lacustrine organic-rich shales in the second member of Kongdian Formation of Cangdong Sag, Bohai Bay Basin, China: Implications for organic matter accumulation. Marine and Petroleum Geology 133, 105244.

Xin, B., Hao, F., Han, W., Xu, Q., Zhang, B., Tian, J., 2021b. Paleoenvironment evolution of the lacustrine organic-rich shales in the second member of Kongdian Formation of Cangdong Sag, Bohai Bay Basin, China: Implications for organic matter accumulation. Marine and Petroleum Geology 133, 105244.

Xu, Z., Lu, H., Zhao, C., Wang, X., Su, Z., Wang, Z., Liu, H., Wang, L., Lu, Q., 2011. Composition, origin and weathering process of surface sediment in Kumtagh Desert, Northwest China. Journal of Geographical Sciences 21, 1062–1076.

Yakubu, J.A., Okeke, F.N., Obiora, D.N., 2020. Estimation of Curie point depth, geothermal gradient and heat flow within the lower Benue trough, Nigeria using high resolution aeromagnetic data. Modeling Earth Systems and Environment 6, 1439–1449.

Yan, C., Jin, Z., Zhao, J., Du, W., Liu, Q., 2018. Influence of sedimentary environment on organic matter enrichment in shale: A case study of the Wufeng and Longmaxi Formations of the Sichuan Basin, China. Marine and Petroleum Geology 92, 880–894.

You, J., Liu, Y., Zhou, D., Zheng, Q., Vasichenko, K., Chen, Z., 2020. Activity of hydrothermal fluid at the bottom of a lake and its influence on the development of high-quality source rocks: Triassic Yanchang Formation, southern Ordos Basin, China. Australian Journal of Earth Sciences 67, 115–128.

Zanguina, M., Bruneton, A., Gonnard, R., 1998. An introduction to the petroleum potential of Niger. Journal of Petroleum Geology 21, 83–103.

Zeng, S., Wang, J., Fu, X., Chen, W., Feng, X., Wang, D., Song, C., Wang, Z., 2015. Geochemical characteristics, redox conditions, and organic matter accumulation of marine oil shale from the Changliang Mountain area, northern Tibet, China. Marine and Petroleum Geology 64, 203–221. https://doi.org/10.1016/j.marpetgeo.2015.02.031

Zhang, C., Chen, J., Song, M., Wang, J., Yuan, B., 2015. Structural interpretation of the Qingdong area in Bohai Bay basin from shipborne gravity data. Polish Maritime Research 22, 100–105.

Zhang, K., Liu, R., Liu, Z., Li, L., Wu, X., Zhao, K., 2020. Influence of palaeoclimate and hydrothermal activity on organic matter accumulation in lacustrine black shales from the Lower Cretaceous Bayingebi Formation of the Yin'e Basin, China. Palaeogeography, Palaeoclimatology, Palaeoecology 560, 110007. https://doi.org/10.1016/j.palaeo.2020.110007

Zhang, L., Dong, D., Qiu, Z., Wu, C., Zhang, Q., Wang, Y., Liu, D., Deng, Z., Zhou, S., Pan, S., 2021. Sedimentology and geochemistry of Carboniferous-Permian marine-continental transitional shales in the eastern Ordos Basin, North China. Palaeogeography, Palaeoclimatology, Palaeoecology 571, 110389.

Zhang, L., Xiao, D., Lu, Shuangfang, Jiang, S., Lu, Shudong, 2019a. Effect of sedimentary environment on the formation of organic-rich marine shale: Insights from major/trace elements and shale composition. International Journal of Coal Geology 204, 34–50.

Zhang, M., Qiao, J., Zhao, G., Lan, X., 2019b. Regional gravity survey and application in oil and gas exploration in China. China Geology 2, 382–390. https://doi.org/10.1016/S2096-5192(19)30188-0

Zhang, S., Liu, C., Liang, H., Wang, J., Bai, J., Yang, M., Liu, G., Huang, H., Guan, Y., 2018. Paleoenvironmental conditions, organic matter accumulation, and unconventional hydrocarbon potential for the Permian Lucaogou Formation organic-rich rocks in Santanghu Basin, NW China. International Journal of Coal Geology 185, 44–60.

Zhang, S.C., Hanson, A.D., Moldowan, J.M., Graham, S.A., Liang, D.G., Chang, E., Fago, F., 2000. Paleozoic oil–source rock correlations in the Tarim basin, NW China. Organic Geochemistry 31, 273–286.

Zhao, B.S., Li, R.X., Wang, X.Z., Wu, X.Y., Wang, N., Qin, X.L., Cheng, J.H., Li, J.J., 2016. Sedimentary environment and preservation conditions of organic matter analysis of Shanxi formation mud shale in Yanchang exporation area, Ordos Basin. Geological Science and Technology Information 35, 109–117.

Zhao, J.-Z., Li, J., Wu, W.-T., Cao, Q., Bai, Y.-B., Er, C., 2019. The petroleum system: a new classification scheme based on reservoir qualities. Petroleum Science 16, 229–251.

Zhong, D.K., Jiang, Z.K., Guo, Q., Sun, H.T., 2015. A review about research history, situation and prospects of hydrothermal sedimentation. J Palaeogeogr 17, 285–296.

Zingerle, P., Pail, R., Gruber, T., Oikonomidou, X., 2020. The combined global gravity field model XGM2019e. Journal of Geodesy 94, 1–12.

Appendix 1

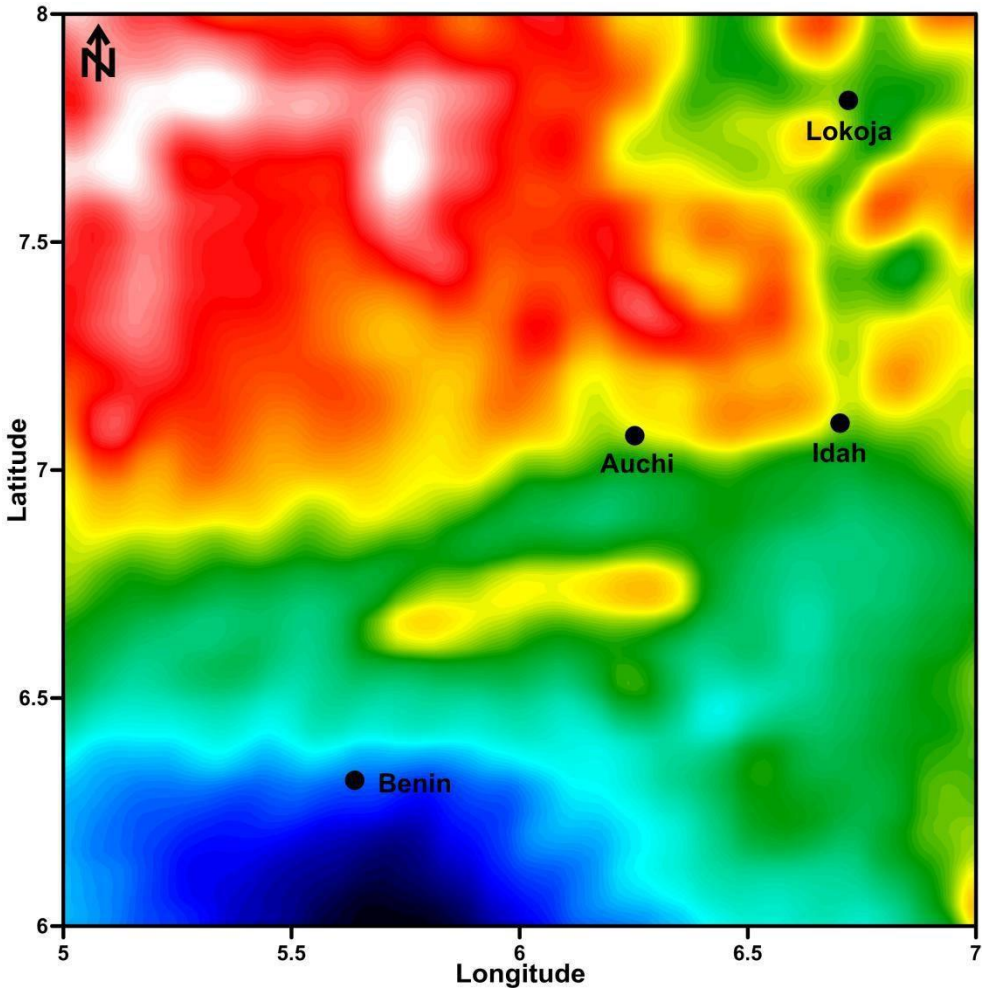

Figure 1: Free-air anomaly map of the study area

Appendix 2

Table 1. Major elements oxides (wt%) and trace elements (ppm) data of the Owan and Ubiaja wells

Well	Sample	Depth (m)	Rock type	SiO_2	Al_2O_3	Fe_2O_3	MgO	CaO	Na_2O	K_2O	TiO_2	P_2O_5	MnO	LOI	Total
Owan	OW1	60	shale	53.60	14.35	4.23	8.09	0.91	0.38	0.81	0.54	0.10	0.05	15.65	99.90
Owan	OW10	103	clayey shale	7.08	2.65	1.19	1.43	47.37	0.18	0.14	0.08	0.03	0.19	39.24	99.94
Owan	OW11	107	shale	29.48	11.62	3.11	3.15	2.07	0.28	0.69	0.47	0.13	0.03	48.53	99.96
Owan	OW14	138	shale	51.34	16.88	4.89	6.53	2.58	0.39	1.32	0.71	0.18	0.05	13.35	99.93
Owan	OW21	192	shale	48.66	22.63	7.36	2.81	0.73	0.16	1.73	1.21	0.07	0.13	14.19	99.95
Owan	OW26	234	shale	52.31	21.30	6.39	1.09	0.25	0.01	0.67	1.50	0.14	0.10	15.68	99.96
Owan	OW29	300	sandy shale	34.96	11.14	23.85	4.43	2.00	0.01	0.21	0.55	0.04	0.20	22.34	99.93
Owan	OW30	340	clayey shale	54.85	21.43	4.55	0.26	0.13	0.01	0.20	1.13	0.11	0.01	16.44	99.93
Owan	OW31	365	silty shale	70.01	14.99	2.54	0.28	0.15	0.01	0.14	1.04	0.08	0.02	10.19	99.92
Owan	OW36	540	shale	72.87	12.97	1.70	0.18	0.16	0.01	0.30	1.46	0.07	0.01	9.27	99.92
Ubiaja	UB03	48	claystone	56.07	27.42	1.53	0.12	0.04	0.01	0.21	2.38	0.07	0.01	11.58	99.96
Ubiaja	UB07	126	shaly sandstone	83.83	5.85	0.70	0.14	3.14	0.01	0.08	0.25	0.04	0.01	5.44	99.90
Ubiaja	UB09	172	shale	84.90	7.97	0.57	0.04	0.45	0.01	0.08	0.48	0.03	0.01	5.30	99.97
Ubiaja	UB17	265	shale	56.98	19.79	2.47	0.11	0.11	0.01	0.18	1.15	0.06	0.01	18.65	99.92
Ubiaja	UB21	305	clayey shale	80.35	11.13	1.40	0.13	0.18	0.01	0.12	0.62	0.05	*0.01*	5.90	99.96
Ubiaja	UB25	357	sandy shale	85.07	7.71	1.03	0.08	0.09	0.01	0.08	0.40	0.03	0.01	5.05	99.93
Ubiaja	UB30	407	shale	54.08	22.80	5.61	0.50	0.20	0.09	0.77	1.48	0.12	0.08	13.75	99.94
Ubiaja	UB32	425	shale	52.95	23.20	4.53	0.32	0.27	0.15	0.55	1.44	0.14	0.06	16.08	99.97
Ubiaja	UB34	612	sandy shale	85.22	4.13	5.49	0.14	0.28	0.01	0.64	0.50	0.05	0.07	3.10	99.97
Ubiaja	UB40	625	shale	46.15	25.53	10.77	0.54	0.49	0.01	0.73	1.51	0.24	0.11	13.81	99.97

Table 1: Continued

	LILE				HFSE							Others							
Sample	**Rb**	**Ba**	**Sr**	**Pb**	**Th**	**U**	**Zr**	**Hf**	**Ta**	**Y**	**Nb**	**Sc**	**Cr**	**Ni**	**Co**	**V**	**Ga**	**Zn**	**Cu**
OW1	33.63	70.24	165.62	12.64	7.63	1.48	88.71	2.41	0.92	9.34	13.73	8.71	120.92	28.24	159.05	149.17	15.99	80.06	10.97
OW10	9.298	18.61	652.3	2.73	1.41	0.45	13.65	0.35	0.1	6.583	2.23	4.65	22	5.89	22.64	25.57	4.55	24.33	2.34
OW11	54.15	132.8	297	18.45	9.57	2.43	108.6	2.82	1.23	16.68	20.75	13.65	114.59	36.28	59.56	152.80	22.22	110.68	14.18
OW14	53.46	111.91	184.3	16	9.054	2.33	110.8	2.914	1.074	12.51	17.43	11.82	149.88	34.62	629.11	145.60	18.53	103.49	10.13
OW21	67.62	136.55	151.9	23.86	13.55	2.37	249.5	6.51	2.49	24.87	42.08	14.67	118.17	44.50	66.65	191.01	29.13	136.46	14.55
OW26	32.82	118.63	166.5	22.56	12.13	2.67	258.5	7.18	2.45	18.61	40.87	11.16	104.16	30.30	298.68	123.00	26.21	85.44	17.62
OW29	11.35	59.99	80.11	12.43	6.73	1.79	81.88	2.346	0.599	12.78	9.053	18.18	92.93	24.40	62.58	158.46	13.75	94.06	9.92
OW30	7.9	99.19	93.13	42.36	19.22	15.27	172.9	5.52	1.74	33.72	26.93	10.29	197.38	32.42	95.92	255.57	33.72	329.84	16.72
OW31	5.779	98.85	59.27	25.8	13.39	5.71	162.4	5.12	1.64	21.52	24.12	9.63	111.33	22.57	98.99	110.82	19.46	148.71	12.94
OW36	13.25	95.28	42.37	17.41	17.73	6.3	338.6	10.46	1.69	23.78	24.079	7.78	66.18	17.28	377.32	78.82	17.53	83.19	12.45
UB03	10.41	143.05	54.14	33.43	21.17	4.6	353.7	9.42	4.11	25.72	71.22	14.11	108.30	17.29	61.60	91.54	35.84	26.84	8.98

UB07	2.98	55.28	45.74	9.15	4.15	0.95	59.12	1.699	0.74	4.73	10.46	3.00	25.36	7.70	205.02	23.81	8.35	23.52	6.47
UB09	4.504	79.29	32.51	20.45	8.93	2.88	129.5	3.6	1.33	10.96	25.85	8.05	61.64	45.83	268.26	44.08	21.53	21.82	15.48
UB17	7.58	117.56	44.26	27.48	12.84	5.76	161.6	4.58	1.53	22.5	32.011	16.21	94.24	32.00	471.34	92.82	26.36	35.83	24.83
UB21	10.92	124.02	46.88	26.16	14.48	3.33	231.6	6.03	2.95	16.79	52.34	10.68	76.71	16.33	249.42	70.61	27.51	26.95	18.25
UB25	4.809	85.58	22.72	16.33	7.3	1.54	114.1	3.19	1.56	7.575	23.4	4.27	38.97	13.18	341.51	29.08	13.22	34.03	8.94
UB30	33.83	346.88	85.44	32.65	16.61	3.54	205.9	5.65	2.44	29.49	42.414	14.09	106.62	39.69	135.04	110.69	32.49	108.79	20.26
UB32	22.93	377.57	82.73	43.12	15.85	3.61	190.9	5.33	2.303	22.7	39.723	13.24	103.67	40.69	102.94	103.78	32.59	82.18	19.46
UB34	16.75	356.47	57.53	16.44	4.985	1.2	160.3	3.92	0.797	9.22	11.23	4.21	40.32	14.14	381.69	39.21	7.22	34.25	11.65
UB40	46.11	588.37	116.6	29.79	13.47	3.69	187.8	5.156	1.9	20.57	30.803	10.99	86.49	50.76	220.40	95.49	26.47	241.60	17.97

Table 1: Continued

	REE																			
Sample	**La**	**Ce**	**Pr**	**Nd**	**Sm**	**Eu**	**Gd**	**Tb**	**Dy**	**Ho**	**Er**	**Tm**	**Yb**	**Lu**	**CIA**	**CIW**	**PIA**	**ICV**	**C-value**	**Fe/Mn**	**D***
OW1	25.72	52.92	5.62	21.03	3.82	0.81	3.22	0.41	2.31	0.43	1.13	0.16	1.06	0.15	87.00	92.00	91.00	1.00	1.90	85.00	0.77
OW10	14.72	27.15	2.81	10.22	1.58	0.35	1.35	0.18	1.07	0.21	0.58	0.08	0.52	0.08	78.00	81.00	81.00	19.00	0.10	6.00	0.65
OW11	36.13	71.10	7.82	30.88	5.87	1.34	5.11	0.66	3.75	0.70	1.88	0.26	1.72	0.25	88.00	92.00	92.00	0.80	0.80	103.00	0.79
OW14	30.76	57.88	6.30	23.56	4.49	1.00	3.81	0.51	2.92	0.56	1.53	0.22	1.46	0.21	86.00	92.00	92.00	0.90	3.10	97.00	0.77
OW21	55.64	113.40	12.44	46.52	9.06	1.94	7.91	1.06	6.14	1.10	2.90	0.40	2.62	0.36	91.00	97.00	95.00	0.60	1.40	56.00	0.75
OW26	46.81	92.82	9.93	35.47	5.99	1.21	4.96	0.68	4.01	0.80	2.33	0.37	2.51	0.36	97.00	99.00	99.00	0.40	1.80	63.00	0.76
OW29	31.90	68.54	7.38	28.02	4.63	0.99	3.70	0.49	2.90	0.58	1.73	0.28	1.83	0.28	98.00	99.00	99.00	2.70	2.50	119.00	0.31
OW30	94.85	224.49	24.03	94.91	17.79	3.65	14.81	1.90	9.81	1.70	4.65	0.71	4.63	0.64	99.00	100.00	100.00	0.30	3.00	455.00	0.82
OW31	46.92	103.28	11.26	44.24	8.49	1.71	7.51	1.02	5.71	1.06	2.87	0.42	2.64	0.37	98.00	99.00	99.00	0.30	2.20	127.00	0.85
OW36	50.92	105.79	11.67	44.72	8.22	1.33	7.19	0.98	5.60	1.10	3.21	0.48	3.10	0.45	97.00	99.00	100.00	0.30	3.90	170.00	0.88
UB03	53.20	89.20	10.78	43.38	9.10	1.96	8.07	1.08	6.01	1.13	3.03	0.43	2.92	0.42	99.00	100.00	100.00	0.20	1.42	153.00	0.95
UB07	17.43	29.42	2.86	9.80	1.64	0.32	1.41	0.19	1.04	0.20	0.54	0.08	0.51	0.07	98.00	99.00	99.00	0.70	2.50	70.00	0.89
UB09	62.22	126.73	11.69	37.31	6.31	1.24	4.81	0.62	3.40	0.61	1.66	0.24	1.65	0.23	98.00	99.00	99.00	0.20	3.70	57.00	0.93
UB17	49.81	101.29	12.44	53.13	12.94	2.68	9.91	1.36	7.57	1.33	3.52	0.50	3.49	0.47	99.00	99.00	100.00	0.20	4.20	247.00	0.88
UB21	62.46	112.47	11.24	38.56	6.66	1.37	5.56	0.72	4.11	0.75	2.05	0.29	1.90	0.27	99.00	99.00	99.00	0.20	2.40	140.00	0.89
UB25	33.13	57.09	5.55	19.04	3.15	0.61	2.66	0.35	1.90	0.35	0.97	0.14	0.89	0.12	98.00	99.00	99.00	0.20	3.90	103.00	0.88
UB30	68.66	145.54	15.57	58.67	11.11	2.39	9.64	1.25	7.01	1.28	3.30	0.45	2.88	0.40	95.00	99.00	98.00	0.30	0.90	70.00	0.80
UB32	65.98	134.33	14.31	51.66	9.39	2.09	7.97	1.01	5.54	1.01	2.65	0.36	2.32	0.33	96.00	98.00	98.00	0.40	0.80	76.00	0.83
UB34	17.36	33.13	3.42	12.59	2.33	0.49	2.19	0.31	1.86	0.39	1.14	0.17	1.25	0.19	85.00	99.00	97.00	1.70	1.20	78.00	0.42
UB40	53.33	112.16	12.28	45.84	8.59	1.98	7.27	0.93	5.18	0.95	2.49	0.35	2.22	0.32	97.00	99.00	99.00	0.60	0.60	98.00	0.70

Table 1: Continued

Sample	V/Cr	Ni/Co	V/V+Ni	Cu/Zn	U/Th	Zr/Sc	Rb/Sr	Th/Sc	Sr/Ba	Zr/Rb	Th/U	P/Ti	Ba/Al
OW1	1.23	0.18	0.84	0.14	0.19	10.18	0.20	0.87	2.35	2.60	5.20	0.12	4.90
OW10	1.14	0.26	0.81	0.10	0.32	2.94	0.01	0.30	35.05	1.50	3.10	0.26	7.00
OW11	1.33	0.61	0.81	0.13	0.25	7.95	0.20	0.70	2.24	2.00	3.90	0.17	11.40
OW14	0.97	0.06	0.90	0.09	0.26	9.38	0.30	0.76	1.65	2.10	3.90	0.14	6.60
OW21	1.62	0.67	0.81	0.11	0.17	17.01	0.50	0.92	1.11	3.70	5.70	0.06	6.00
OW26	1.18	0.10	0.80	0.21	0.22	23.17	0.20	1.09	1.40	7.90	4.50	0.04	5.60
OW29	1.71	0.39	0.86	0.03	0.27	4.50	0.10	0.37	1.34	7.20	3.80	0.06	5.40
OW30	1.29	0.34	0.88	0.05	0.79	16.80	0.10	1.87	0.94	21.80	1.30	0.06	4.60
OW31	0.99	0.23	0.83	0.09	0.43	16.86	0.10	1.39	0.59	28.10	2.40	0.04	6.60
OW36	1.19	0.06	0.82	0.15	0.36	43.52	0.30	2.28	0.44	25.50	2.80	0.03	7.30
UB03	0.85	0.28	0.84	0.33	0.22	25.06	0.20	1.50	0.37	33.90	4.60	0.02	5.20
UB07	0.94	0.04	0.75	0.28	0.23	19.71	0.10	1.38	0.83	19.80	4.40	0.08	9.50
UB09	0.72	0.17	0.49	0.71	0.32	8.05	0.10	1.11	0.41	28.70	3.10	0.04	10.00
UB17	0.98	0.07	0.74	0.69	0.45	9.97	0.20	0.79	0.38	21.30	2.20	0.03	5.90
UB21	0.92	0.06	0.80	0.68	0.23	21.68	0.20	1.36	0.38	21.20	4.40	0.03	11.00
UB25	0.75	0.04	0.68	0.26	0.21	26.72	0.20	1.71	0.27	23.70	4.70	0.04	11.10

UB30	1.04	0.29	0.74	0.19	0.21	14.61	0.40	1.18	0.25	6.10	4.70	0.04	15.20
UB32	1.00	0.40	0.72	0.24	0.23	14.42	0.30	1.20	0.22	8.30	4.30	0.05	16.30
UB34	0.97	0.04	0.73	0.34	0.24	38.08	0.30	1.18	0.16	9.60	4.20	0.09	86.30
UB40	1.10	0.23	0.65	0.07	0.27	17.09	0.40	1.23	0.20	4.10	3.70	0.04	23.10

Appendix 3

Table 2. Total Organic Carbon data of the Owan and Ubiaja wells Anambra Basin

No.	Sample	Depth (m)	TOC
1	OW 07	60	0.50541
2	OW 09	99	0.50285
3	OW 11	107	0.052855
4	OW 12	122	0.456
5	OW 14	138	0.63613
6	OW 15	147	0.33885
7	OW 16	153	0.32878
8	OW 18	172	0.41131
9	OW 19	182	0.24472
10	OW 20	187	0.49709
11	OW 22	194	21.9796
12	OW 24	199	1.36699
13	OW 25	210	0.60718
14	OW 26	234	0.43245
15	OW 27	256	0.63392
16	OW 28	278	0.65796
17	OW 29	300	0.68782
18	OW 30	340	1.88117
19	OW 31	365	2.40266
20	OW 34	443	1.40862
21	OW 36	540	0.67812
22	UB 03	48	0.12199
23	UB 06	70	0.33409
24	UB 9	172	1.84256
25	UB 17	265	4.07955

26	UB 18	272	1.04715
27	UB 19	280	0.79497
28	UB 20	298	0.55083
29	UB 21	305	0.66833
30	UB 22	318	0.62114
31	UB 27	370	1.26105
32	UB 28	390	1.90958
33	UB 29	397	1.3996
34	UB 30	407	2.0074
35	UB 32	425	2.74932
36	UB 33	436	1.67161
37	UB 36	615	2.53447
38	UB 39	623	1.38682
39	UB 40	625	2.19686
40	UB 43	629	2.27246

Note: OW=Owan, UB= Ubiaja